INFORMATION TO USERS

This dissertation was produced from a microfilm copy of the original document. While the most advanced technological means to photograph and reproduce this document have been used, the quality is heavily dependent upon the quality of the original submitted.

The following explanation of techniques is provided to help you understand markings or patterns which may appear on this reproduction.

1. The sign or "target" for pages apparently lacking from the document photographed is "Missing Page(s)". If it was possible to obtain the missing page(s) or section, they are spliced into the film along with adjacent pages. This may have necessitated cutting thru an image and duplicating adjacent pages to insure you complete continuity.

2. When an image on the film is obliterated with a large round black mark, it is an indication that the photographer suspected that the copy may have moved during exposure and thus cause a blurred image. You will find a good image of the page in the adjacent frame.

3. When a map, drawing or chart, etc., was part of the material being photographed the photographer followed a definite method in "sectioning" the material. It is customary to begin photoing at the upper left hand corner of a large sheet and to continue photoing from left to right in equal sections with a small overlap. If necessary, sectioning is continued again — beginning below the first row and continuing on until complete.

4. The majority of users indicate that the textual content is of greatest value, however, a somewhat higher quality reproduction could be made from "photographs" if essential to the understanding of the dissertation. Silver prints of "photographs" may be ordered at additional charge by writing the Order Department, giving the catalog number, title, author and specific pages you wish reproduced.

University Microfilms

300 North Zeeb Road
Ann Arbor, Michigan 48106

A Xerox Education Company

72-25,011

BOETTINGER, William James, 1946-
SURFACE RELIEF CINEMICROGRAPHY OF THE UNSTEADY SOLIDIFICATION OF THE LEAD-TIN-CADMIUM TERNARY EUTECTIC.

The Johns Hopkins University, Ph.D., 1972
Materials Science

University Microfilms, A XEROX Company, Ann Arbor, Michigan

© 1972

WILLIAM JAMES BOETTINGER

ALL RIGHTS RESERVED

THIS DISSERTATION HAS BEEN MICROFLIMED EXACTLY AS RECEIVED

Surface Relief Ciremicrography
of the
Unsteady Solidification of the Lead-Tin-Cadmium Ternary Eutectic

by

William James Boettinger

A dissertation submitted to
The Johns Hopkins University
in conformity with the requirements for
the degree of Doctor of Philosophy

Baltimore, Maryland
1972

PLEASE NOTE:

Some pages may have

indistinct print.

Filmed as received.

University Microfilms, A Xerox Education Company

Abstract

An experimental technique is developed to directly observe the solidification of alloys. This technique utilizes the microscopic observation of the topography produced by the microstructure on a free surface of a .25 mm thick foil, which is suspended on an oblong wire loop. Directional growth is obtained by electrically heating one end of the wire loop. For the Pb-Sn-Cd ternary eutectic, information regarding the motion of the liquid-solid interface and the Pb-rich and Sn-rich lamellae is recorded cinemicrographically. Metallographic sectioning of the foils after solidification shows no sign of microstructural differences between the interior and the exterior of the foil.

This technique is applied to the study of the unsteady solidification of the Pb-Sn-Cd ternary eutectic. It is well known that changes in solidification velocity have a profound effect on inter-lamellar spacing; but the dynamics of such effects have not been documented. In the present work, it is found that the lamellar spacing does not begin to change until the ratio of the interface velocity to the initial (steady) velocity reaches a critical value. This critical value depends heavily on the uniformity of the lamellar structure. Also when the final steady interface velocity is more than four times the initial steady velocity, the lameller spacing does not decrease uniformly in time but decreases in

stages. It was also found that after a velocity change from one steady value to another the product $\lambda^2 n$ does not return to its original value. A steady state theory of ternary lamellar solidification is formulated and used as a basis for a discussion of the non-steady results.

Acknowledgements

To Professor Robert B. Pond, I owe many thanks. He has been a constant source of encouragement and guidance throughout my undergraduate and graduate years at Johns Hopkins. He has not only instilled in me a deep interest in Materials Science, but has played an intangible role in helping me attain manhood. His life will always serve as an inspiration for me.

Special thanks must be extended to Professor Robert E. Green, Jr. for his interest and support throughout this research.

To Mr. Russell Vane III, I extend my thanks for his conscientious aid with much of the photographic work and for a computer program to compute a mathematic solution found in this work. To Mrs. Mary Thuma is due my gratitude for typing this manuscript.

Lastly, I would like to thank my wife, Sharon, for making my life very pleasant during all of this work.

Table of Contents

		Page No.
	Abstract	ii
	Acknowledgements	iv
	Table of Illustrations	vi
I.	Introduction	1
II.	Survey of Experimental Techniques to Study Solidification	5
III.	Survey of Current Knowledge of Lamellar Eutectic Solidification	11
IV.	Purpose of Program	25
V.	A Steady State Theory of Ternary Lamellar Solidification	26
VI.	Experimental Procedures	40
VII.	Treatment of Data	50
VIII.	Results and Discussion	57
	1. Constant Interface Velocity	57
	2. Increases in Interface Velocity	57
	3. Decreases in Interface Velocity	82
	4. Oscillating Interface Velocity	97
IX.	Conclusions	102
	Bibliography	105
	Vita	109

Table of Illustrations

		Page No.
Fig. 1	Cline's apparatus for directly observing solidification (28)	10
Fig. 2	a) Binary eutectic phase diagram with extended liquidi	14
	b) Binary lamellar liquid-solid interface	14
	c) Binary eutectic diagram with parameters, $C_o^{\alpha}, C_o^{\beta}, C_e$	14
Fig. 3	$\Delta T = K_1 \lambda v + K_2/\lambda$ plot	18
Fig. 4	Ternary eutectic phase diagram (49)	27
Fig. 5	a) Ternary lamellar liquid-solid interface	29
	b) Isothermal section of a ternary eutectic diagram at the eutectic temperature with compositions of solid phases labeled	29
Fig. 6	Liquidus surface for Pb-Sn-Cd system (atomic %) (50)	35
Fig. 7	Composition distribution in the liquid at the interface	36
Fig. 8	Extrapolated pyramid showing effects of composition and interface curvature on temperature of interface	38
Fig. 9	a) Sketch of wire loop with alloy foil, spacer loop, and cover glass	42
	b) Wiring diagram for spark welder	42
Fig 10	a) Micrograph of transverse section of foil showing topography produced by microstructure at top surface of foil	45
	b) Micrograph of top surface of foil showing liquid and solid phases	45
Fig. 11	Micrograph of longitudinal section of foil showing ternary lamellar structure (Nital etch)	46
Fig. 12	Wiring diagram for current supply	48

		Page No.
Fig. 13	a) Low magnification micrograph of moving liquid-solid interface on the surface of the foil	49
	b) Micrograph of longitudinal section of foil showing "quenched interface"	49
Fig. 14	A typical plot of interface position vs. time data	55
Fig. 15	Inclined lamellae to foil	56
Fig. 16	Steady state $\lambda^2 v$ data superimposed on the data of Kerr et al.	60
Fig. 17	Sequence of enlargements from movie film at 0.6 second intervals for velocity increase test	61
Fig. 18	Data for velocity increase tests	62
Fig. 19	Data for velocity increase tests	63
Fig. 20	Data for velocity increase tests	64
Fig. 21	Data for velocity increase tests	65
Fig. 22	Micrograph taken from movie film for each test showing structure uniformity no. (velocity increase tests)	68
Fig. 23	Micrograph taken from movie film for each test showing structure uniformity no. (velocity increase tests)	69
Fig. 24	Two ways of decreasing lamellar spacing by formation of new lamellae	74
Fig. 25	Correlation of v_d/v_i with structure uniformity, acceleration, and v_f/v_i (velocity increase tests)	76
Fig. 26	Formation of concavities in the α lamellae liquid-solid interface due to velocity increase	81
Fig. 27	Sequence of enlargements from movie film at 2.4 second intervals for velocity decrease test	85
Fig. 28	Data for velocity decrease tests	86
Fig. 29	Data for velocity decrease tests	87
Fig. 30	Data for velocity decrease tests	88

		Page No.
Fig. 31	Data for velocity decrease tests	89
Fig. 32	Micrographs taken from movie film for each test showing structure uniformity no. (velocity decrease tests)	91
Fig. 33	Micrographs taken from movie film for each test showing structure uniformity no. (velocity decrease tests)	92
Fig. 34	Correlation of v_d/v_i with structure uniformity no., acceleration, and v_f/v_i (velocity decrease tests)	96
Fig. 35	Data for oscillating velocity tests	98
Fig. 36	Data for oscillating velocity tests	99
Fig. 37	Values of v_d/v_i along with $\Delta T/\Delta T_e = \frac{1}{2}\left[\left(\frac{v}{v_i}\right)^{-\frac{1}{2}} + \left(\frac{v}{v_i}\right)^{\frac{1}{2}}\right]$	101

I. INTRODUCTION

The ultimate goal of a macroscopic physical theory is the prediction of the state of a body subject to certain exterior conditions. Continuum Mechanics and Modern Thermodynamics deal with the prediction of the density, motion and temperature at each point in a body for all future time, when the body is subjected to forces, displacements, heatings and temperatures on the exterior. Among the great variety of problems which can be approached through these theories, those problems involving a physical phase transition are rarely pursued. For example, the mechanical response of a body of water partly liquid and partly solid and capable of melting or freezing during the mechanical process would be quite complicated.

The definition of a physical phase transition has classically been made in two ways. The more intuitive way is by defining a phase as that part of a body which is physically and chemically homogeneous, and then the transition as that process which changes part of a body from one phase to another. This definition of a phase transition is not without its flaws but can be adopted as a working definition. The more analytic way is by defining a phase transition as that process whereby a body suffers a discontinuity of the temperature derivative of some objective energy function of the material at a moving surface in the body. This surface then divides the body into portions which are different phases. This definition is a general-

ization of the classical definition of a first-order phase transition. Solidification mechanics is the study of the motion of such surfaces of discontinuity when at least one phase is a liquid and one is a solid and the surface moves toward the liquid phase.

The existence of phase diagrams in metallurgy and physical chemistry indicate that, under certain conditions, many phase transitions occur at specific values of the variables which in some sense define the local state of a body. These diagrams have been determined in the context of the old thermodynamics or more properly thermostatics, in which the local state of a body was considered to be the same at different places in the body, and that "processes" occurred very slowly. For these reasons phase diagrams are often called equilibrium phase diagrams. The extension of such phase diagrams from global, static states to local, dynamic processes is the first step in establishing the basis for solidification mechanics. This extension must be made carefully, incorporating information known about the microscopics of phase transitions. The fact that these equilibrium diagrams cannot be directly extended to a local description of phase transitions greatly complicates solidification mechanics and makes it excitingly interesting at the same time.

This work deals with the solidification of a ternary eutectic alloy, often called a eutectic reaction. This reaction

is a polyphase transition; i.e., it involves more than two phases. In an n component system a eutectic reaction is the simultaneous precipitation of n solid phases from a single liquid phase. According to the Gibbs Phase Rule, a result valid in the context of equilibrium phase diagrams, such reactions should occur at a fixed temperature and fixed liquid composition, rather than over a range of temperatures and compositions if the pressure is held constant. That is, a liquid of any other composition would not simultaneously precipitate n phases upon cooling. Whether these reactions actually do occur isothermally and only at one composition will be discussed later, but these reactions do occur in nature and one hopes that deviations from the equilibrium behavior will not be too great.

After a eutectic reaction in an n component system, n solid phases will exist in the solid state. The prediction of the spatial distribution of these phases in the solid, or the microstructure, is one of the primary goals of any theory of eutectic solidification. The solid microstructure of many eutectics has been known for some time. Three excellent review articles (1,2,3) have been written on eutectic solidification in binary alloys but a brief history of the early understanding of eutectics will be presented here.

Eutectics were first recognized and named as that alloy in a given system having a minimum freezing temperature by Guthrie (4) in 1884. That solid binary eutectic alloys consisted

of two phases was shown by Ponsot (5) in 1895. Rosehain and Tucker (6), Tammann (7), Lamplough and Scott (8), Desch (9), Vogel (10), Brady (11), Portevin (12) were among those attempting to classify solid eutectic microstructures by microscopic examination. Of the great variety of two-phase solid structures observed, the ones commanding the most interest were lamellar eutectic structures in which each separate lamination is single-phase. Vogel (10) in 1912 showed that the lamellar structures grew from the liquid in an edgewise manner. Tammann and Moritz (13) showed that the crystallization velocity of eutectics was considerably slower than either of the pure components when cast under similar conditions. Thus they realized that the growth of a lamellar eutectic was diffusion controlled. Bochvar and Gorev (14) showed that the ternary eutectic of Pb-Sn-Cd was lamellar. Winegard et al. (15) in 1951 showed that both phases in binary eutectics grew simultaneously from the melt and that the lamellar spacing was a function of growth rate. Since that time, most of the research, both theoretical and experimental, on lamellar eutectics has been to determine the relationship between lamellar spacing and growth velocity. Almost all of the research has been done on binary lamellar eutectics, and all but qualitative results correspond to eutectic structures produced by steady growth velocities. This work will study the effect of non-steady growth velocities on the lamellar spacing in a ternary lamellar eutectic.

II. SURVEY OF EXPERIMENTAL TECHNIQUES USED TO STUDY SOLIDIFICATION

The earliest information regarding the solidification of metals and alloys was at best very indirect. Surface shrinkage patterns and internal solid microstructures produced by various casting conditions have been examined for centuries with the naked eye and the optical microscope (16). Much of the work of this type was performed for reasons other than the study of solidification. The more conscientious investigators of phase diagrams using metallographic techniques were aware of the effects that casting conditions had on ingot structure. For example, Phragmen (17) in his monumental work on the constitution of alloys of Al with Fe, Cu, Si, Mg and Mn performed castings in molds which were originally hot or cold, made of cast iron or a refractory and then furnace- or air-cooled. Although much useful knowledge about solidification was obtained in these manners, the conditions of solidification were far too complicated and the observation techniques were too limited to yield systematic and error-free knowledge about the mechanics of solidification.

The development of unidirectional solidification was the beginning of modern solidification research. This technique was originally invented by Tammann (7) in 1925 and developed by many others with the purpose of growing metal single crystals from the melt. The method was not, however, used greatly in research on solidification until the late 1940's and early 1950's.

With appropriate placement of heat sinks, heat sources and insulators, the direction of the temperature gradient was held nearly constant throughout a long cylindrical mold. This simple arrangement greatly simplified the understanding of solid microstructures produced by solidification and permitted more detailed information regarding the solidification conditions. By placing one or more small thermocouples in the melt at various positions, the liquid-solid interface position and velocity as well as the temperature gradient were surmised. Even with this technique of solidification, unless a complicated heating and cooling program is used at the ends of the mold, the growth conditions will vary greatly from one end of the mold to the other.

The purpose of the next development in experimental solidification research was to produce uniform solidification conditions throughout a directionally solidified ingot. Again this development was made in the single crystal field. Bridgeman (18) was the first to lower a long cylindrical mold through a temperature gradient provided by a furnace. All of these methods attempted to simplify the conditions under which a metal or alloy was to become a solid. Direct observation of the motion of the liquid-solid interface was not made, and solidification velocity could only be guessed at from the thermocouple data or the mold removal rate from a gradient furnace. In the event that the solidification velocities were unsteady, these indirect measurements of solidification velocity were useless.

To gain more precise information regarding the exact shape and position of the liquid-solid interface at any instant, two techniques were developed. Pond and Kessler (19) and Weinberg and Chalmers (20,21) were among the first to decant the remaining liquid during the course of unidirectional solidification to expose the liquid-solid interface. Some questions always remained regarding distortion of the interface shape by residual liquid. The other technique employed a sudden, drastic increase in solidification velocity during the course of solidification. Because the fineness of the microstructure is usually determined by solidification velocity, a demarcation of the interface at the time of the drastic change in velocity is recorded in the microstructure. Both of these techniques added greatly to the knowledge of solidification mechanics, but still they did not directly observe the moving interface and the microstructure it produced.

Glicksman (22) has recently reviewed direct methods of observing solidification for both optically transparent and opaque materials. Much information regarding metallic solidification has been obtained by Jackson and Hunt (23) and others by using transparent organic materials that solidify like metals do. However, methods of observing such systems will not be reviewed here. Techniques used to directly observe the solidification of optically opaque (metallic) materials are given by Glicksman (22) in Table 1.

Table 1

1. Surface-reflection microscopy
2. Ultra-violet transmission
3. Polarized light microscopy
4. Transmission electron microscopy
5. Radiography
6. Autoradiography
7. Ultrasonic reflection

Rosenberg and Winegard (24) and Schaefer and Glicksman (25) have used reflected light microscopy with surface relief contrast to study dendritic growth in supercooled tin. Here a transparent flux was used to maintain an oxide-free surface for observation. This technique has not been used for eutectic solidification due to the fineness of eutectic structures compared to single-phase structures produced by similar growth rates (22).

Ultraviolet transmission microscopy has been used by Woodruff and Forty (26) on alloys of potassium and sodium, metals which have low absorption coefficients in the ultraviolet. Polarized light microscopy has been used by several authors to study eutectic solidification. This technique utilizes the rotation of polarized light reflected from non-cubic crystalline surfaces. Davies (27) made the first direct studies of metallic eutectic growth in the systems Bi-Sn, Bi-Cd, Sn-Zn and Pb-Sn. Through direct observation, he established the dependence of interlamellar spacing on solidification velocity for steady growth. He also attempted to classify non-lamellar binary eutectics on the basis of the lead of one phase over

another in growth into the melt. Cline (28) greatly improved the resolution of this technique for the Pb-Sn eutectic in order to determine the shape of the interface on a lamellar scale. His apparatus is shown in Figure 1. Cline also reported on the lamellar interface shape change during a change in growth rate. These results will be discussed in a later section. Because these observations were made with glass in intimate contact with the alloy during solidification, questions arise as to how representative these surface observations are of the interior microstructure, and whether the presence of the glass affected the heat flow in the mold. Both Davies and Cline state that no appreciable difference in microstructure was seen when the solid specimens were sectioned and examined metallographically.

Electron transmission microscopy has been extensively used to observe the solidification of pure and dilute binary metal systems. These experiments, however, have not utilized unidirectional solidification because the heating is applied by the electron beam itself. This produces a pool of liquid metal in the specimen. The resolution of electron microscopy is, of course, at least ten times better than optical microscopy; but the necessarily thin specimens that must be used and the time required to expose a photographic film greatly limit this technique in applicability to systems of practical size and practical growth velocities. With the exception of Takahashi and Ashinuma (29) this method has not been applied to eutectic solidification.

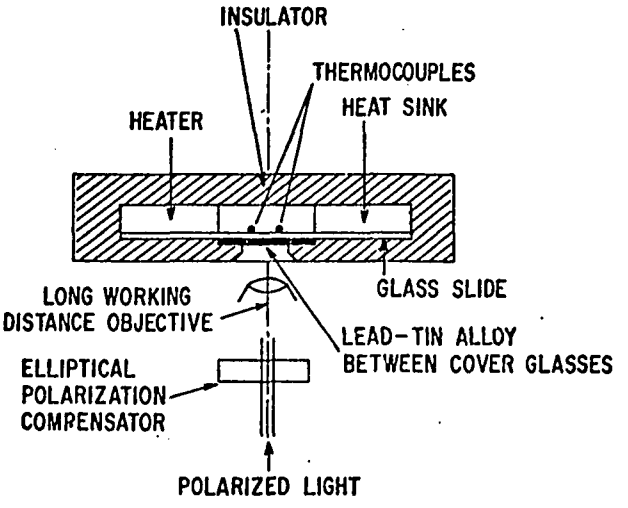

Fig. 1. Cline's apparatus for directly observing solidification (28).

They employed an interesting method of obtaining thin foils of the Pb-Sn eutectic by dipping a wire loop into the molten eutectic, and directly examining these foils after solidification by electron microscopy. Although they attempted to observe melting by heating with the electron beam, vaporization of the foils greatly restricted their attempts to directly observe the melting and solidification process.

Radiography, autoradiography and ultrasonic reflection off of interfaces are useful for macroscopic information about the solidification process. However, none yield information about the solid microstructure so vital to the study of polyphase solidification. Microradiography might have some interesting possibilities when employed with a very fast sensing instrument.

III. SURVEY OF CURRENT KNOWLEDGE OF LAMELLAR EUTECTIC SOLIDIFICATION

Theory for steady growth of a binary lamellar eutectic. Attempts to understand eutectic solidification have been most successful for the steady growth of lamellar eutectics of two component systems. The ideas of Scheil (30) and others about the coupled region, and the ideas of Zener (31) about the eutectoidal decomposition of austenite were formalized by Tiller (32) and refined by Jackson and Hunt (33) to produce the current theory of the solidification of such eutectics. Of the other

theories developed, only one employs a truly different analysis. This will be presented later.

The preliminary assumptions of the Jackson-Hunt theory, and for that matter, of almost all metallurgical phase transition thinking, will now be stated. Consider the interface between the liquid phase and the solid phase. The first preliminary assumption is that with but two exceptions, the temperature at each point on the interface will be given in terms of the liquid composition at that point on the interface by the liquidus curve for that solid phase in the equilibrium phase diagram. This assumption immediately limits the description of the local state of the body to temperature and composition. Such quantities as deformation are not included. The first exception concerns the change in the equilibrium transition temperature due to the curvature of the interface. The quantitative expression used for this change comes from thermostatic arguments applied to interfaces between fluids in equilibrium, and expressed in a form applicable to solidification where the pressure is assumed constant. These arguments have been performed by many authors in different ways and the effect is often called the Gibbs-Thomson effect. This classical relationship states that the transition temperature given by the phase diagram is depressed by an amount proportional to the mean curvature of the interface with the interface convex toward the liquid phase. The second exception concerns the ability, or rather the necessity, for a phase transition to occur at a temperature lower

than its equilibrium value, that is supercooling. This supercooling has nothing to do with the local adjustment of the transition temperature to the local composition, that is, constitutional supercooling. This true supercooling, which is often called kinetic supercooling, is considered necessary to drive the process forward, that is, solidify. This kinetic supercooling is usually considered small and often is neglected; but it is a real and measurable deviation from the equilibrium transition temperature predicted by the composition and the interface curvature. The second preliminary assumption applies particularly to eutectic solidification, which is actually a polyphase transition. In a binary equilibrium diagram containing a eutectic point, the liquidus curves for the two solid phases terminate at the eutectic point. In the event that the liquid composition value adjacent to the liquid-solid interface for a particular solid phase is not contained on the liquidus curve for that solid phase, the liquidus for that phase is extrapolated beyond the eutectic point. (See Figure 2a) This extrapolation yields values of the equilibrium transition temperature for that phase when the local composition of the liquid at the interface does not lie on the liquidus proper. Other preliminary assumptions are that the diffusion in the liquid can be described by simple Fick-type equations, that there is no diffusion in the solid and that there is no fluid motion.

The details of the Jackson-Hunt theory begin by consid-

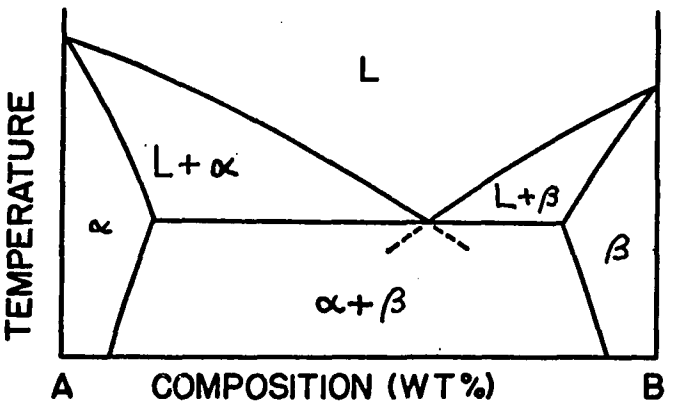

Fig. 2a. Binary eutectic phase diagram with extended liquidi.

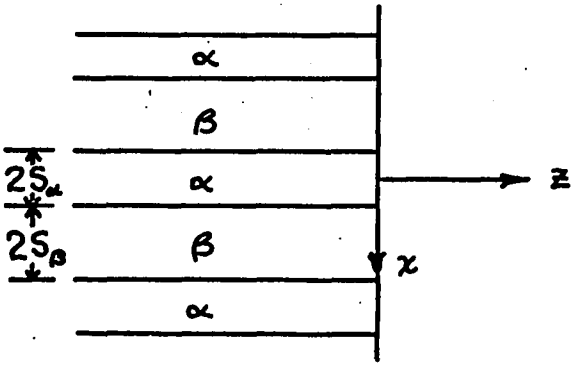

Fig. 2b. Binary lamellar liquid-solid interface.

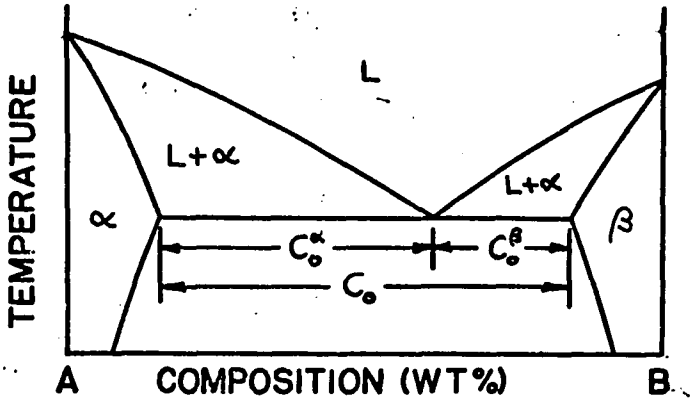

Fig. 2c. Binary eutectic diagram with parameters, $C_o^\alpha, C_o^\beta, C_o$

ering the planar interface shown in Figure 2b with a coordinate system fixed to the interface which moves at a constant velocity v. The assumption of a planar interface is made only for the diffusion analysis that follows and is relaxed later in the theory. Because the compositions of the α and β phases are each drastically different than the liquid (eutectic) composition, the liquid adjacent to each phase must be enriched in that component which is the minor constituent of that phase, that is, the solute in the phase. Thus the individual interface of each lamella can be represented as a moving surface which constantly rejects solute into the liquid phase. By assuming that the total interface is a plane moving perpendicular to the lamellae, a diffusion problem can be formulated to find the details of the composition distribution in the liquid.

In the moving frame of reference, the diffusion equation for a steady distribution becomes

$$\nabla^2 C + \frac{v}{D} \frac{\partial C}{\partial z} = 0$$

where D is the linear diffusion coefficient. A two-dimensional solution $C(x,z)$ is sought in the region $0 \leq x \leq S_\alpha + S_\beta$, $z \geq 0$, where S_α and S_β are the individual lamellar half-widths, with the following boundary conditions:

$$C(x,\infty) = C_E = \text{EUTECTIC COMPOSITION}$$

$$\frac{\partial C}{\partial x}(0,z) = \frac{\partial C}{\partial x}(S_\alpha + S_\beta, z) = 0 \quad \text{FOR ALL } z$$

$$\frac{\partial C}{\partial z}(x,0) = -\frac{v C_o^{\alpha}}{D} \quad \text{FOR} \quad 0 \le x \le S_\alpha$$

$$\frac{\partial C}{\partial z}(x,0) = \frac{v C_o^{\beta}}{D} \quad \text{FOR} \quad S_\alpha \le x \le S_\alpha + S_\beta$$

where C_o^{α} and C_o^{β} are shown in Figure 2c. With the assumption that $\pi/S_\alpha+S_\beta >> \frac{v}{2D}$ the solution is

$$C(x,z) = C_E + B_o \exp\left(-\frac{v}{D}z\right) + \sum_{n=1}^{\infty} B_n \cos\left(\frac{n\pi x}{S_\alpha+S_\beta}\right)\exp\left(-\frac{n\pi z}{S_\alpha+S_\beta}\right)$$

$$B_o = \frac{C_o^{\alpha}S_\alpha - C_o^{\beta}S_\beta}{S_\alpha+S_\beta} \quad , B_n = \frac{2}{(n\pi)^2}(S_\alpha+S_\beta)\frac{v}{D}C_o \sin\left(\frac{n\pi S_\alpha}{S_\alpha+S_\beta}\right).$$

Jackson and Hunt next consider the situation at the interface in front of, for example, the α phase. The composition is to the right of the eutectic composition (Figure 2c) according to the above calculation. Solid α phase and liquid phase exist together at all points on this interface. This implies that the equilibrium freezing temperatures, in the absence of curvature effects, must be given by the extension of the liquidus curve beyond the eutectic point as mentioned previously.

Using these ideas as a basis, Jackson and Hunt consider the actual temperature of every point on the interface $T_I(x)$. If no solidification is taking place and the interface is flat, then $T_I(x) = T_E$ where T_E is the eutectic temperature. In general for a non-planar solidifying interface, the difference $T_E - T_I(x)$ will be composed of three parts. The first is ΔT_c due to the departure of the local composition from the eutectic composition. In front of each phase, this can be written as $\Delta T_c = m\left(C_E - C(x,0)\right)$ where m is the slope (including

sign) of the liquidus curve of the relevant phase. The second contribution due to a non-planar interface is ΔT_σ which can be written $\Delta T_\sigma = a\,K(x)$ where $K(x)$ is the mean curvature of the interface and a is a constant given by the Gibbs-Thomson Relationship $a = \frac{\sigma T_E}{L}$ where σ is the relevant solid-liquid interface energy, L is the heat of fusion of the relevant phase. The third is the kinetic supercooling ΔT_K mentioned before. Thus

$$\Delta T(x) = T_E - T_I(x) = m\left(C_E - C(x,0)\right) + a\,K(x) + \Delta T_K .$$

Next ΔT_K is neglected. It has been measured in tin by Tiller and Kramer (34) to be $\sim 10^{-2}$°C. Because the gross interface deviates from planarity only very slightly, and the temperature gradient in the liquid is assumed to be perpendicular to the interface and to be about $10^{\circ}C/cm.$, the difference $T_E - T_I(x)$ is assumed to be a constant for all points x on the interface. Therefore the average value of the difference computed over each lamellar width will also be the same constant. For each phase then the average undercooling is

$$\overline{\Delta T}^{\alpha} = m^{\alpha}\left(C_E - \bar{C}^{\alpha}\right) + a^{\alpha}\,\overline{K}^{\alpha}$$

$$\overline{\Delta T}^{\beta} = m^{\beta}\left(C_E - \bar{C}^{\beta}\right) + a^{\beta}\,\overline{K}^{\beta}$$

where m^{α} and m^{β} are the slopes of the respective liquidus curves (both positive). After some algebraic calculations and

the assumption that $\frac{S_\alpha}{S_\beta}$ = constant, one obtains

$$\Delta T = K_1 \lambda v + \frac{K_2}{\lambda}$$

where $\lambda = 2(S_\alpha + S_\beta)$ and K_1, K_2 are constants for a given eutectic system. For a fixed velocity the undercooling is a function of the lamellar spacing as shown in Figure 3.

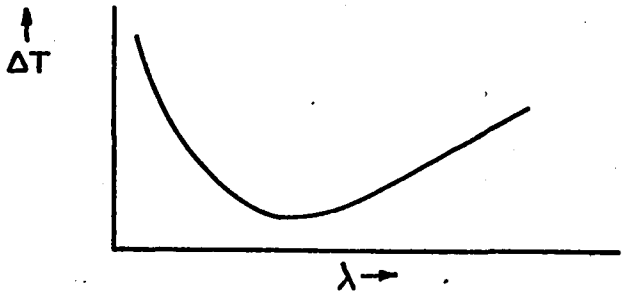

Figure 3

Jackson and Hunt next discuss the principle of growth at the extremum which has two expressions which are equivalent for this particular undercooling relationship: i.e., that the correct value of the lamellar spacing for a given (steady) velocity will be one which minimizes the undercooling, or that the correct value of the lamellar spacing will be one which maximizes the growth velocity for a fixed undercooling. Minimizing the undercooling at fixed velocity as a function of lamellar spacing, one gets

$$\frac{d(\Delta T)}{d\lambda} = K_1 v - \frac{K_2}{\lambda^2} = 0$$

OR $$\lambda^2 v = \frac{K_2}{K_1} .$$

Maximizing the growth velocity at fixed undercooling as a function of lamellar spacing, one gets

$$v = \frac{\Delta T}{K_1 \lambda} - \frac{K_2}{K_1 \lambda^2}$$

$$\frac{dv}{d\lambda} = -\frac{\Delta T}{K_1 \lambda^2} + \frac{2K_2}{K_1 \lambda^3} = 0$$

OR $\quad \Delta T = \frac{2K_2}{\lambda}$

BUT $\quad \Delta T = K_1 \lambda v + \frac{K_2}{\lambda} \quad \Rightarrow \quad \lambda^2 v = \frac{K_2}{K_1}$.

Jackson and Hunt next describe possible growth which does not occur at the extremum condition. According to arguments of Cahn (35), which they present, growth to the left of the minimum (see Figure 3) is "inherently unstable." This argument is based on whether a slight perturbation of lamellar spacing at a constant growth rate causes an alteration of the growth conditions such as to restore the spacing to the unperturbed value. Jackson and Hunt state that the growth to the right of the minimum is possible up to a certain value of lamellar spacing. This limiting value is obtained by investigating the motion of lamellar faults. Thus their conclusion is that growth is possible over a range of lamellar spacings at a given velocity.

One other work is to be mentioned regarding steady state lamellar eutectic growth. Li and Weart (36) used the thermodynamics of irreversible process by applying the principle of minimum entropy production. The total rate of entropy production is assumed to consist of contributions from heat of transformation, heat and mass transfer within the system, formation of inter-

phase boundaries and heat transfer between the system and the environment. This analysis leads to an expression

$$\lambda v = \text{constant.}$$

Theory for steady growth of ternary lamellar eutectics. No theory exists for the steady growth of ternary lamellar eutectics. All of the work done on ternary eutectics has been an attempt to classify ternary eutectic microstructures, using ideas generated during attempts to classify binary eutectic microstructures. Kerr, Bell and Winegard (37) have discussed the microstructure of Pb-Sn-Cd and Zn-Sn-Pb in terms of phase lead at the interface as determined by constitution supercooling. Cooksey and Hellawell (38) have discussed the dissimilarity of ternary eutectic microstructures and the eutectic microstructures of the three binary combinations of the same components, and also the effects of interfacial energies on ternary eutectic microstructures. Crivelli-Visconti (39) has discussed constitutional supercooling in front of various phases in ternary eutectics in an attempt to understand their microstructures.

Experimental knowledge of lamellar eutectic solidification. -- Many authors have obtained $\lambda^2 v = \text{constant}$ for steady state binary lamellar eutectic solidification (1,40,41,42,43,44). All but Davies measured the velocity of solidification indirectly by measuring the gradient furnace rate. In addition, Hunt and Chilton (45) and Moore and Elliot (46) measured the

undercooling at the interface to be that predicted in the Jackson-Hunt (33) Theory. $(\Delta T \sim v^{\frac{1}{2}})$. This presents strong arguments for the Jackson-Hunt Theory including the idea of growth at the extremum. It has also been shown that these results seem to be independent of imposed thermal gradient (42).

For a ternary lamellar eutectic of Pb-Sn-Cd, two papers have investigated the relation of interlamellar spacing to (steady growth) velocity. Kerr et al. (37) have obtained the same $\lambda^2 v$ = constant relation for this ternary eutectic. The stacking of this triple lamellar structure is ABCBABCBA where A is the Sn-rich phase, B is the Pb-rich phase and C is the cadmium-rich phase. The interlamellar spacing is defined as the distance between the centers of consecutive Sn (or Cd) phases. Crivelli-Visconti (47) has also experimented with this eutectic and found somewhat different results in that $\lambda^n v$ = constant, $3 \leq n \leq 5$.

Unsteady solidification of lamellar eutectics. -- Information concerning the unsteady solidification of lamellar eutectics is quite sparse. Three groups of researchers have discussed the effects of change of solidification velocity on the lamellar structure in binary eutectics: Hunt and Jackson (33), Mollard and Flemings (48) and Cline (28). Cline, using a direct observation technique in Pb-Sn, states some qualitative aspects of the effect of rate change. "Increases in spacing occur by termination of the growth of individual lamellae, while decreases

in spacing occur by a lamella tip first becoming concave, then becoming forked to form two lamella." Judging from a picture shown in this article, when the spacing increased, it did so by the termination of Pb-rich lamella and a transition from a lamellar structure to a spheroidized structure in which lead particles formed in front of the interface. This was attributed by Cline to the compositions being slightly to the Pb-rich side of the eutectic composition. Mollard and Flemings (48) treat the effect of rate changes on lamellar composites theoretically. Because they are mainly interested in growing lamellar composites different from the eutectic composition, the assumption is made in their analysis that the composition of the alloy is much different from the eutectic composition. However, this assumption is shown to be valid experimentally when the difference is as small is 1/2%. Their theory predicts a change in the average solid composition from the nominal alloy compositions when the rate is changed. However, this deviation, at its maximum, is proportional to the difference in the alloy composition from the eutectic composition. Thus one might infer that no such deviation should occur for an alloy of eutectic composition. No information was given in this paper regarding lamellar spacing changes caused by rate changes.

Jackson and Hunt develop some theoretical ideas about lamellar spacing changes in binary eutectics due to changes of growth velocity based on their observations of such phenomenon

in organic eutectics. In addition to the small adjustment of lamellar spacing due to the motion of lamellar faults which have already been mentioned, they discuss catastrophic changes in lamellar spacing caused by interface shape instabilities and boundary layer instabilities. Interface shape instabilities occur when a pocket forms in the center of the lamellae. In such a case the pocket drops progressively farther back from the interface and the other phase forms in the pocket to produce a new lamella. Thus, interface shape instabilities produce decreases in inter-lamellar spacing. Quantitative estimation of the deviation from the extremum condition that would cause such an instability is made by realizing that the formation of such a pocket requires the slope of the interface with respect to a direction perpendicular to the solidification direction to become infinite. Since from the Jackson-Hunt theory presented previously,

$$\Delta T = m\left(C_E - C(x,0)\right) + a\,K(x) = \text{CONSTANT}$$

$$K(x) = \frac{\Delta T - m\left(C_E - C(x,0)\right)}{a}$$

$$\frac{\frac{d^2y}{dx^2}}{\left(1+\left(\frac{dy}{dx}\right)^2\right)^{3/2}} = \frac{\Delta T - m\left(C_E - C(x,0)\right)}{a}$$

where $y = y(x)$ is the shape of the interface.

Using the value of compositions obtained from a steady-state calculation corresponding to a value of solidification velocity, this can be integrated using information about $\frac{dy}{dx}$ at the center of lamella and the edges to yield an expression for $\frac{dy}{dx}$ as a function of χ which is independent of ΔT . Letting $\frac{dy}{dx} = \infty$ at $\chi = 0$ and $\chi = S_\alpha + S_\beta$, expressions are obtained for the value of $\lambda^2 v$ required for this sort of instability. This value of $\lambda^2 v$ required for instability is a function only of properties of the alloy used such as latent heats, diffusion constant, liquidus slopes, ratio of lamellar widths, etc. If the two lamella are of the same width, the instability should occur in both simultaneously. If one is wider, the instability occurs in that one. For a lamella of equal width the value of $\lambda^2 v$ for instability is about ten times the extremum value of $\lambda^2 v$. They also state that in an imperfect lamellar structure; i.e., one with grain boundaries, fault lines or interface depressions where the local lamellar spacing is wider than the rest of the structure, instabilities will occur at lower values of $\lambda^2 v$ than predicted above. Boundary layer instabilities apply mostly to alloys solidifying with an off eutectic composition where the average composition of the liquid at the interface is different from the nominal alloy composition. In such cases changes in growth rate alter the average composition of the liquid out of the coupled region (the region between extended liquidi) thus making the growth of one of the phases unfavorable. In this

case one phase will be pinched off by the adjacent lamella and consequently increase the lamellar spacing. In the event that the alloy is of eutectic composition, Jackson and Hunt state that pinch off may occur at irregularities in the lamellar structure.

IV. PURPOSE OF PROGRAM

The purpose of this research program is two-fold: first, to develop a relatively simple method of observing and recording the actual process of solidification in alloy systems; and second, to apply this technique to the study of the non-steady solidification of a ternary eutectic alloy. In particular, information is sought regarding the time rate of change of the interlamellar spacing produced at the liquid-solid interface by various non-steady (time dependent) solidification velocities. Three types of experiments are performed: increases in solidification velocity from one steady value to another, decreases in solidification velocity from one steady value to another, and fluctuations in the solidification velocity. Included in the information obtained, should be statements about the time required for the adjustment of the spacing to its steady state value after a velocity change; and whether a uniform (constant lamellar spacing) lamellar structure can be produced with an oscillating solidification velocity. Details of the mechanism of lamellar spacing change are sought especially for the case of triple lamellar

structure. To facilitate the discussion of non-steady growth of a ternary eutectic, a steady-state theory of ternary lamellar eutectic solidification will be presented.

V. A STEADY STATE THEORY OF TERNARY LAMELLAR EUTECTIC SOLIDIFICATION

Using the basic concepts of binary lamellar growth as presented by Jackson and Hunt (33), a theory of ternary lamellar eutectic growth can be formulated, which while not different in basic concept requires quite different detail. This theory does not explain why a particular lamellar eutectic is lamellar, or why a particular arrangement of lamellae is found, but attempts to describe the physical situation that might be present in the growth of such a structure. The preliminary assumptions of this theory coincide with those of the Jackson-Hunt theory.

First consider the three-component equilibrium phase diagram at constant pressure of a system having a ternary eutectic reaction. (See Figure 4). The compositions of the three solid phases α , β , γ which will precipitate from a liquid of eutectic composition are drastically different than the eutectic composition. Just as in the case of binary lamellar growth, this causes rejection of the various components into the liquid at the interface. Unlike the binary case where only the solute in each phase is rejected into the liquid, in a ternary system all three components can in general be rejected (positively or negatively) into the liquid.

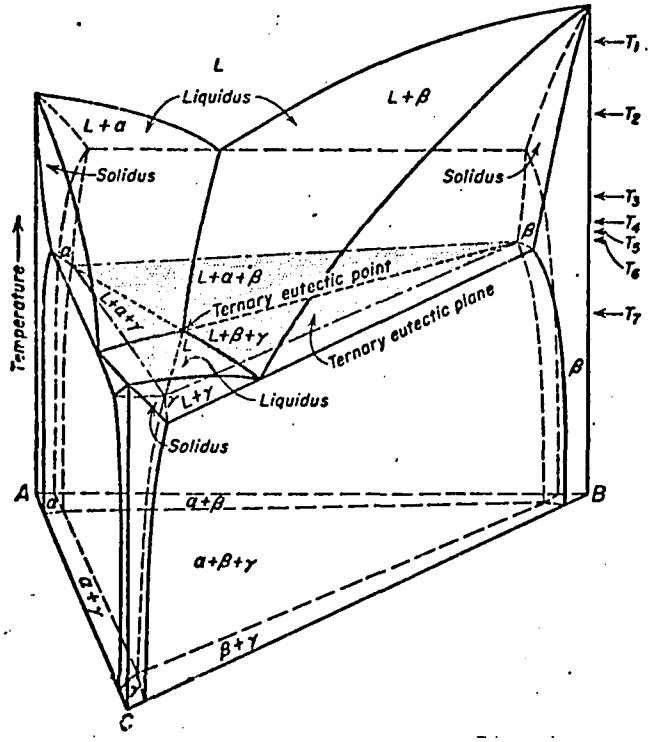

Fig. 4. Ternary eutectic phase diagram (49).

In an infinite body, consider the composition distribution in front of a triple lamellar interface with stacking $\alpha\beta\gamma\beta\alpha\beta\gamma\beta\alpha$ which is growing edgewise into the liquid at a constant velocity v. The interface will be assumed planar for the diffusion analysis. This assumption will later be relaxed. In a coordinate system fixed on the flat interface as shown in Figure 5a, the linear constant coefficient diffusion equations for a steady (non-time dependent) distribution become

$$D_{11}\left(\frac{\partial^2 C_1}{\partial x^2}+\frac{\partial^2 C_1}{\partial z^2}\right)+D_{12}\left(\frac{\partial^2 C_2}{\partial x^2}+\frac{\partial^2 C_2}{\partial z^2}\right)+v\frac{\partial C_1}{\partial z}=0$$

$$D_{21}\left(\frac{\partial^2 C_1}{\partial x^2}+\frac{\partial^2 C_1}{\partial z^2}\right)+D_{22}\left(\frac{\partial^2 C_2}{\partial x^2}+\frac{\partial^2 C_2}{\partial z^2}\right)+v\frac{\partial C_2}{\partial z}=0.$$

A solution $C_1(x,z), C_2(x,z)$ will be sought in the region $z\geq 0$, $0\leq x\leq S_\alpha+2S_\beta+S_\gamma$. The boundary conditions are

$$C_1(x,\infty)=C_1^E$$

$$C_2(x,\infty)=C_2^E$$

$$\frac{\partial C_1}{\partial x}=\frac{\partial C_2}{\partial x}=0 \quad \text{AT } x=0 \text{ AND } x=S_\alpha+2S_\beta+S_\gamma \text{ FOR ALL } z$$

$$\left.\begin{aligned} v C_1^{\alpha_0} &= -\left(D_{11}\frac{\partial C_1}{\partial z}+D_{12}\frac{\partial C_2}{\partial z}\right) \\ v C_2^{\alpha_0} &= -\left(D_{21}\frac{\partial C_1}{\partial z}+D_{22}\frac{\partial C_2}{\partial z}\right) \end{aligned}\right\} \begin{array}{l}\text{AT } z=0 \\ 0\leq x\leq S_\alpha\end{array}$$

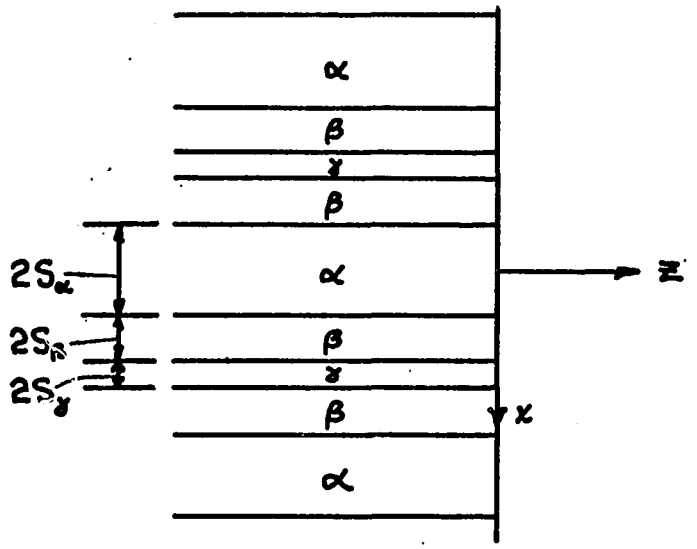

Fig. 5a. Ternary lamellar liquid-solid interface.

a – COMPOSITION OF α PHASE (C_1^α, C_2^α)

b – COMPOSITION OF β PHASE (C_1^β, C_2^β)

c – COMPOSITION OF γ PHASE (C_1^γ, C_2^γ)

d – EUTECTIC COMPOSITION (C_1^E, C_2^E)

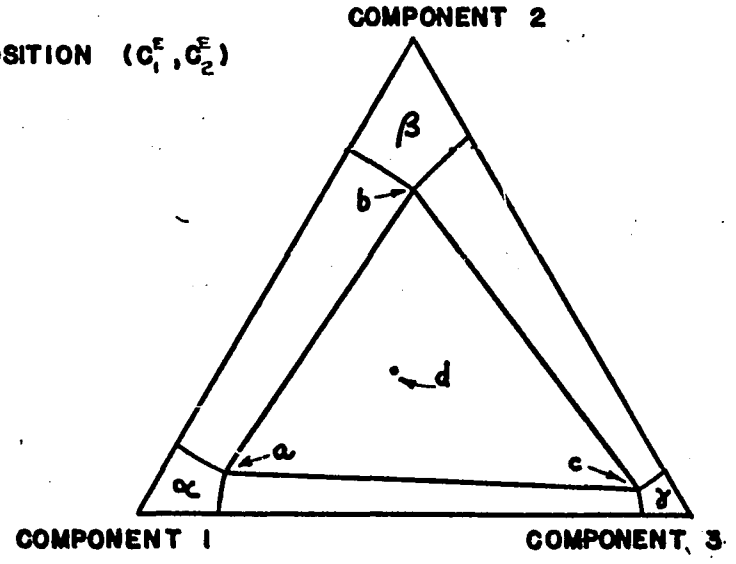

Fig. 5b. Isothermal section of a ternary eutectic diagram at the eutectic temperature with compositions of solid phases labeled.

$$\left.\begin{aligned} v C_1^{\beta_0} &= -\left(D_{11}\frac{\partial C_1}{\partial z} + D_{12}\frac{\partial C_2}{\partial z}\right) \\ v C_2^{\beta_0} &= -\left(D_{21}\frac{\partial C_1}{\partial z} + D_{22}\frac{\partial C_2}{\partial z}\right) \end{aligned}\right\} \quad \begin{aligned} &\text{AT } z=0 \\ &S_\alpha \le \chi \le S_\alpha + 2S_\beta \end{aligned}$$

$$\left.\begin{aligned} v C_1^{\gamma_0} &= -\left(D_{11}\frac{\partial C_1}{\partial z} + D_{12}\frac{\partial C_2}{\partial z}\right) \\ v C_2^{\gamma_0} &= -\left(D_{21}\frac{\partial C_1}{\partial z} + D_{22}\frac{\partial C_2}{\partial z}\right) \end{aligned}\right\} \quad \begin{aligned} &\text{AT } z=0 \\ &S_\alpha + 2S_\beta \le \chi \le S_\alpha + 2S_\beta + S_\gamma \end{aligned}$$

where

$C_1^{\alpha_0} = C_1^E - C_1^\alpha$ $\qquad$ $C_1^{\beta_0} = C_1^E - C_1^\beta$ $\qquad$ $C_1^{\gamma_0} = C_1^E - C_1^\gamma$

$C_2^{\alpha_0} = C_2^E - C_2^\alpha$ $\qquad$ $C_2^{\beta_0} = C_2^E - C_2^\beta$ $\qquad$ $C_2^{\gamma_0} = C_1^E - C_1^\gamma$

and C_1^E, C_2^E is the eutectic composition, C_1^α, C_2^α is the composition of the α phase, C_1^β, C_2^β is the composition of the β phase, and C_1^γ, C_2^γ is the composition of the γ phase. The boundary conditions were formulated using the following considerations. Far away from the interface the composition should be the original alloy composition, that is, the eutectic composition. The composition distribution should be symmetric with respect to the centers of the α and γ phases. This yields a condition on the χ derivatives at $\chi = 0$ and $\chi = S_\alpha + 2S_\beta + S_\gamma$. The flux conditions at the interface are obtained by considering conservation of each component at the interface in front of each phase. The mass of liquid

solidifying per unit time per unit area of interface is ρv where ρ is the density of the liquid. Because this solidified liquid must be of composition C_1^α, C_2^α for, say, the α phase, then $(C_1^L - C_1^\alpha)\rho v, (C_2^L - C_2^\alpha)\rho v$ must be the mass of components one and two respectively which are rejected into the liquid, where C_1^L, C_2^L is the composition of the liquid at the interface. In terms of Fick-type diffusion analysis, the mass flux of component one is given by $-\left(\rho D_{11}\frac{\partial C_1}{\partial z} + \rho D_{12}\frac{\partial C_2}{\partial z}\right)$, and so on for the other component. Then an approximation is made that

$$C_1^L - C_1^\alpha \approx C_1^E - C_1^\alpha$$
$$C_2^L - C_2^\alpha \approx C_2^E - C_2^\alpha$$

and so on for the other phases. This assumption is consistent with that made by Jackson and Hunt. It means simply that deviations from the eutectic composition in the liquid are small compared to the difference between the liquid composition and composition of the solid phases.

In order to easily estimate the solution, the assumption that $D_{12} = D_{21} = 0$ will now be made. The differential equations become

$$D_{11}\left(\frac{\partial^2 C_1}{\partial x^2} + \frac{\partial^2 C_1}{\partial z^2}\right) + v\frac{\partial C_1}{\partial z} = 0$$

$$D_{22}\left(\frac{\partial^2 C_2}{\partial x^2} + \frac{\partial^2 C_2}{\partial z^2}\right) + v\frac{\partial C_2}{\partial z} = 0 \quad ;$$

these equations are decoupled and can be solved independently. Letting $C_i(x,z)$, $i=1,2$ be the two solutions, they are:

$$C_i(x,z) = C_i^E + B_i^o \exp\left(-\frac{\pi}{D_{ii}} z\right) + \sum_{n=1}^{\infty} B_i^n \cos\left(\frac{n\pi x}{S_\alpha+2S_\beta+S_\gamma}\right) \exp\left(\frac{-n\pi z}{S_\alpha+2S_\beta+S_\gamma}\right)$$

where the assumption that $\pi/S_\alpha+2S_\beta+S_\gamma >> \frac{\pi}{2D_{ii}}$ has been made. This assumption is again consistent with the Jackson-Hunt theory. The coefficients B_i^o and B_i^n can readily be evaluated using the boundary conditions.

$$B_i^o = \frac{1}{S_\alpha+2S_\beta+S_\gamma}\left[S_\alpha C_i^{\alpha_o} + 2S_\beta C_i^{\beta_o} + S_\gamma C_i^{\gamma_o}\right]$$

$$B_i^n = \frac{2\pi}{D_{ii}} \frac{(S_\alpha+2S_\beta+S_\gamma)}{(n\pi)^2}\left[\left(C_i^{\alpha_o} - C_i^{\beta_o}\right)\sin\frac{n\pi S_\alpha}{S_\alpha+2S_\beta+S_\gamma}\right.$$

$$\left. + \left(C_i^{\beta_o} - C_i^{\gamma_o}\right)\sin\frac{n\pi(S_\alpha+2S_\beta)}{S_\alpha+2S_\beta+S_\gamma}\right] .$$

The average composition in front of each lamella at can be computed for later use from the composition distribution just obtained. $\overline{C_i}^{\alpha}$, the average composition of the i component in front of the α phase, is given by

$$\overline{C_i}^{\alpha} = \frac{1}{S_\alpha}\int_0^{S_\alpha} C_i(x,0)\,dx = C_i^E + B_i^o + \frac{\lambda\pi}{D_{ii}} P_i^{\alpha}$$

where P_i^{α} are functions of $\frac{S_\alpha}{\lambda}$, $\frac{S_\alpha+2S_\beta}{\lambda}$ only , with $\lambda = 2(S_\alpha+2S_\beta+S_\gamma)$. Similarly the compositions in front of

the β and γ phases can be computed. Here the distribution in front of the β lamella is not necessarily symmetric with the center of the lamella.

$$\overline{C_i}^{\beta} = \frac{1}{2S_\beta} \int_{S_\alpha}^{S_\alpha+2S_\beta} C_i(x,0)\,dx = C_i^E + B_i^o + \frac{\lambda v}{D_{ii}} P_i^{\beta}$$

$$\overline{C_i}^{\gamma} = \frac{1}{S_\gamma} \int_{S_\alpha+2S_\beta}^{S_\gamma+2S_\beta+S_\gamma} C_i(x,0)\,dx = C_i^E + B_i^o + \frac{\lambda v}{D_{ii}} P_i^{\gamma}$$

where P_i^{β} and P_i^{γ} are functions of $\frac{S_\alpha}{\lambda}$, $\frac{S_\alpha+2S_\beta}{\lambda}$ only.

The assumption will now be made that the liquidus surfaces for each of the three solid phases can be extrapolated below the eutectic temperature in the equilibrium diagram in order to accommodate possible liquid compositions in front of each phase which are not contained on the liquidus surface proper for that phase. These three extrapolated liquidus surfaces will form a triangular pyramid when intersected by an isothermal plane below the eutectic temperature. The vertex of the pyramid is the eutectic point and the edges of the pyramid, which intersect the vertex, will be the extrapolated space curves of binary crystallization.

Using the solution found previously, the composition distribution in the liquid was computed for the Pb-Sn-Cd ternary eutectic. For this solution, the ratios $S_\alpha/S_\alpha+2S_\beta+S_\gamma$ and $S_\alpha+2S_\beta/S_\alpha+2S_\beta+S_\gamma$ were 0.433 and 0.867 respectively. These were determined from Figure 11. The compositions of the solid phases at the eutectic temperature are not known. They were estimated

by picking values which are consistent with the binary solid solubilities. These values in weight fractions are

$$C_1^{\alpha} = .928 \qquad C_1^{\beta} = .175 \qquad C_1^{\gamma} = .000$$

$$C_2^{\alpha} = .025 \qquad C_2^{\beta} = .792 \qquad C_2^{\gamma} = .000$$

where component one is Sn, and component two is Pb. The eutectic composition was taken to be $C_1^E = .494$, $C_2^E = .323$ (37). This solution is shown in Figure 7.

The temperature of the interface $T_I(X)$ can now be found. In general $T_E - T_I(X)$ will be composed of three parts, just as in binary lamellar solidification. The first is ΔT_c due to the departure of the local composition from the eutectic composition. In front of each phase this can be written as

$$\Delta T_c = m_1\left[C_1^E - C_1(x,o)\right] + m_2\left[C_2^E - C_2(x,o)\right]$$

where $m_1 = \left.\frac{\partial T_L}{\partial C_1}\right|_{C_i = C_i^E}$ and $m_2 = \left.\frac{\partial T_L}{\partial C_2}\right|_{C_i = C_i^E}$ and $T_L = T_L(C_1, C_2)$ is the equation of the liquidus surface for the relevant phase. The second contribution, due to a possibly non-planar interface, is ΔT_σ and can be written $\Delta T_\sigma = a\,K(X)$ where a is a constant given by the Gibbs-Thomson relationship for the relevant phase $\left(a = \frac{\sigma T_E}{L}\right)$, and $K(X)$ is the mean curvature of the liquid-solid interface for the relevant phase. The third contribution is the kinetic supercooling ΔT_K necessary to drive the process forward.

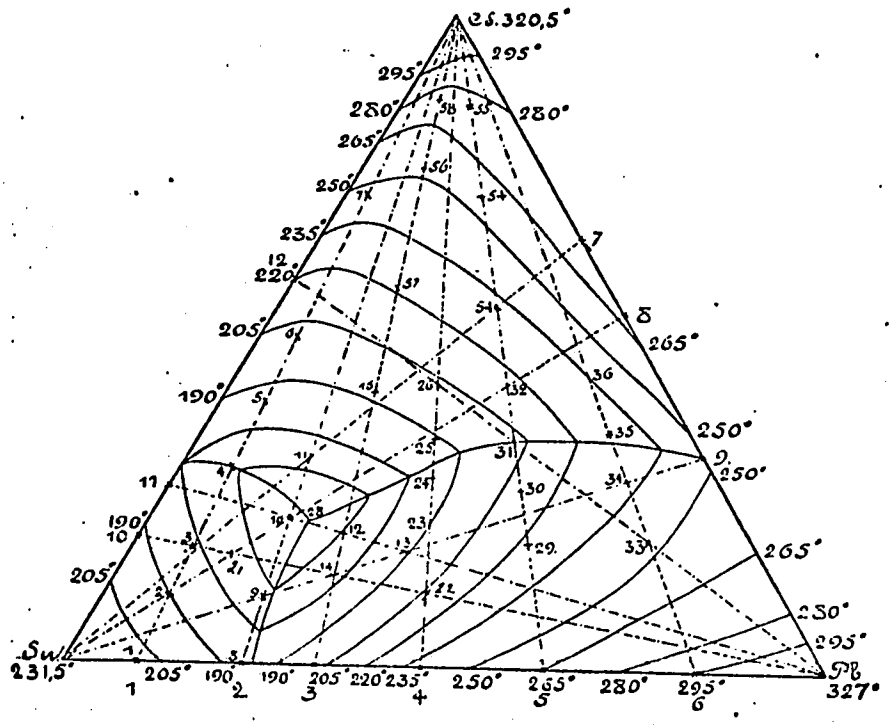

Fig. 6. Liquidus surface for Pb-Sn-Cd system (atomic %) (50).

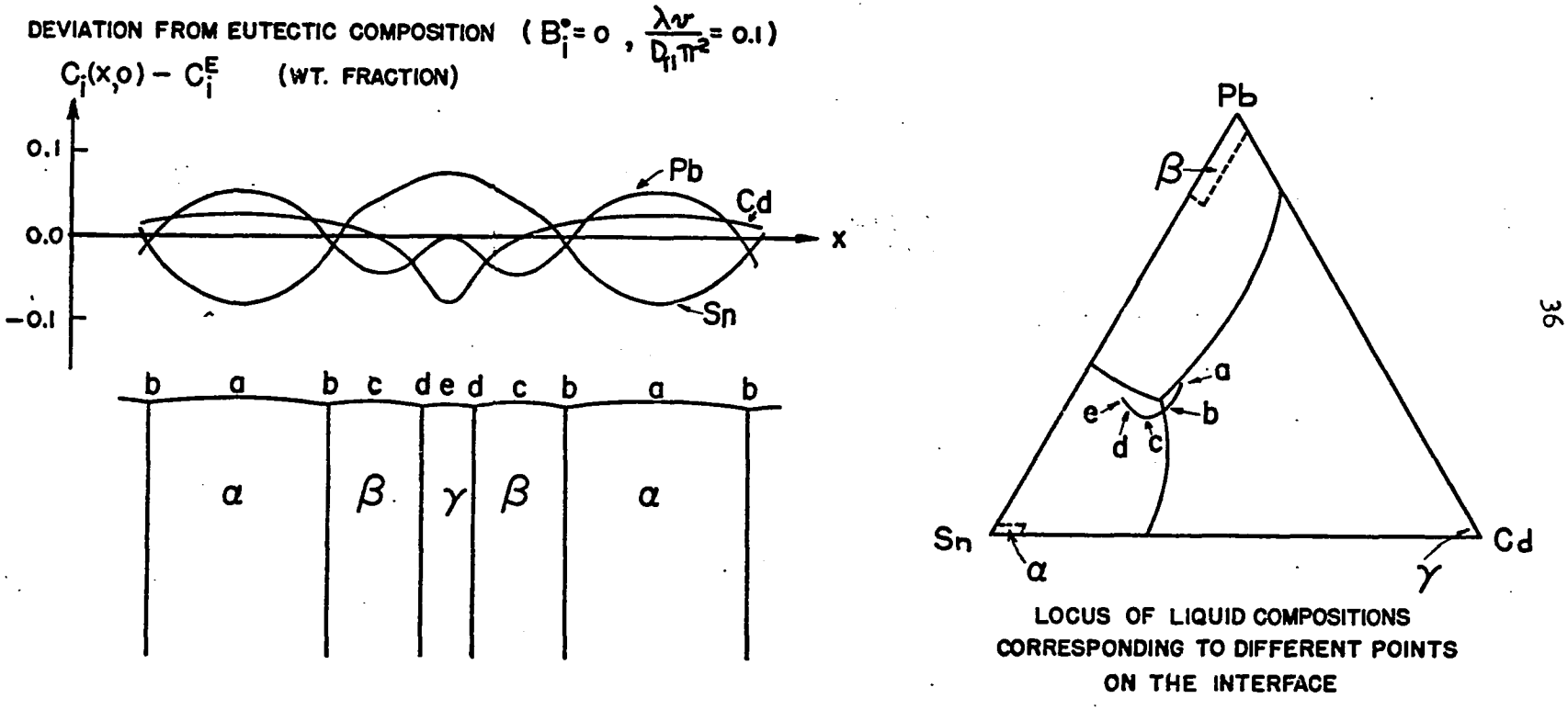

Fig. 7. Composition distribution in the liquid at the interface.

Because the gross interface deviates from planarity only very slightly, the temperature gradient in the liquid is approximately perpendicular to the interface, and its value is about $10^{\circ}C/cm$, the difference $T_E - \overline{T}_I(x)$ is assumed to be constant for all points on the interface. From the schematic composition diagram and the extrapolated pyramid one can visualize the equilibrium liquidus temperature in the absence of curvature effects at different points on the interface. (See Figure 8). Because the undercooling $T_E - \overline{T}_I$ is a constant, the average value of $T_E - \overline{T}_I$ over each lamellar width will be the same constant. For each phase the average undercooling $\overline{\Delta T}$ is

$$\overline{\Delta T}^{\alpha} = m_1^{\alpha}\left[C_1^E - \overline{C}_1^{\alpha}\right] + m_2^{\alpha}\left[C_2^E - \overline{C}_2^{\alpha}\right] + a^{\alpha}\overline{K}^{\alpha}$$

$$\overline{\Delta T}^{\beta} = m_1^{\beta}\left[C_1^E - \overline{C}_1^{\beta}\right] + m_2^{\beta}\left[C_2^E - \overline{C}_2^{\beta}\right] + a^{\beta}\overline{K}^{\beta}$$

$$\overline{\Delta T}^{\gamma} = m_1^{\gamma}\left[C_1^E - \overline{C}_1^{\gamma}\right] + m_2^{\gamma}\left[C_2^E - \overline{C}_2^{\gamma}\right] + a^{\gamma}\overline{K}^{\gamma}$$

where the kinetic supercooling has been neglected. The average value of the interface curvature over each lamellar width can be computed without a knowledge of the detailed shape of the lamellar interface. In a manner similar to that used by Jackson and Hunt except that the shape of the β phase interface is not necessarily symmetric with respect to its center, the average curvature for a lamella can be computed as follows:

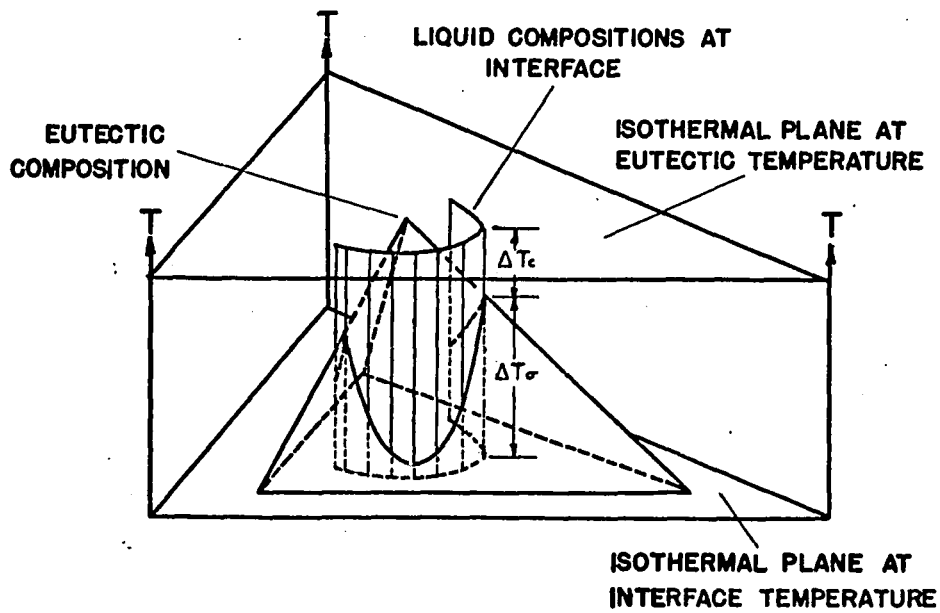

Fig. 8. Extrapolated pyramid showing effects of composition and interface curvature on temperature of interface.

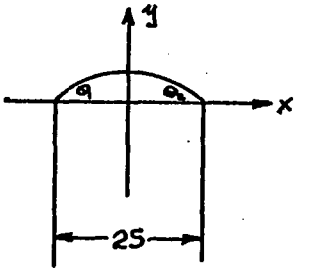

$$\overline{K} = \frac{1}{2S}\int_{-S}^{S} \frac{-\frac{d^2y}{dx^2}}{\left(1+\left(\frac{dy}{dx}\right)^2\right)^{3/2}}\,dx$$

$$= -\frac{1}{2S}\sin\tan^{-1}\left(\frac{dy}{dx}\right)\Bigg]_{-S}^{S}$$

$$= \frac{1}{2S}\left(\sin\theta_1 + \sin\theta_2\right).$$

For the α and γ phases $\theta_1 = \theta_2$, so

$$\overline{K}^{\alpha} = \frac{1}{S_\alpha}\sin\theta_\alpha^L$$

$$\overline{K}^{\beta} = \frac{1}{2S_\beta}\left(\sin\theta_{1\beta}^L + \sin\theta_{2\beta}^L\right)$$

$$\overline{K}^{\gamma} = \frac{1}{S_\gamma}\sin\theta_\gamma^L .$$

These angles are assumed to be constant as determined by the simplest of arguments concerning surface tension. The solid-solid interfacial tension and the two solid-liquid interfacial tensions must be in mechanical equilibrium at the points where the liquid and two lamellae come in contact. If the assumption is also made that the relative volume fractions of the phases in the eutectic solid are constant, then $\frac{S_\alpha}{\lambda}$, $\frac{S_\alpha + 2S_\beta}{\lambda}$ are constants. Then the average undercoolings in front of each phase can be expressed

$$\overline{\Delta T}^{\alpha} = m_1^{\alpha} B_1^{o} + m_2^{\alpha} B_2^{o} + \lambda v\left[m_1^{\alpha} P_1^{\alpha} + m_2^{\alpha} P_2^{\alpha}\right] + \frac{\Lambda^{\alpha}}{\lambda}$$

$$\overline{\Delta T}^{\beta} = m_1^{\beta} B_1^{o} + m_2^{\beta} B_2^{o} + \lambda v\left[m_1^{\beta} P_1^{\beta} + m_2^{\beta} P_2^{\beta}\right] + \frac{\Lambda^{\beta}}{\lambda}$$

$$\overline{\Delta T}^{\gamma} = m_1^{\gamma} B_1^{o} + m_2^{\gamma} B_2^{o} + \lambda v\left[m_1^{\gamma} P_1^{\gamma} + m_2^{\gamma} P_2^{\gamma}\right] + \frac{\Lambda^{\gamma}}{\lambda}$$

where $P_i^\alpha, P_i^\beta, P_i^\gamma, \Lambda^\alpha, \Lambda^\beta, \Lambda^\gamma$ are constants and $\overline{\Delta T}^\alpha = \overline{\Delta T}^\beta = \overline{\Delta T}^\gamma$.

An expression for the undercoolings which is independent of B_1° and B_2° can be obtained by solving for B_1° and B_2° in terms of λ and v. This is done by equating the expressions given above for the undercoolings. The solutions are

$$B_1^\circ = a\lambda v + b/\lambda$$

$$B_2^\circ = c\lambda v + d/\lambda$$

where a, b, c, d are constants.

Hence $\overline{\Delta T}^\alpha = \overline{\Delta T}^\beta = \overline{\Delta T}^\gamma = \Delta T = K_1\lambda v + \frac{K_2}{\lambda}$ where K_1, K_2 are constants. This expression has the same form as that derived in the Jackson-Hunt theory for binary eutectic growth. If one wishes to apply the principle of growth at the extremum; i.e., the correct value of the lamellar spacing for a given (steady) velocity will be the one which minimizes the undercooling, one obtains $\lambda^2 v$ = constant.

VI. EXPERIMENTAL PROCEDURES

Alloys of composition* 49.4% Sn, 32.3% Pb, 18.3% Cd were prepared from 99.99% Sn, 99.998% Pb and 98+% Cd components by first melting the cadmium in a pyrex beaker and then successively dissolving the lead and the tin into the molten cadmium. The melt temperature was quickly reduced to minimize vaporization

*weight per cent

losses. After stirring with a glass rod, the dross was reduced with stearic acid and the sediment removed with a stiff paper spatula because the temperature was too low to ignite the by-products of the reduction. A small ingot was chill cast at this point, and subsequently examined for evidence of microconstituents other than ternary eutectic as a check on the composition of the alloy.

Small wire loops were prepared by electrically welding a straight piece of .017" Nichrome wire to a long U-shaped piece of .009" steel wire as shown in Figure 9. The loops were about 8 mm. long and about 2.5 mm. wide. The welding was accomplished by the discharge of a 9000 μf capacitor through both joints when the U-shaped wire is touched to the Nichrome wire (see Figure 9b).

The loops were then washed in acetone, pickled briefly in 17% HCl, washed in water and fluxed in saturated $ZnCl_2$ solution for about 30 seconds. After shaking off the excess $ZnCl_2$ solution from the loop, the loop, lying horizontally, was dipped into the molten alloy which had recently been stirred and which was held at 170°C with a hot plate. After clearing away the thin dross with a piece of stiff paper, the loop was lifted out of the melt. Usually a molten foil of alloy was left suspended on the loop. Because a drip usually formed on the underside of the foil before it had frozen completely, the end of the loop was tilted down slightly when being removed from the

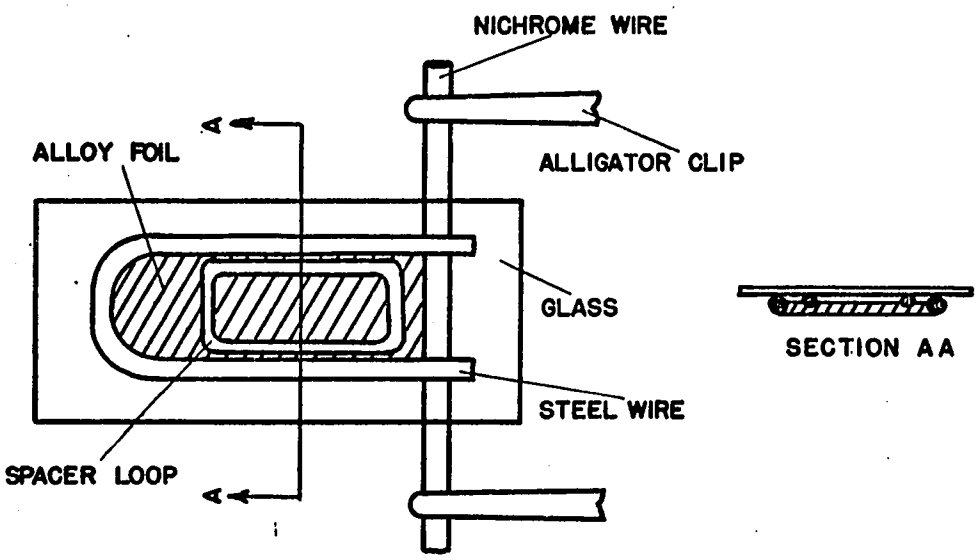

Fig. 9a. Sketch of wire loop with alloy foil, spacer loop, and cover glass.

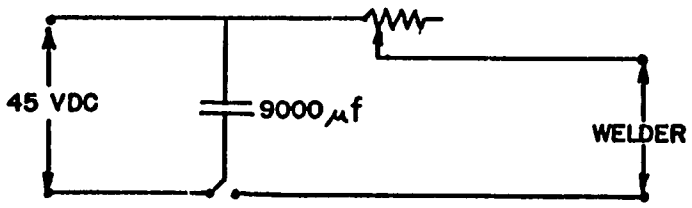

Figure 9b. Wiring diagram for spark welder.

alloy so that the drip would form near the end of the foil. After the formation of the drip, the loop was quickly tilted back to horizontal to prevent excessive thinning of the foil at the end near the Nichrome wire. After a few seconds, the foil had solidified and was carefully examined for holes or excessive oxide film on the surface of the foil. This method produces foils about .009" thick.

For the solidification experiment, the foil was held horizontally with two "alligator" clips connected to the ends of the Nichrome wire (see Figure 9a). The "alligator" clips were attached to a movable stage on a metallographic bench microscope. Electrical power to heat the foil was supplied through these "alligator" clips.

To prevent oxidation of the surface of the foil while in the molten state, about two drops of dibutylphthalate, an oily transparent organic fluid, were placed on the top of the foil. A loop of .009" steel wire, slightly narrower than the foil and about 5 mm. long, was then placed on top of the foil. Then a piece of Corning No. 1 cover glass was placed on top of the inner wire loop and the foil. This leaves a space between the foil and the glass which was of course filled with dibutylphthalate and was necessary for the full development of the surface microtopography.

The ability to observe the microstructure of the solid part of the foil is a consequence of the topography produced by

the microstructure at the surface of the foil. Figure 10a is a micrograph of a section through the foil transverse to the solidification direction. (The method of this solidification will be described later.) The light lamella are the Sn-rich phase, the grey lamella are the Pb-rich phase, and the thin black colored lamella are the cadmium-rich phase. The microstructure can also be seen in Figure 11. One can see that the Sn-rich lamella are higher at the surface than the Pb-rich and Cd-rich lamella. With a microscope, shadows produced by this topography are clearly visible on the surface when illuminated with oblique light. On the surface, the tin-rich lamella are bright and the composite of Pb and Cd rich lamellae, which almost always occur together, are dark. (See Figure 10b). Thus the liquid which is essentially flat, and the Sn-rich lamella, and the Pb-rich Cd-rich lamellar composite are discernible. Unfortunately the thickness of the Cd lamella is too small to observe it separately. Figure 10a also shows that the microstructure at the surface is truly representative of the interior microstructure.*

Observations of the solidification and resulting microstructure were made through a Bausch and Lomb bench microscope with an objective lens of 0.65 N A and a 20x eyepiece. The observations were recorded on 16 mm. Kodak Plus X Negative film

---

*This interior microstructure is also the same as that observed by many authors (37,38,47) in bulk ingots.

Fig. 10a. Micrograph of transverse section of foil showing topography produced by microstructure at top surface of foil.

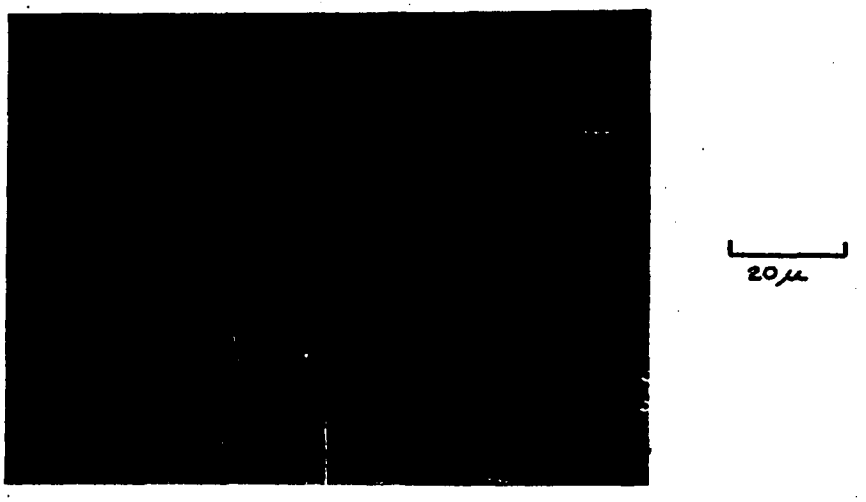

Fig. 10b. Micrograph of top surface of foil showing liquid and solid phases.

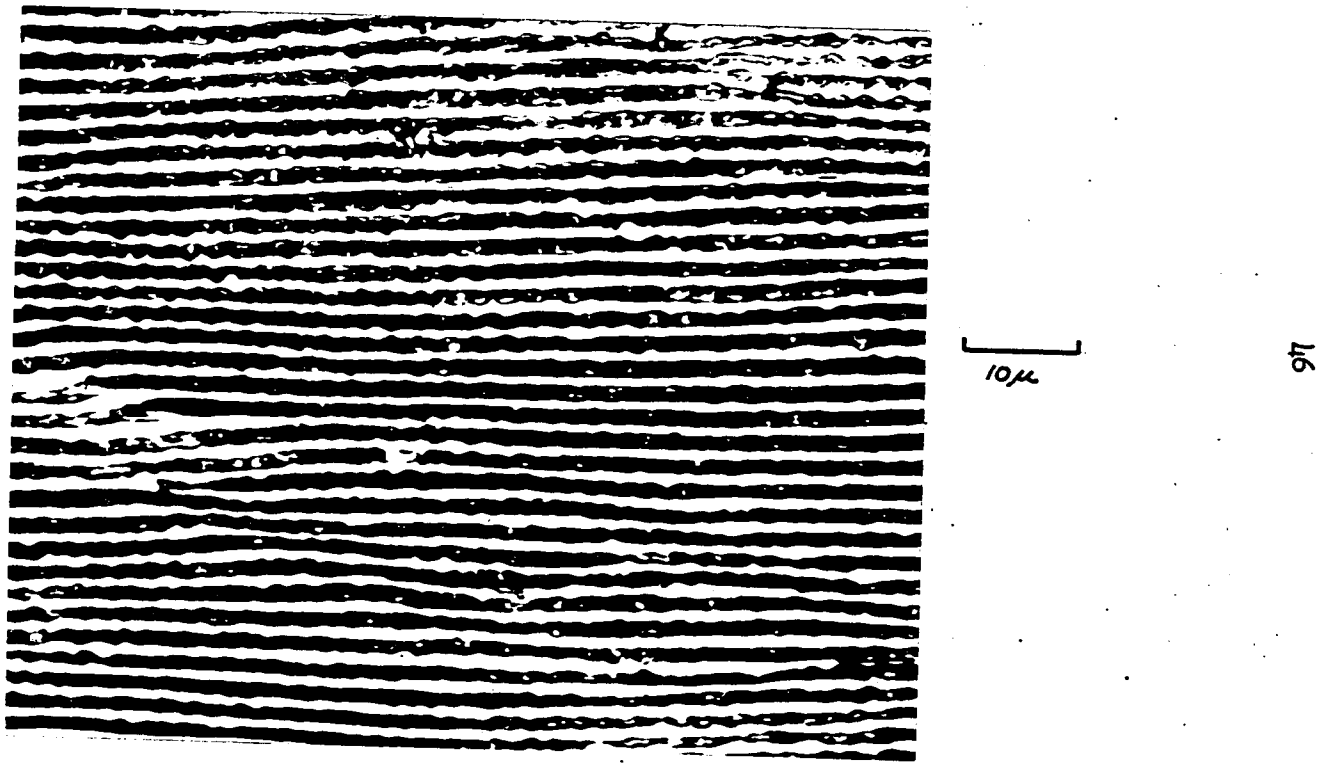

Fig. 11. Micrograph of longitudinal section of foil showing ternary lamellar structure (Nital etch).

using a Bolex reflex movie camera with an electric drive. An f 1.9 lens with a 1/4" extension tube was used on the camera. The camera was supported independently of the microscope and placed as close to the eyepiece of the microscope as possible without touching it. A sleeve of black paper was placed around the camera lens and the eyepiece tube. The camera lens was stopped fully open and focused at infinity. The image focus and light intensity were then controlled by using the microscope focus and aperture diaphram. Before each test, a photograph was taken through the system of a Bausch and Lomb Calibrator Grid, to be used for later magnification calculations.

As has been previously mentioned, an electrical current was supplied to the foil through the two alligator clips which hold the foil. This current was supplied by batteries and could be controlled by rheostats (see Figure 12). By properly controlling these rheostats, it was possible to melt part of the foil. After stabilizing the position of the liquid-solid interface, solidification was accomplished by slightly lowering the current. Admittedly, the heat flow in the foil is quite complex; but directional solidification with an almost planar interface and with a constant velocity could be obtained. Figure 13a is an enlargement of a single frame of film showing at relatively low magnification the shape of the liquid-solid interface as it intersects the top surface of the foil. Cinemicrographic observations were always made on a single grain (there

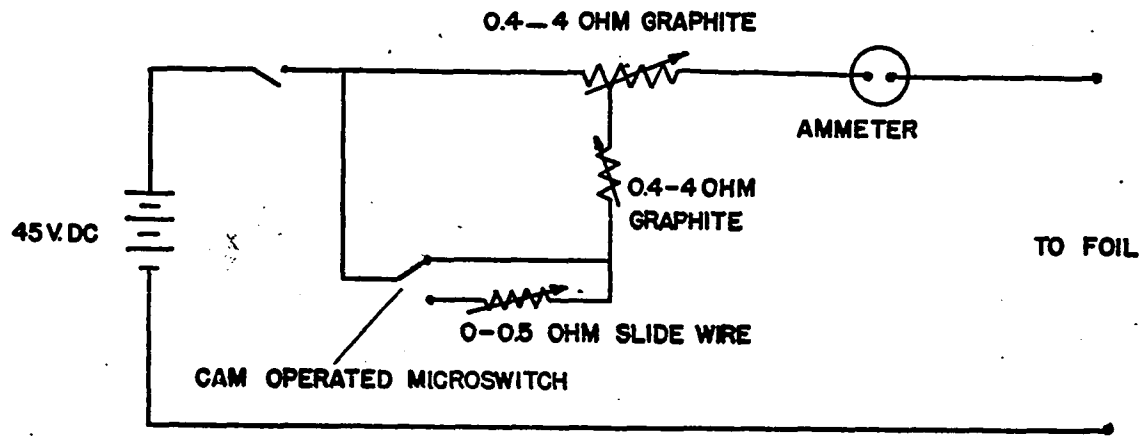

Fig. 12. Wiring diagram for current supply.

Fig. 13a. Low magnification micrograph of moving liquid-solid interface on the surface of the foil.

Fig. 13b. Micrograph of longitudinal section of foil showing "quenched interface."

are several in this picture) in the center of the foil. Figure 13b shows a micrograph of a section of a foil parallel to the solidification direction and perpendicular to the surface of the foil. Shown in the micrograph is a demarcation of the approximate interface position at a particular instant while solidifying. This demarcation is made by causing a drastic increase in solidification velocity by cutting the heating current to zero. This "quenched" interface shows the remarkable planarity of the interface inside the foil and also the perpendicularity of the interface to the top surface. This last point is very important, because only in this case would the velocity of the liquid-solid interface as measured on the top surface of the foil coincide with the true interface velocity.

In order to effect the changes in solidification velocity that were sought, a microswitch, which was operated by a slow-speed motor-operated cam, was used to insert or remove a very small (.05Ω) resistance in series with the fine control rheostat (see Figure 12). This slightly increased or decreased the electrical current, and consequently decreased or increased the solidification velocity respectively.

Three types of tests were performed: increases in solidification velocity, decreases in solidification,and oscillations in solidification velocity. Before any tests were performed, the foil was first melted past the spacer loop to seat it into the alloy (see Figure 9a). This seating prevented air bubbles from entering the interior of the spacer loop and also checked

for defective foils which break. The first two types of tests were performed as follows. The foil was remelted about half-way down its length. After stabilizing the position of the interface, the electrical current was slightly reduced using the fine adjust rheostat to begin solidification at roughly a constant velocity. Because eutectic grains nucleate at random orientations to the final growth direction, before performing an experiment the foils were allowed to solidify for at least 2 mm. so that only grains with lamellae nearly parallel to the growth direction remained. During all of this, the stage was translated to keep the interface in the field of view. When the test began, the stage was left in one position and the camera and cam drive motor were started. After a time sufficient to record the initial steady solidification velocity (about 2 to 3 seconds), the cam would activate the microswitch, consequently increasing or decreasing the heating current depending on the initial position of the microswitch. For these tests the period of the cam operation was large so that the switch would not change again until the test was completed. For the oscillating tests, exactly the same procedure was followed except that the period of the microswitch operation was shorter (1 to 4 seconds) and it was running throughout the entire procedure.

A great variety of tests were performed. Tests with relatively fast and slow initial interface velocities, large and small changes in velocity for the first two types of experiments;

and fluctuating tests with different periods and changes in velocity. These were all accomplished by a somewhat trial-and-error adjustment of the fine and course adjust rheostats for initial velocities and the slide wire for the changes in velocity. Since the velocity is to be taken as the independent variable which controls the microstructure, no further attempt to describe the reaction of the velocity to certain current changes will be made.

VII. TREATMENT OF DATA

The information sought from each test was the liquid-solid interface velocity as a function of time, and the interlamellar spacing produced at the interface as a function of time. With this purpose, sequences of movie film of good photographic quality, and an interesting spectrum of velocity changes, were enlarged ten frames to an 8" x 10" sheet of photographic paper. In all cases, the edges of the movie film frames were included in the enlargement to serve as a reference for later measurements. The movie of the calibration grid was enlarged along with the sequence to yield the overall magnification of the microscope, camera, enlarger combination.

To obtain the velocity of the liquid-solid interface, it was of course necessary to obtain the interface position as a function of time. Due to the fact that the interface was never perfectly planar on the scale of many lamellae, and did not

propagate as a parallel surface, it was necessary to define first the mean solidification direction and second the mean interface position in that direction. The mean solidification direction was obtained by tracing the shape of the interface at intervals of about twenty frames throughout the sequence on a common piece of paper (using the edges of the frame as a common reference). The mean solidification direction was then chosen as a perpendicular to those parallel straight lines which best approximated the interface throughout the sequence. This solidification direction sometimes deviated from a direction square with the movie frame because the foil was not perfectly square with the microscope stage, and the whole interface across the foil was slightly convex. (See Figure 13a). Two measurements of the interface position were made in each frame by measuring the distances along the solidification direction from the same point on the edge of the frame to the most advanced (into the liquid) part of the interface and the most recessed part of the interface. The mean of these two distances was taken as the mean interface position. In no case did the difference of these measurements exceed 5 μ in real space over a 35 μ width of interface. Because in some cases, grain boundaries, surface oxide, or just poor focus were present in part of the field of view, the region of the frame used for these measurements was often restricted. The region was restricted to regions free of these items by lines contained com-

pletely within the field of view and parallel to the mean solidification direction. The width of region used was always greater than 35 μ . The same set of lines in reference to the edges of the frame were used in all frames of a given sequence. Measurements were taken every five frames (.3 second) or every two frames (.12 second) depending on the acceleration of the interface. The framing rate of the camera, which was set at eighteen frames per second, was calibrated and found to be 16.67 frames per second. Using this and the above mentioned measurements, the mean interface position x was plotted as a function of time t . A typical plot of x vs. t data is shown in Figure 14 with a smooth curve drawn through the points. The interface velocity was found by differentiating this smooth curve using a Gerber Derivameter at .3 second or .12 second intervals depending again on the acceleration. These data yield a plot of interface velocity as a function of time.

To obtain the interlamellar spacing as a function of time, a single frame at the end of the particular sequence was used. As has been described in Section VI, the Sn-rich lamellae appear bright on the surface of the foil. Since the lamellar spacing is defined as the distance between centers of Sn-rich lamellae, an apparent lamellar spacing at any position in the solidification direction could be obtained by simply counting the number per unit length of bright lamellae intersected by a line perpendicular to the solidification direction at that position. This was done at positions 2.4 μ or 4.7 μ apart depend-

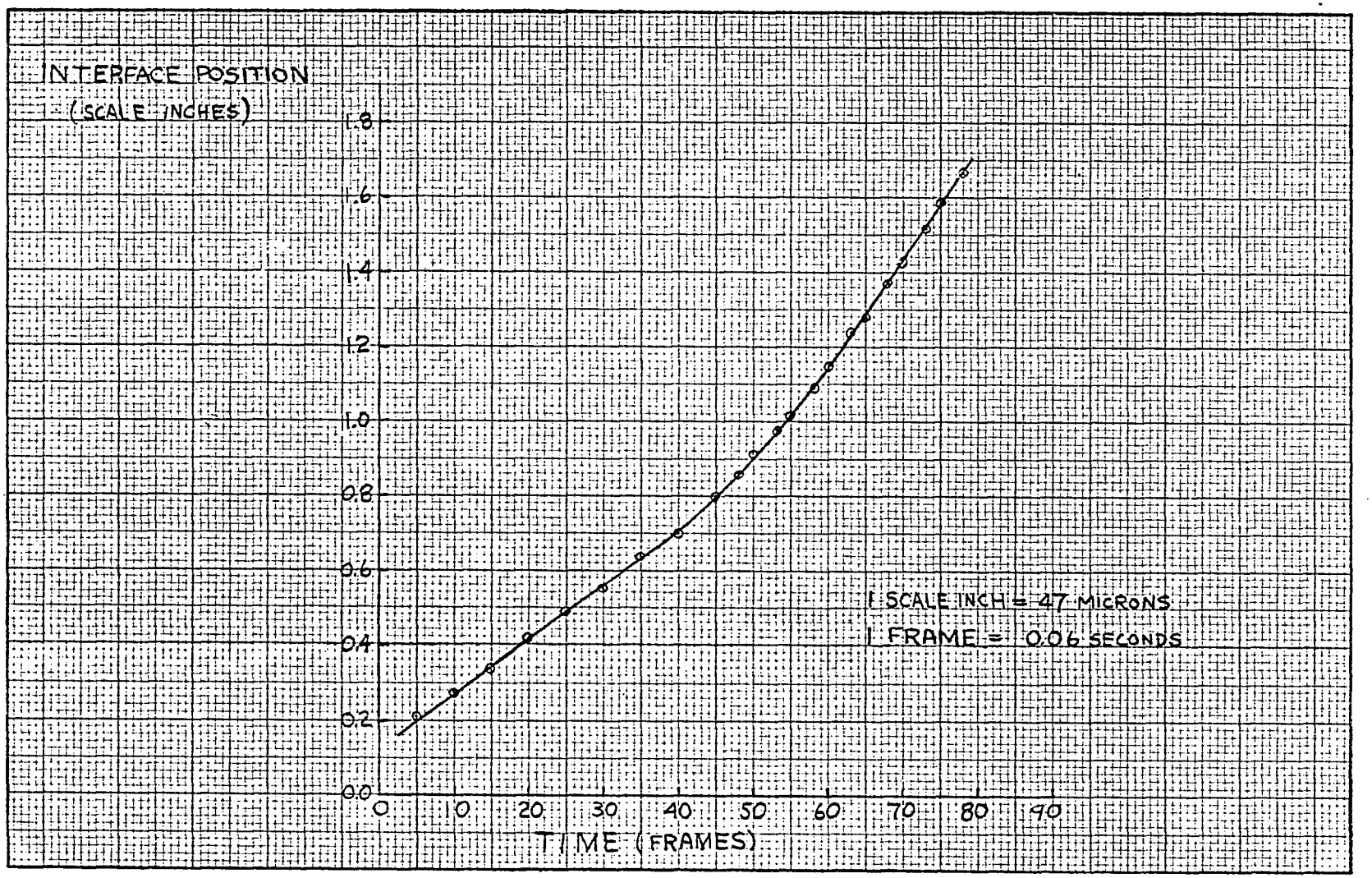

Fig. 14. A typical plot of interface position vs. time data.

ing on the rate of change of the lamellar spacing. The reciprocal of the number of Sn-rich lamellae per unit length is only an apparent lamellar spacing because the lamella need not be perpendicular to the top surface of the foil. This can be seen in Figure 15, where the solidification is out of the paper and λ and λ' are the true and apparent lamellar spacings, and Θ is the angle the lamellae make with the foil.

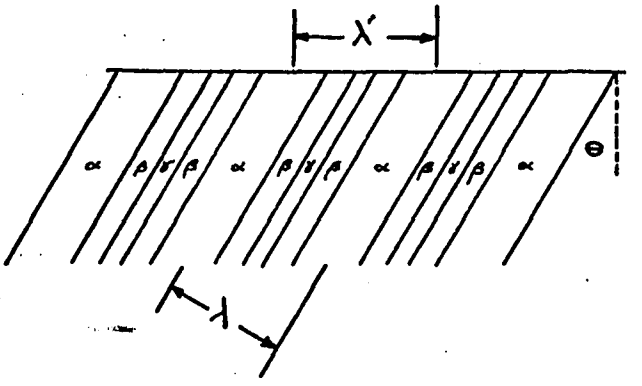

Figure 15

Assuming Θ were known, λ can obviously be given by

$$\lambda = \lambda' \sec \Theta \quad .$$

It is implicitly assumed in all of this work that within a given eutectic grain Θ is a constant. This assumption, while not directly verified, is justified based on the following two points. First, the rotation of lamellar habit planes in the solidification direction have been studied in Al-Zn eutectic and shown to be about 10°/per inch (51). Over the lengths observed in this study (.125 mm.), these rotations are certainly negligible. Secondly, when the rate is changed many individual lamellae are connected throughout the transient region, eliminating the possibility of a new eutectic grain (different Θ)

having nucleated. Generally only changes in lamellar spacing will be discussed, so that not knowing the true spacing will be no real limitation. In a few cases, where the true lamellar spacing was needed, the solidified foils were sectioned transversely to the solidification direction at a position where the solidification velocity had been previously determined. In these transverse sections, there was a range of spacings found from grain to grain. The minimum was used since it corresponds to a grain growing with lamellar habit planes lying exactly in the solidification direction, if one assumes the true spacing is the same in all grains. Practically, this determination of true spacing could only be done in a region over which the solidification velocity was steady over a distance of about 1/4 mm., due to difficulty in sectioning. The apparent lamellar spacing-position data can be converted into apparent lamellar spacing-time data because there exists a one-to-one correspondence between interface position and time as derived before. This is true as long as the solidification velocity is a non-zero positive number. Thus one can easily obtain the apparent lamellar spacing which is produced at the interface as a function of time.

Possible sources of error in these data will now be discussed. For the interface velocity time curves, the major source of error is the differentiation of the interface position-time curves. Systematic errors in the position-time data will be unimportant since usually ratios of velocities are used in the

discussion to follow. The effect of random errors in the position-time data on the velocity is minimized by the placement of a smooth curve through the position-time data points. For the scales used for the plotting of the data, the use of the Gerber Derivameter to differentiate the position-time curves can cause a maximum error in the velocity of $\sim$ 4% at 3μ/sec. and a maximum error of $\sim$ 2% at 16μ/sec. Hence the time when the velocity begins to change from a steady value may be in slight error if the velocity changes very slowly. The apparent lamellar spacing could be measured with a maximum error of 3%. Hence the time when the lamellar spacing begins to change from a steady value might be in question. But when the spacing changes rapidly as it does in most of the tests performed, the error in this time is small. The lamellar spacing usually changes by the formation or termination of individual lamellae. It is also possible that the position where a lamella forms or terminates might be misjudged in position in the microstructure by as much as 2/3 μ. This is an approximate limit to the resolution of the total optical system. Hence at a velocity of 20μ/sec, the time of the event could be misjudged by .03 sec. At a velocity of 1μ/sec the misjudgment in time might be .67 sec. Hence times when the lamellar spacing begins to change are most accurate when the interface is moving fast.

VIII. RESULTS AND DISCUSSION

The results of four groups of tests, based on velocity program, will be presented and discussed separately.

1. Constant Interface Velocity ---- Four tests were performed to check the steady state relationship between interlamellar spacing and interface velocity. For these tests the true interlamellar spacing was found using the sectioning technique mentioned previously. These data are shown in Figure 16 superimposed on the data of Kerr et al. (37). The average value of the product $\lambda^2 v$ for these four tests was 25.6 μ^3/sec. as opposed to Kerr's value of 10.1 μ^3/sec. The work of Kerr et al. was for slower velocities, however, Although this discrepancy is large enough to bring one or both of these results into question, it will be shown later that an error of 30% can be expected in some "steady state" measurements.

2. Increases in Interface Velocity ---- Eight tests were performed in which the interface velocity increased by factors of from 2.1 to 19.5 from one steady value to another. A typical sequence of pictures from the movie film is shown in Figure 17. The ratios of interface velocity v, apparent lamellar spacing λ', and the product $\lambda'^2 v$ to their initial steady values v_i, λ'_i, $\lambda'^2_i v_i$ are plotted as functions of time in Figures 18, 19, 20, 21. With the assumption stated previously that the orientation of lamellae is constant within a grain, one should note that $\frac{\lambda'}{\lambda'_i} = \frac{\lambda}{\lambda_i}$ and $\frac{\lambda'^2 v}{\lambda'^2_i v_i} = \frac{\lambda^2 v}{\lambda^2_i v_i}$. The

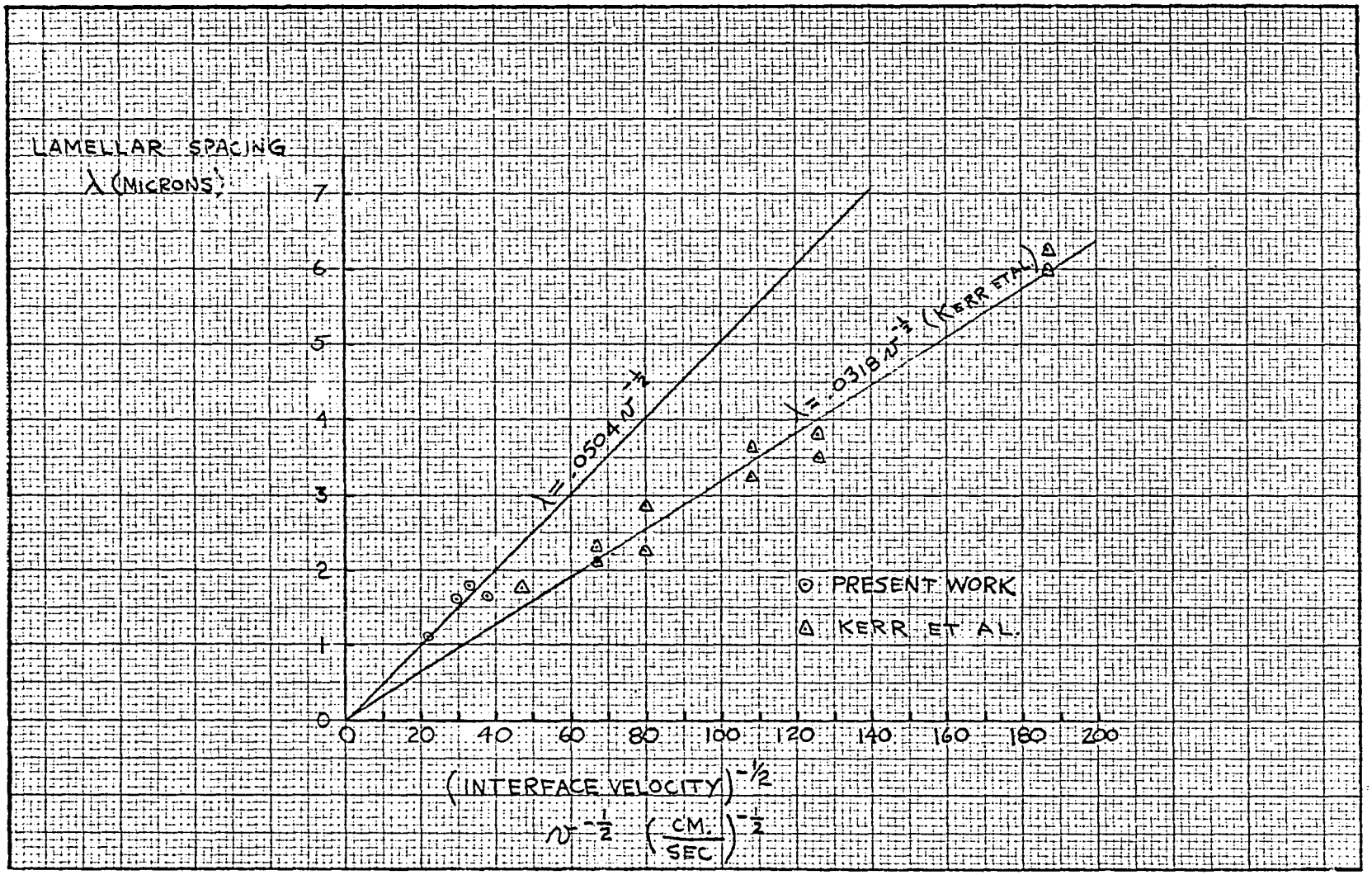

Fig. 16. Steady state $\lambda^2 v$ data superimposed on the data of Kerr et al.

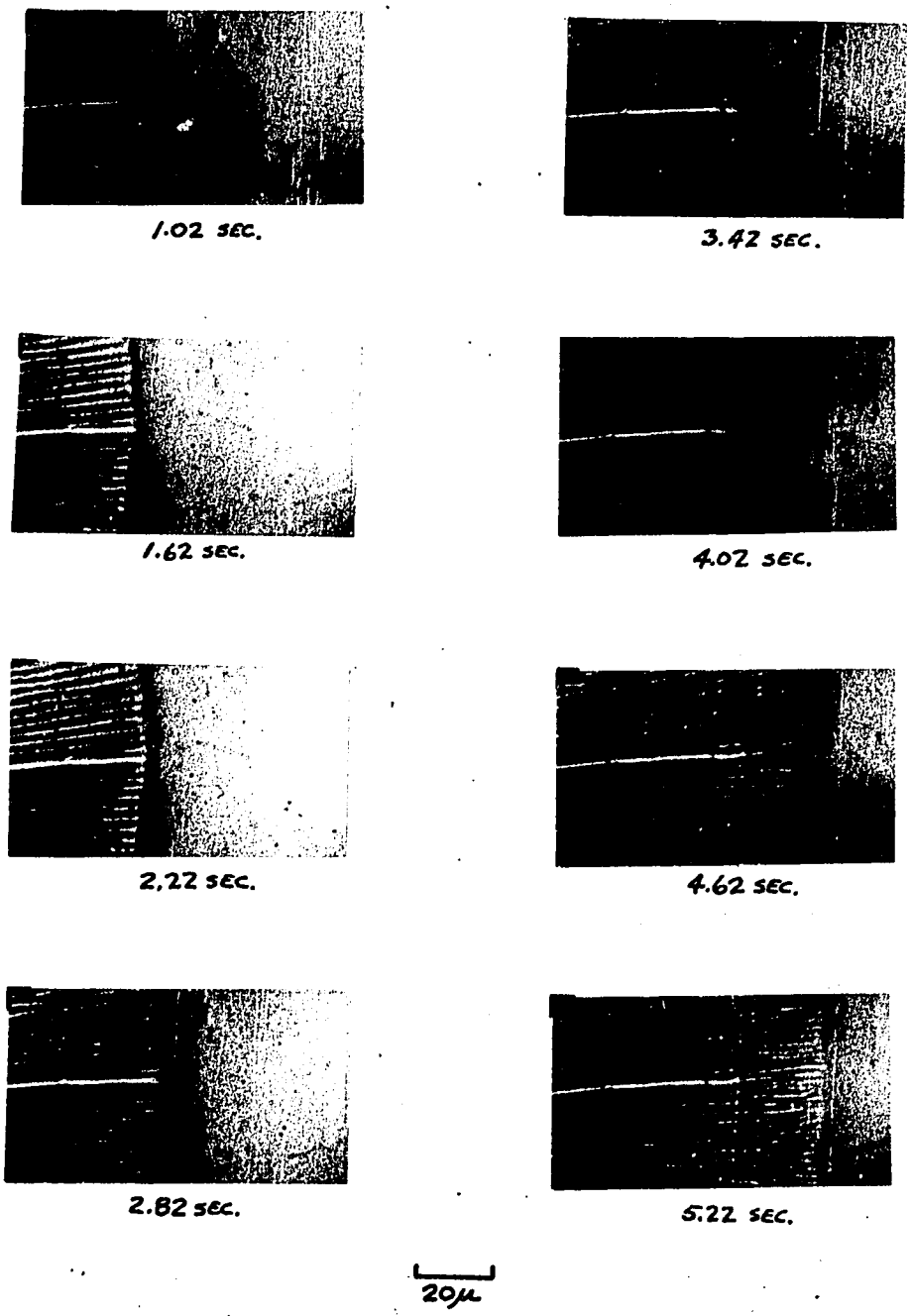

Fig. 17. Sequence of enlargements from movie film at 0.6 second intervals for velocity increase test. (I2)

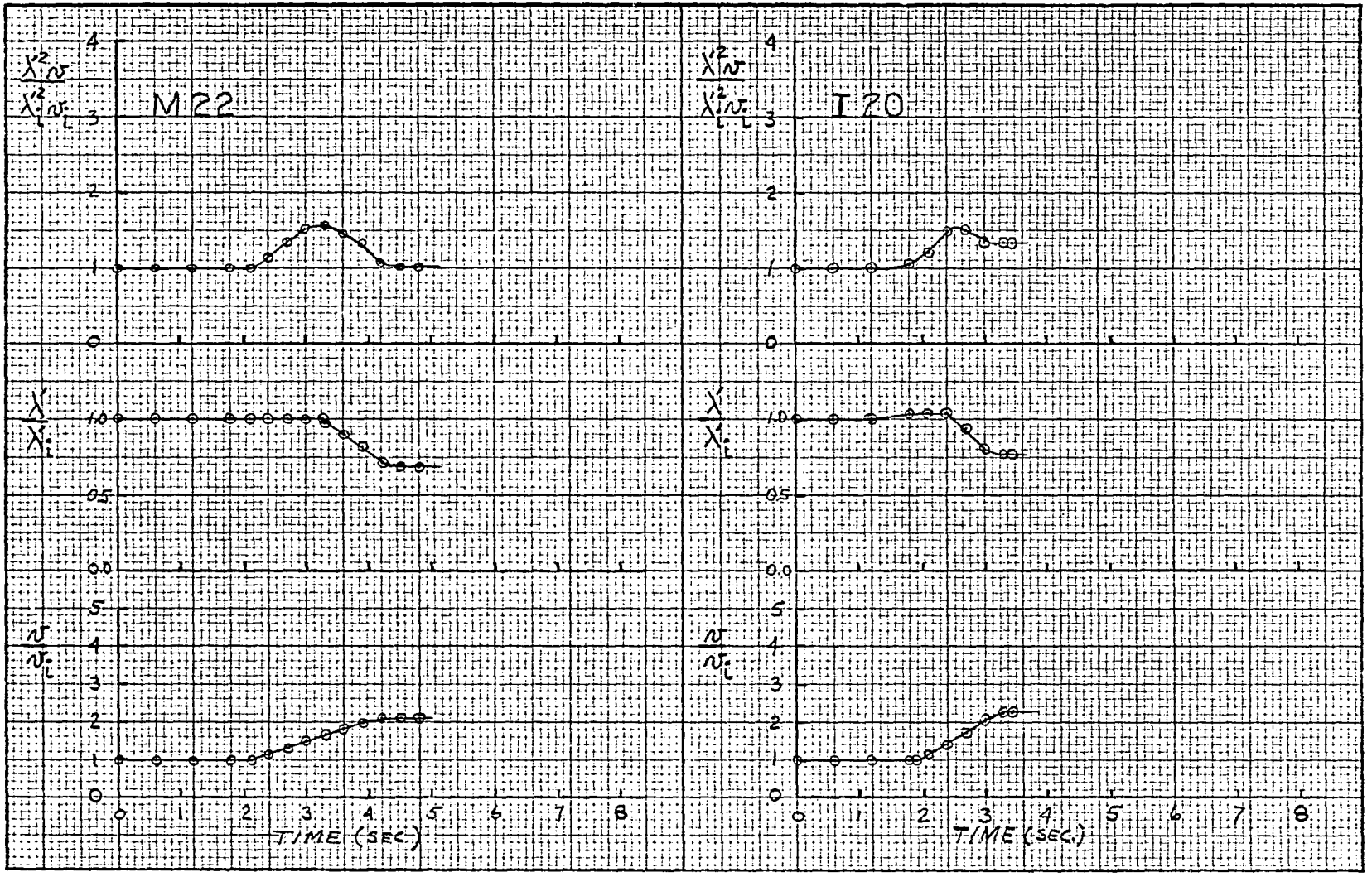

Fig. 18. Data for velocity increase tests.

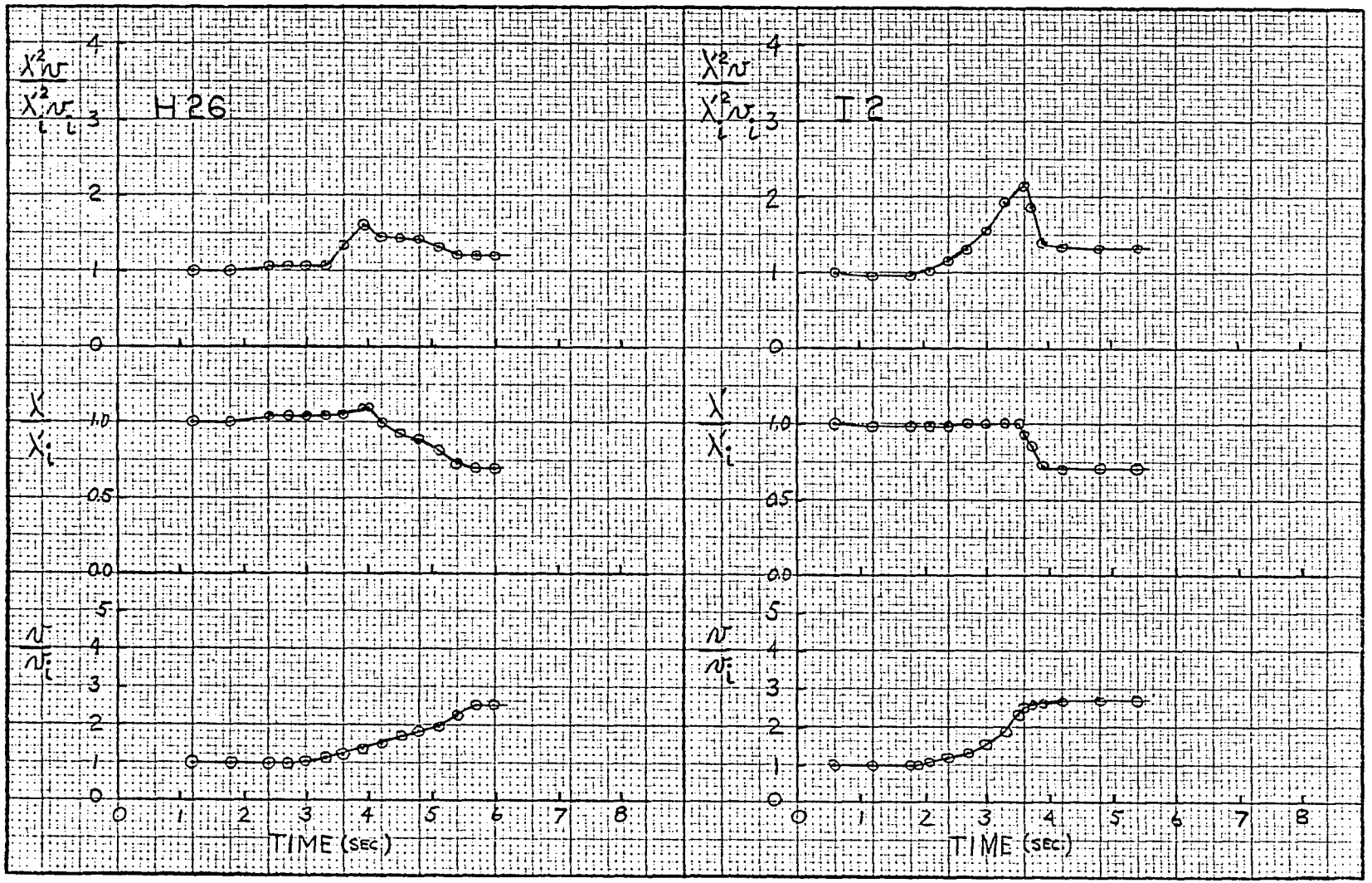

Fig. 19. Data for velocity increase tests

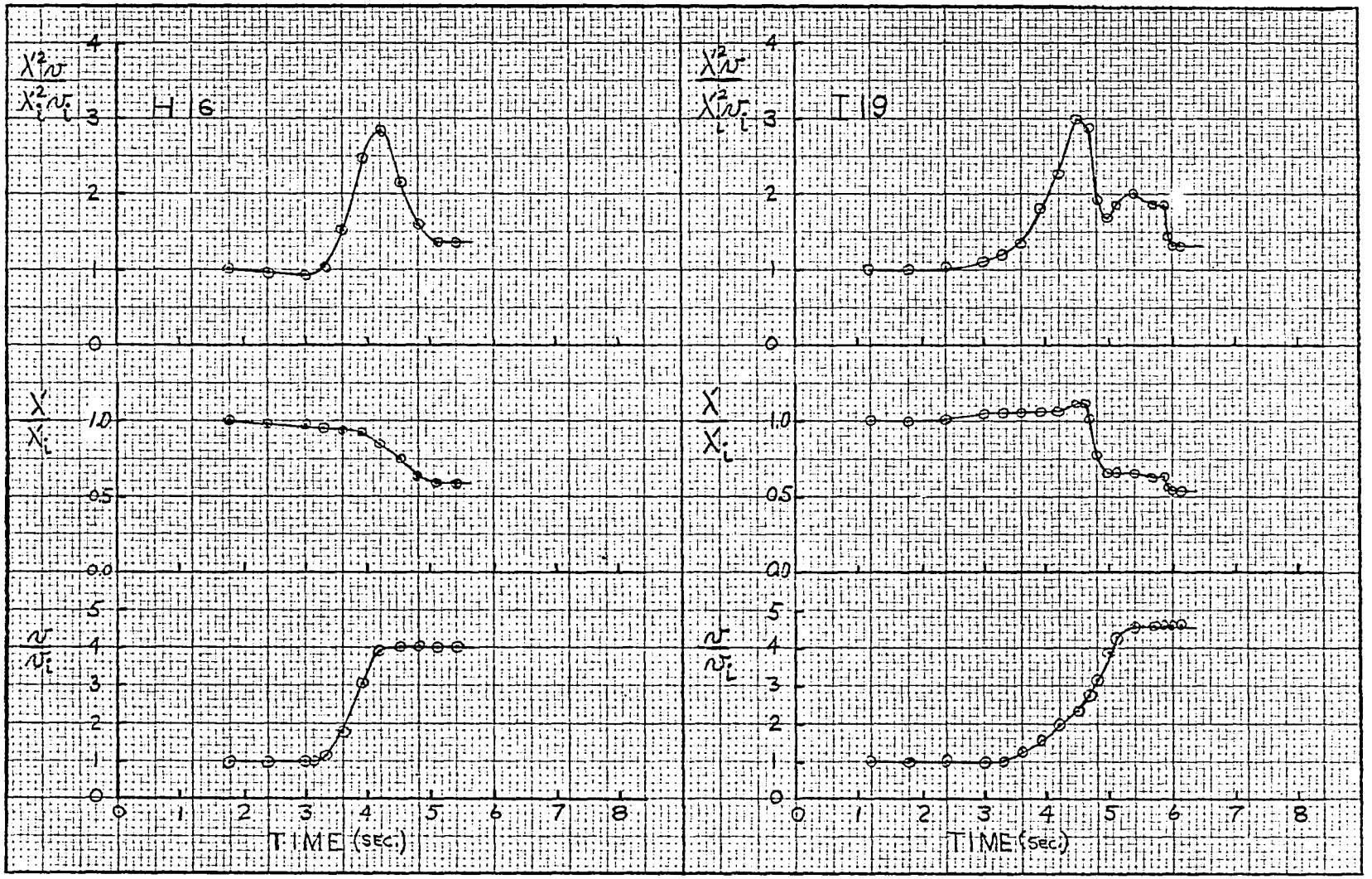

Fig. 20. Data for velocity increase tests.

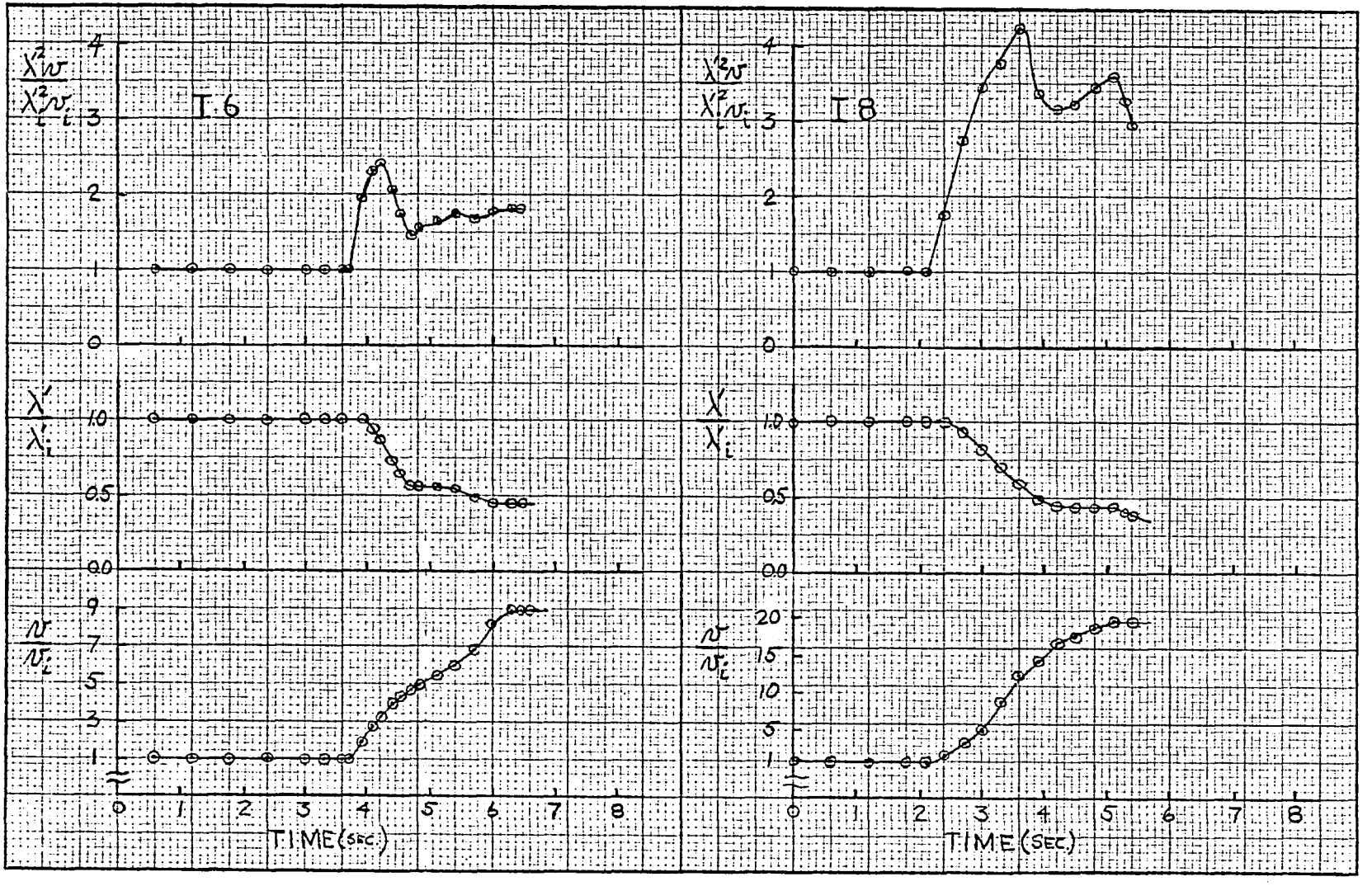

Fig. 21. Data for velocity increase tests.

initial values of these quantities are given in Table 2 along with the ratio of interface velocity v_d to the initial velocity at the instant when λ' begins to decrease, the ratio of the final (steady) interface velocity v_f to the initial velocity, the ratio of the final apparent lamellar spacing λ'_f to the initial apparent lamellar spacing, the ratio of the final value of the product $\lambda'^2_f v_f$ to its initial value. Also given in Table 2 is the approximate time delay Δt between the instant when the velocity begins to increase and the instant when the lamellar spacing begins to decrease, the distance Δd between the interface positions corresponding to the above instants in time, and the average acceleration of the interface $\frac{v_d - v_i}{\Delta t}$ between the same two instants in time. Shown in Figures 22, 23 for later consideration are micrographs taken from the movie film of the surface of the foil at the end of each of the tests. It is during the course of the solidification of the material in the field of view that the above data were taken. These micrographs have been numbered according to increasing uniformity of the lamellar structure to the right (cold) side of the place where the lamellar spacing began to decrease. Points considered in this ordering are freedom from lamellar faults, mismatch surfaces (or rather their traces as seen on the surface of the foil) and isolated products of primary crystallization. Points not considered in this ordering are the size of the apparent lamellar spacing and the photographic focus and contrast of

TABLE 2 (VELOCITY INCREASE TESTS)

TEST	v_i	v_f	$\frac{v_f}{v_i}$	λ_i	$\frac{\lambda_f}{\lambda_i}$	$\lambda_i^2 v_i$	$\frac{\lambda_f^2 v_f}{\lambda_i^2 v_i}$	Δt	Δd	$\frac{v_d}{v_i}$	$\frac{v_d - v_i}{\Delta t}$	STRUCT. UNIFORM-ITY
#	$\frac{\mu}{\text{SEC.}}$	$\frac{\mu}{\text{SEC}}$	·	μ	·	$\frac{\mu^3}{\text{SEC.}}$	·	SEC.	μ	·	$\frac{\mu}{\text{SEC.}^2}$	#
M 22	11.13	23.48	2.11	1.83	0.69	37.3	1.02	1.17	17.4	1.65	6.18	4
I 20	19.43	43.91	2.26	1.41	0.77	38.6	1.32	0.51	12.2	1.40	15.23	3
H 26	6.27	15.68	2.50	2.63	0.70	43.4	1.21	1.26	8.9	1.36	1.79	1
I 2	5.64	15.06	2.67	2.59	0.71	37.8	1.33	1.56	13.2	2.33	4.81	7
H 16	3.92	15.68	4.00	2.77	0.59	30.1	1.36	0.78	4.7	2.90	9.54	2
I 19	7.52	34.44	4.58	1.93	0.54	28.0	1.31	1.32	16.0	2.59	9.05	8
I 6	2.98	26.67	8.95	3.24	0.45	31.3	1.81	0.24	0.9	1.95	11.79	6
I 8	2.04	39.70	19.46	2.63	0.39	14.1	2.95	0.30	0.7	1.77	5.23	5

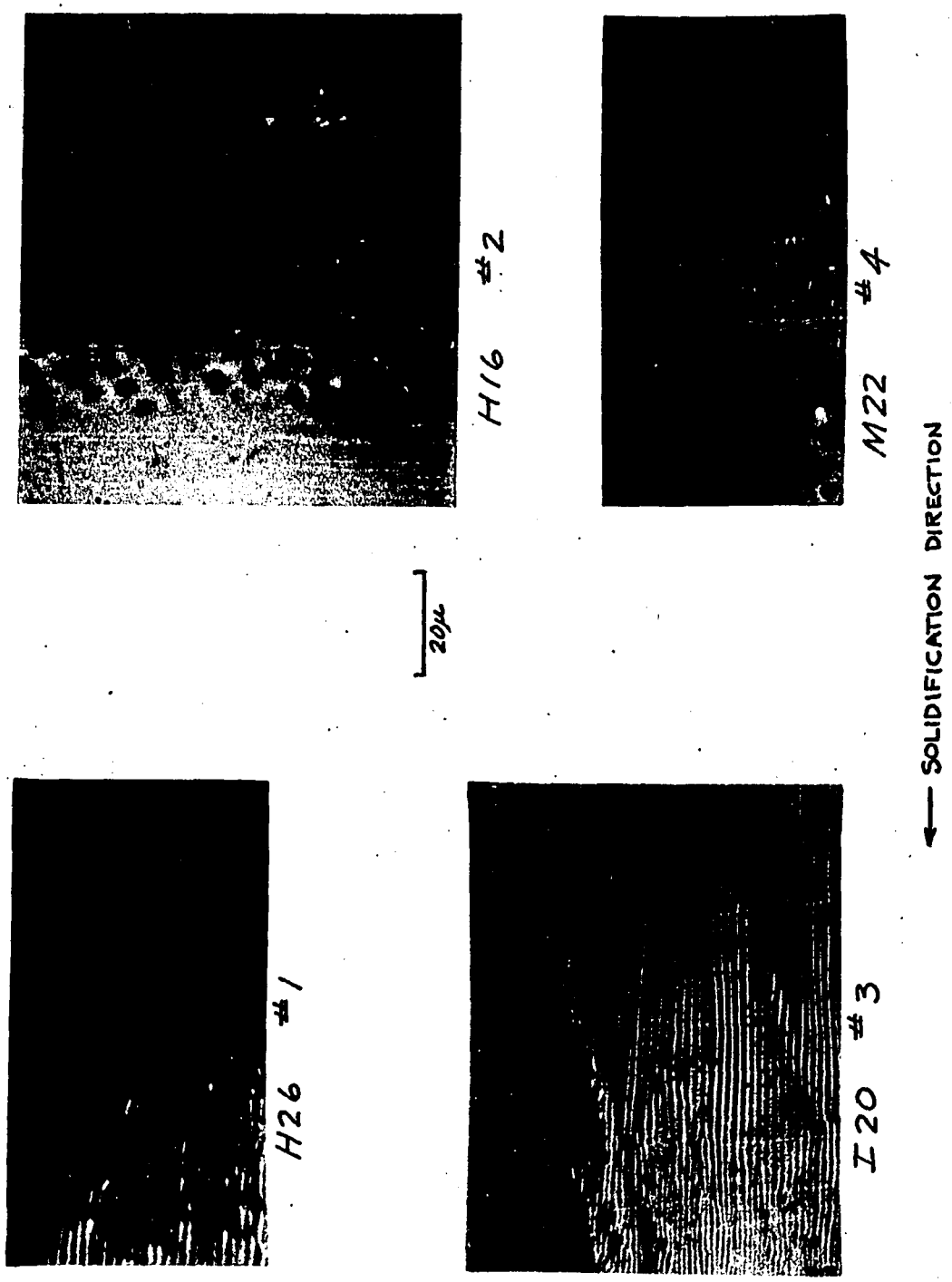

Fig. 22. Micrograph taken from movie film for each test showing structure uniformity no. (velocity increase tests).

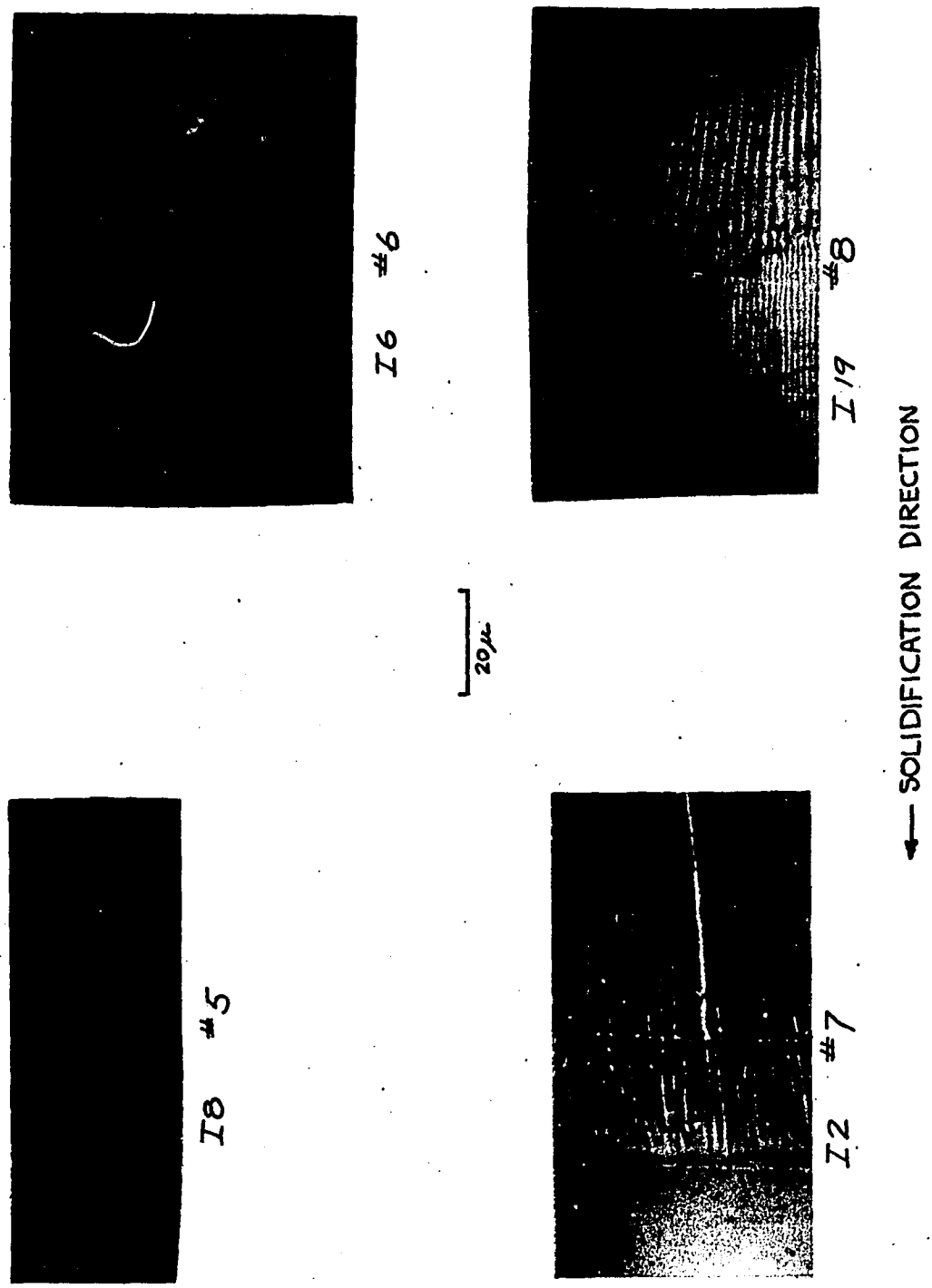

Fig. 23. Micrograph taken from movie film for each test showing structure uniformity no. (velocity increase tests).

the micrographs. Pictures #1 and #2 have a large number of faults, Picture #3 has a large number of traces of mismatch surfaces, and Picture #4 has what is believed to be isolated products of primary crystallization. From these micrographs one can see lamellar spacing decreases by the splitting of an individual lamella and the formation of a different lamella in this split. It must be remembered that the dark lamellae in these micrographs are actually a composite of Pb-rich and Cd-rich lamellae. In four of these micrographs, one can definitely see places where a light lamella splits and a dark lamella forms in the split and also places where a dark lamella splits and a light lamella forms in the split. There is no definite preference for either of these in these four micrographs.

The following aspects of these data and curves will be discussed: the final value of the lamellar spacing after a steady state velocity has been re-established, the details of the lamellar spacing change, and the initial response of the lamellar spacing to the velocity change. The first point to be noticed about these data is that in none of the tests did the final value of $\lambda'^2 v$ return to exactly its original value after the change in lamellar spacing was completed. With the exception of tests I6 and I8, the values of $\frac{\lambda_f'^2 v_f}{\lambda_i'^2 v_i}$ ranged between 1.02 and 1.36. Tests I6 and I8 showed much larger values of this parameter. These are also the tests with the largest overall changes in velocity. In light of a phenomenon to be discussed

later, it is felt that the reason for the high value of this parameter for tests I6 and I8 is because the solidification was not observed over a long enough distance. Although the possibility exists that the other tests were not observed long enough, it is thought that the failure of $\lambda'^2 v$ to return to its original value after the spacing change indicates that a lamellar structure can really solidify over a range of lamellar spacings for a given steady velocity. This effect has been discussed by Jackson and Hunt and is presented in Section III. Further adjustment of the lamellar spacing to a value nearer the extremum spacing is accomplished by the slower process of lamellar spacing change, the motion of lamellar faults. The largest value of the parameter $\frac{\lambda'^2_f v_f}{\lambda'^2_i v_i} = 1.36$ indicates an upper limit on the value which the lamellar spacing can have for a steady velocity. One might also speculate that overall changes in velocity of less than 1.36 would not cause a change in lamellar spacing by the formation of new lamellae.

The second point to be noticed about the data concerns the details of the lamellar spacing change. For all tests where the final velocity was less than or equal to four times the initial velocity $\left(v_f/v_i \leq 4\right)$ the apparent lamellar spacing changed from its initial value to its final value in one stage. For all tests where $v_f/v_i > 4$ the apparent lamellar spacing changed from its original value to its final value in two or more stages. This multi-staged spacing change is seen in tests I19, I6 and I8

and is even more apparent in the shape of the $\frac{\lambda'^2 v}{\lambda'^2_i v_i}$ vs. time plots. These show two or more maxima as opposed to the one maximum seen for the other tests. These plots are an indication of the deviation at a given time of the physical situation from the extremum condition. These curves always rise to some value and then fall only after the lamellar spacing has begun to decrease. For the tests with a multi-staged change in spacing, after reaching a minimum the curve again rises and falls to a new minimum which is closer to unity. This process could go on until the value of $\frac{\lambda'^2 v}{\lambda'^2_i v_i}$ is close enough to its original value to not require further adjustment by the formation of new lamellae. This value was discussed previously. Unfortunately the solidification was not observed over a distance long enough to exhibit more than two stages.

This multi-staged spacing change for $v_f/v_i > 4$ places some rather interesting restrictions on the possible mechanism of lamellar spacing decrease. If one assumes that the $\lambda^2 v$ = constant law will at least serve as a guide to the initial and final values of lamellar spacing and interface velocity, one can easily show that $\frac{v_f}{v_i} = \frac{\lambda_i^2}{\lambda_f^2} = \frac{\lambda'^2_i}{\lambda'^2_f}$ since the orientation of the lamellae is assumed to be constant. When the final velocity is less than four times the original velocity, the final lamellar spacing should be greater than 1/2 times the original lamellar spacing. When the final velocity is greater than four times the original velocity, the final lamellar spacing should be

less than 1/2 times the original spacing. Hence, multi-staged spacing changes were observed only when the final lamellar spacing was required to be less than 1/2 of the original spacing. Thus it seems that this halving of lamellar spacing is a limit to the amount of lamellar spacing change which can be accommodated in one stage. When the spacing must change by more than a factor of 1/2, two or more stages occur. Each stage of course need not reduce the spacing by exactly one-half; any value between one and 1/2 is permissible in each stage. These variations are possibly due to slight perturbations to the system which will allow some lamellae to split earlier than others. Figure 24 shows the only two ways that the triple lamellar structure can halve its lamellar spacing in one stage while maintaining its $\alpha\beta\gamma\beta\alpha\beta\gamma\beta\alpha$ stacking, and while maintaining the continuity of at least some of the lamellae. These sketches are consistent with the types of lamella formation seen in the micrographs. It is possible to consider ways in which the spacing might cut its value in thirds but 1/3 is not the limiting value observed in the experiments, nor were these types of lamella formation observed. These sketches are meant to show a case of spacing change of exactly one-half. Smaller changes are easily accommodated by merely skipping a few new lamellar formations in the stacking. Hence any model of lamellar spacing change must optimally produce changes as seen in these diagrams; i.e., in a given region either splits must occur in the Sn-rich

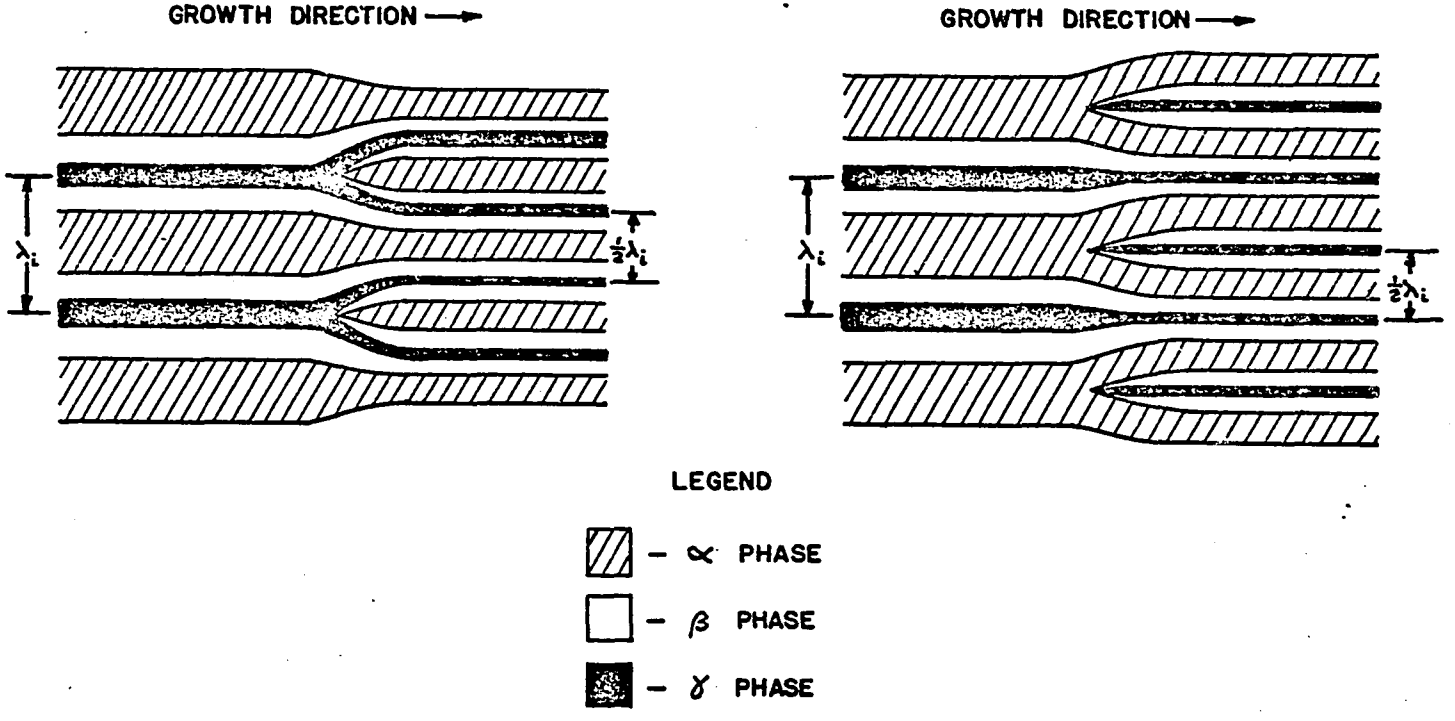

Fig. 24. Two ways of decreasing lamellar spacing by formation of new lamellae.

α phase with the β-γ-β composite forming in the splits, or the splits must occur in the β-γ-β composite with the α phase forming in the splits. In different regions in the structure these two possibilities could be found without noticeably changing the ability of the lamellar spacing to be reduced to 1/2 of its original value.

The third point to be noticed about the data concerns the initial change in lamellar structure. There is a delay between the time when the velocity begins to increase and the time when the spacing begins to decrease. The spacing does not change when the velocity does. In fact, the lamellar spacing begins to decrease only after the velocity has increased from its original value by a factor of from 1.36 to 2.90 depending on the particular test. This is seen in Table 2 by the values of $\mathcal{V}_d/\mathcal{V}_i$. The size of these ratios is well correlated with the structure uniformity number as shown in the bar graph in Figure 25. They however are not simply correlated with the average accelerations or the magnitude of the total velocity changes $\mathcal{V}_s/\mathcal{V}_i$ as shown in Figure 25. Thus it seems that the important factor in determining the velocity change required to initiate the lamellar spacing change is the uniformity of the lamellar structure, not the details of the velocity change. The more uniform the lamellar structure is, the larger the velocity change required to initiate the structure change.

One is now in a position to consider the mechanism by

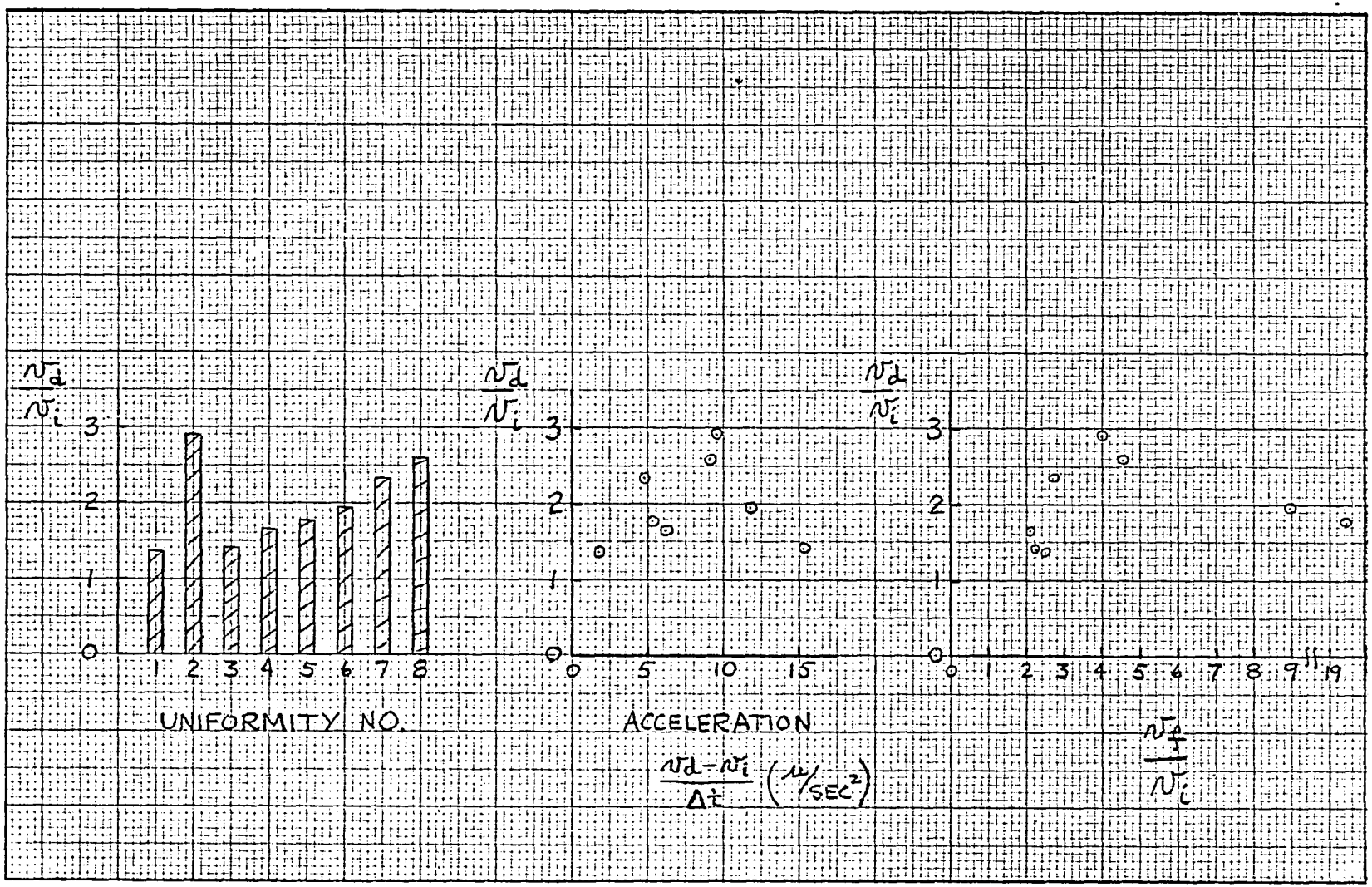

Fig. 25. Correlation of v_d/v_i with structure uniformity, acceleration and v_f/v_i (velocity increase tests).

which a lamella will split and a different lamella form in the split. This mechanism will be discussed first for a perfect lamellar structure. As the velocity of the interface increases from its original value and the lamellar spacing remains constant, three things happen: the composition distribution of the liquid changes, the temperature of the interface changes, and the shape of the liquid-solid interface changes on a lamellar scale. These of course are not independent. None of these changes were measured directly, but they can be estimated by a careful application of some of the results of Section V. Somewhere in these changes must lie the reason for the formation of new lamellae.

The composition in the liquid is shown in Figure 7 for a fixed lamellar spacing and a fixed steady interface velocity. The amplitude of the oscillations about the eutectic composition increase linearly with the interface velocity. At a particular interface velocity which is increasing, the deviation of the composition distribution from the eutectic composition will exceed the deviation that one predicts for that same velocity, if the velocity is steady. This excess should be a function of the acceleration of the interface. As the interface velocity increases, the liquid-solid interface of each phase rejects more solute for that phase into the liquid than can diffuse away from the interface in a given time. Hence the solute concentration in the liquid must increase at the interface

for each phase. If a new steady velocity is achieved, the excess solute at the interface will have time to diffuse away from the interface and reduce its value to the new steady state value. The slower the acceleration of the interface, the smaller this effect should be. Hence for a slowly changing velocity, the steady-state prediction of the liquid composition distribution should be a good approximation to the actual situation. For all of the tests conducted in this section, the value of the acceleration of the interface seemed to have no effect on the initial decrease in lamellar spacing. Hence, the steady state prediction of the composition distribution will be employed for further discussion. It should not be forgotten, however, that for extremely large accelerations, the composition distribution can differ from the steady state prediction for a given velocity.

In the context of these remarks, the undercooling of the interface at a fixed lamellar spacing λ_i and any velocity v will be given by the equation found in Section IV.

$\Delta T = K_1 \lambda v + K_2/\lambda$ where K_1, K_2 are constants.

Hence as the velocity increases, the temperature of the interface will decrease. The temperature would be even lower if the value of the acceleration mattered. In order to gain an expression for ΔT which is independent of the constants K_1 and K_2, one can form the ratios of ΔT with either ΔT_i or ΔT_e. ΔT_i is the undercooling of the interface initially if the

initial velocity and initial lamellar spacing satisfy the extremum conditions $\left(\lambda_i^2 v_i = \frac{K_2}{K_1}\right)$. ΔT_e is the undercooling that the interface would have if at the velocity v, the lamellar spacing had changed to satisfy the extremum condition for that velocity $\left(\lambda^2 v = \frac{K_2}{K_1}\right)$; i.e.,

$$\Delta T_i = K_1 \lambda_i v_i + K_2/\lambda_i = 2\sqrt{K_1 K_2}\, v_i^{1/2}$$

$$\Delta T_e = K_1 \lambda v + K_2/\lambda = 2\sqrt{K_1 K_2}\, v^{1/2}.$$

Hence the ratios $\frac{\Delta T}{\Delta T_i}$ and $\frac{\Delta T}{\Delta T_e}$ are given by

$$\frac{\Delta T}{\Delta T_i} = \frac{K_1 \lambda_i v + K_2/\lambda_i}{2\sqrt{K_1 K_2}\, v_i^{1/2}} = \frac{1}{2}\left[1 + \frac{v}{v_i}\right]$$

$$\frac{\Delta T}{\Delta T_e} = \frac{K_1 \lambda_i v + K_2/\lambda_i}{2\sqrt{K_1 K_2}\, v^{1/2}} = \frac{1}{2}\left[\left(\frac{v}{v_i}\right)^{\frac{1}{2}} + \left(\frac{v}{v_i}\right)^{-\frac{1}{2}}\right].$$

It is interesting to note that $\Delta T \geq \Delta T_e$ for all $\frac{v}{v_i}$. This is merely a statement of the extremum condition itself; i.e., at a given velocity the lamellar spacing which minimizes the undercooling is the "extremum" spacing. Any other spacing yields a higher undercooling. At the instant when the lamellar spacing begins to change, $v = v_d$ and the undercooling of the interface at this instant will be ΔT_d, where

$$\frac{\Delta T_d}{\Delta T_i} = \frac{1}{2}\left[1 + \frac{v_d}{v_i}\right] \quad \text{OR} \quad \frac{\Delta T_d}{\Delta T_e} = \frac{1}{2}\left[\left(\frac{v_d}{v_i}\right)^{\frac{1}{2}} + \left(\frac{v_d}{v_i}\right)^{-\frac{1}{2}}\right].$$

The shape of the lamellar liquid-solid interface can be obtained by using another expression which was found in Section V. The undercooling at each point χ on the interface is given by

$$\Delta T = m_1\left[C_1^E - C_1(x,0)\right] + m_2\left[C_2^E - C_2(x,0)\right] + a\,K(x)$$

where m_1, m_2, and a are different for each phase. One can solve for the curvature $K(x)$ and integrate to find the slope of the interface since ΔT is not a function of χ and $C_1(x,0)$ and $C_2(x,0)$ are known. Jackson and Hunt (33) have done this for a binary eutectic and found that as the velocity of the interface increases, concavities will form in the widest lamellae. Although this integration was not performed for the ternary eutectic, it is felt the concavity will also form in the widest of the three lamellae in the ternary case, because of the similarity of the expressions for the curvature in the binary and ternary case. Qualitatively what happens can be seen in Figure 26. For a given steady velocity, the undercooling ΔT_c due to composition variation is shown along with the undercooling ΔT_σ due to the curvature for all positions on the interface. As the velocity increases, ΔT_c will increase to a value where ΔT_σ must be negative for certain parts of the interface to maintain an isothermal interface. This negative undercooling due to curvature requires that the curvature in that region of the interface be negative and hence a concavity. This con-

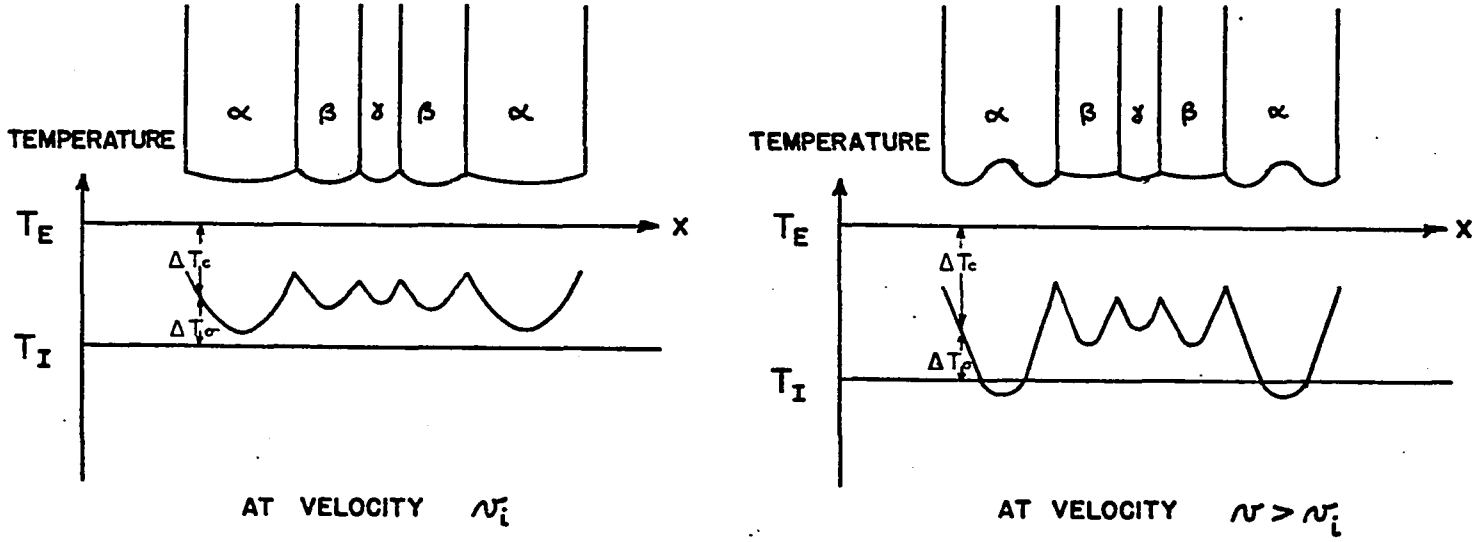

AT CONSTANT LAMELLAR SPACING λ_i

Fig. 26. Formation of concavities in the α lamellae liquid-solid interface due to velocity increase.

cavity will deepen with increasing velocity as long as the lamellar spacing remains constant. If the lamellar spacing remains constant and the velocity continues to increase, concavities can also form first in β lamellae and second the γ lamellae.

Jackson and Hunt's hypothesis that the formation of a new phase in the concavity when the sides of the concavity become infinitely steep would partially explain the splitting of the α phase and the formation of different phases in the concavity, but their hypothesis is inconsistent with the observation that in some regions in microstructure the β-γ-β composites also split with α lamellae forming in the splits at values of λ_d/λ_i similar to those for α phase splits.

While it is indisputable that the existence of concavities in the interface will aid in the nucleation of new lamellae, nucleation of new lamellae must be possible without the formation of concavities with infinitely steep sides. It is proposed that the temperature and liquid composition at the interface are at least equally as important as interface shape in the nucleation of new lamellae. As the velocity of the interface increases, the temperature of the interface decreases. Because the possibility for the nucleation of any new phase will occur where the liquid is richest in that component which is the solvent for that phase, one can look at the composition distribution at the interface and pick out the places where the new phases are likely

to nucleate. Now since under steady velocities, nucleation of new lamellae does not occur at these positions, some alteration of the conditions present during steady growth must be necessary. This alteration is precisely the increase in solute composition in front of each phase and the lowering of the temperature of the interface. Both of these favor the nucleation of new lamellae. In fact, for a very uniform lamellar structure, the value of the velocity at which the lamellar spacing begins to change and hence the value of the velocity at which nucleation occurs, is about 2.5 times the initial velocity. Hence

$$\frac{\Delta T_d}{\Delta T_i} = \frac{1}{2}\left[1+\frac{v_d}{v_i}\right] = \frac{1}{2}\left[1+2.5\right] = 1.75 \;;$$

i.e., when the undercooling of the interface reaches 1.75 times its original undercooling, the nucleation of new phases begins. In a later part of this section, more will be said about this undercooling change required to bring about the change in lamellar structure.

Several questions remain regarding the details of the nucleation of the new lamellae at the interface. First, the exact position on the interface where new α lamellae will nucleate is still uncertain. A possibility might be the groove on the interface formed by the β-γ interface. It can be seen from the composition distribution diagram (Figure 7) that the composition here is still quite favorable for the nucleation of a

α lamella. Second, nothing is known about the dual or even triple nucleation necessary for the formation of a β-γ-β composite in the α phase concavity.

The effect of lamellar structure uniformity on the change in velocity required to change the lamellar spacing has been mentioned before. At positions on the interface where any non-uniformity in the lamellar structure occurs, there will be slight perturbations in the conditions at the interface. Some of these perturbations will be of a type to cause nucleation in that vicinity to occur at a lower velocity change than is required for other points on the interface. Only a few perturbations of this type are needed to initiate an earlier change in lamellar spacing.

3. Decreases in Interface Velocity ---- Seven tests were performed in which the final interface velocities decreased to values of from .87 to .08 times the original velocities. A sequence of pictures from the movie film of a test of this type is shown in Figure 27. For each test the same quantities that were plotted for the velocity increase tests are given in Figures 28, 29, 30, and 31. Also in Table 3 will be found the same quantities for these tests that were tabulated for the velocity increase tests with the exception now that the value V_d represents the interface velocity at the instant when the lamellar spacing begins to increase. Also shown in Figures 32 and 33, for later consideration, are micrographs of the foil at the

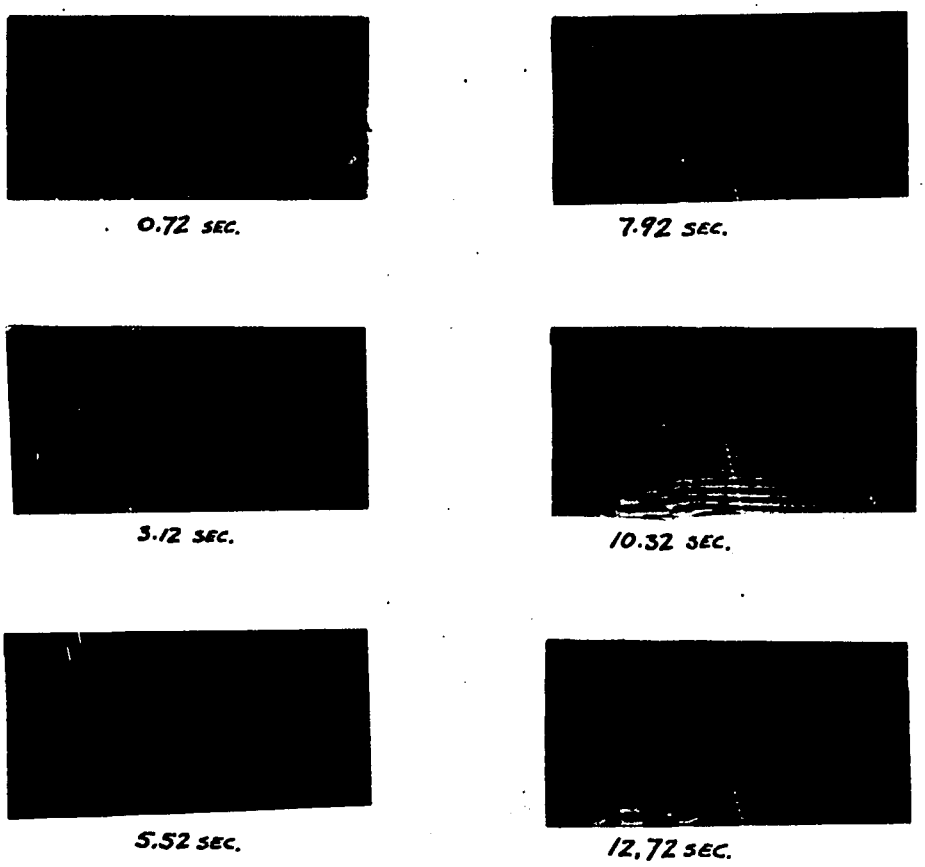

Fig. 27. Sequence of enlargements from movie film at 2.4 second intervals for velocity decrease test. (L19)

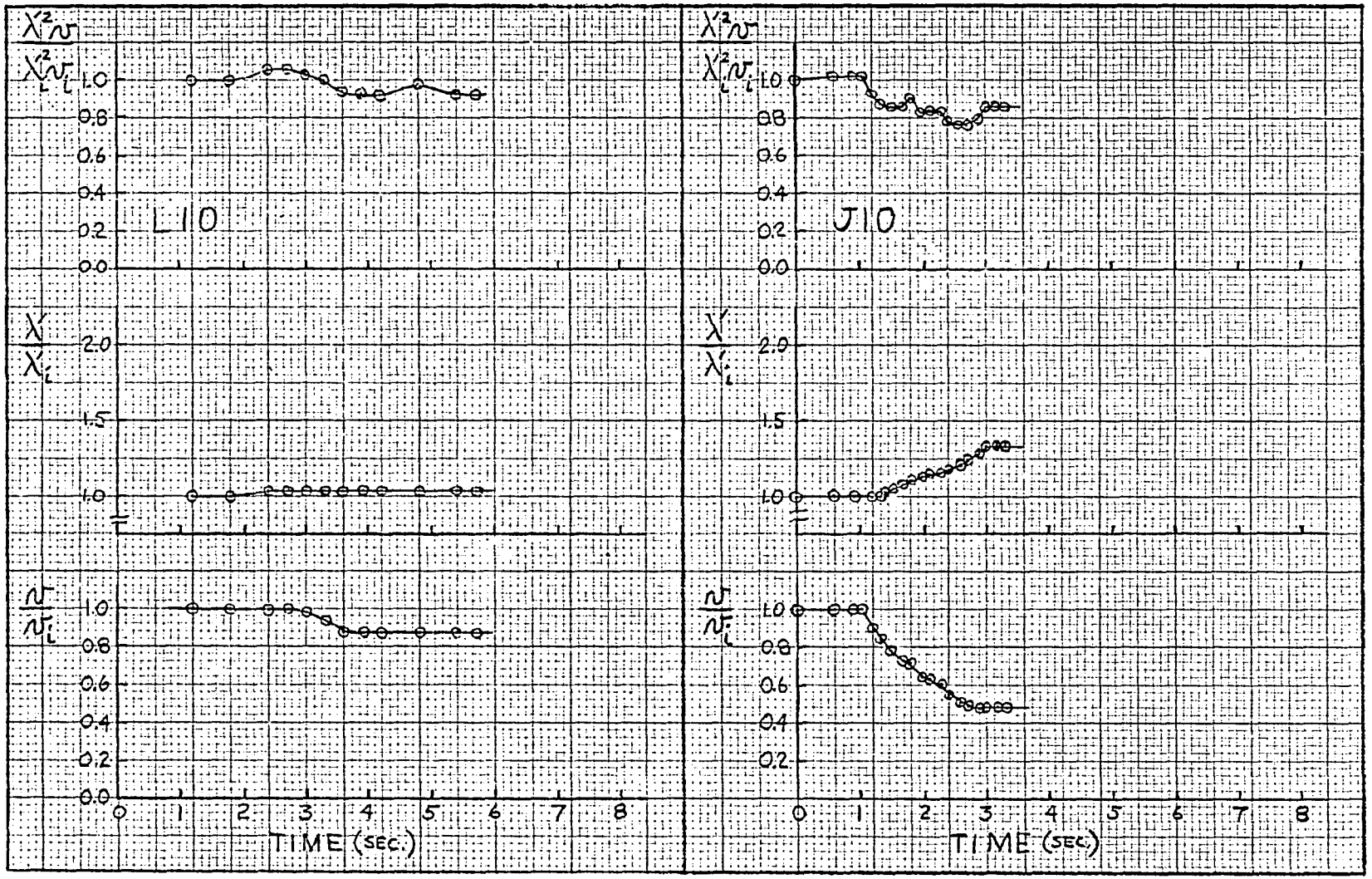

Fig. 28. Data for velocity decrease tests.

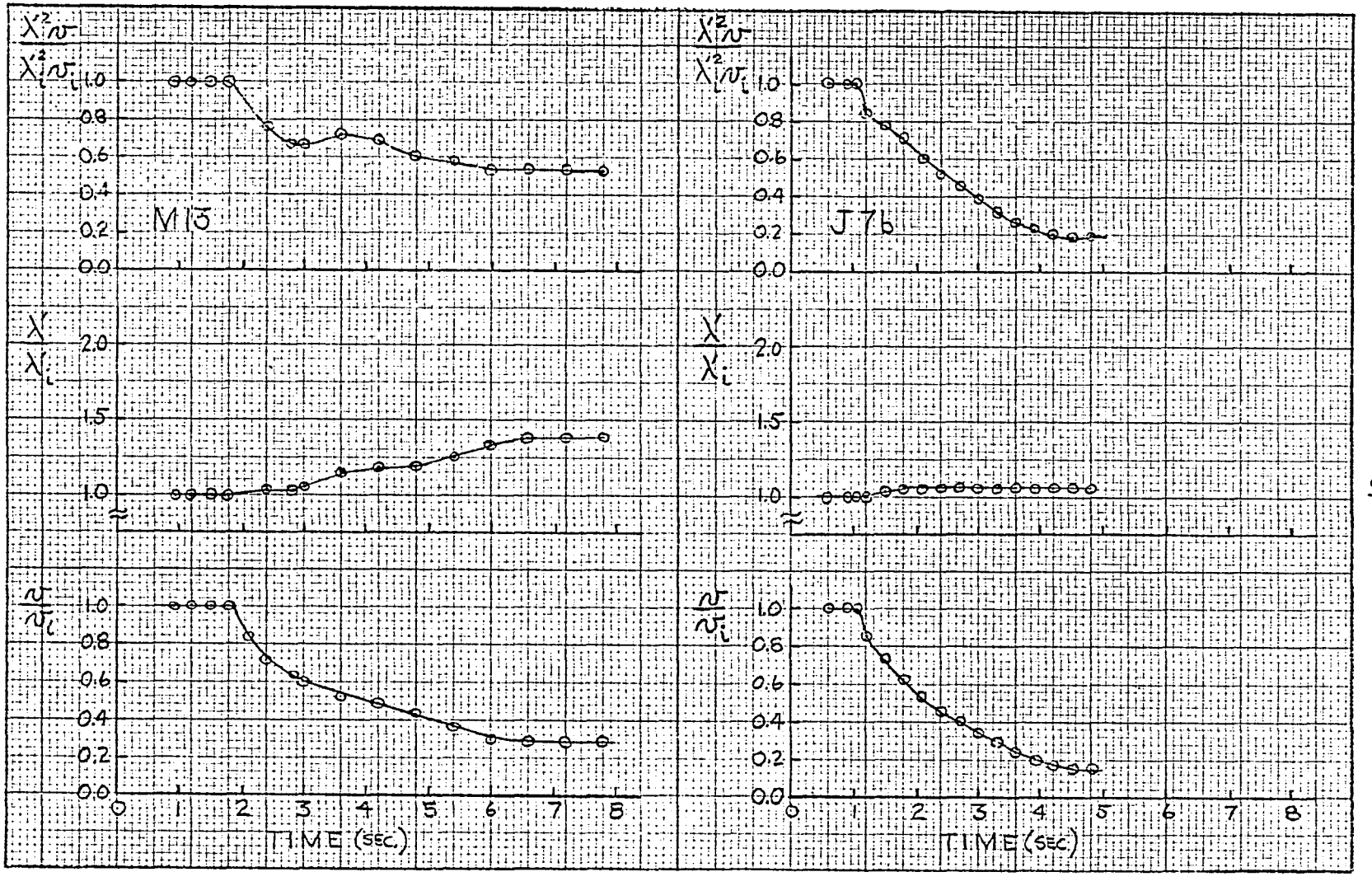

Fig. 29. Data for velocity decrease tests.

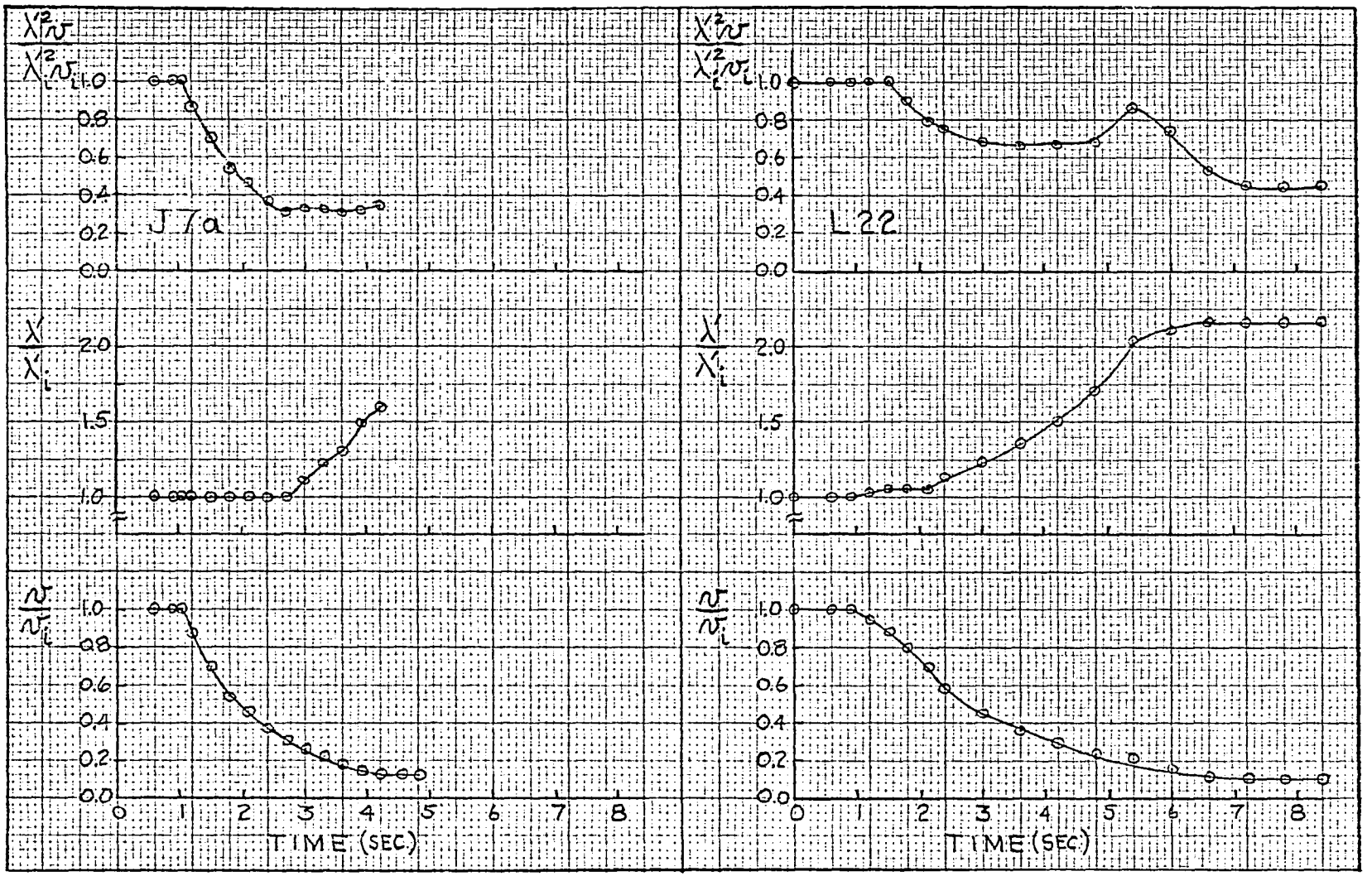

Fig. 30. Data for velocity decrease tests.

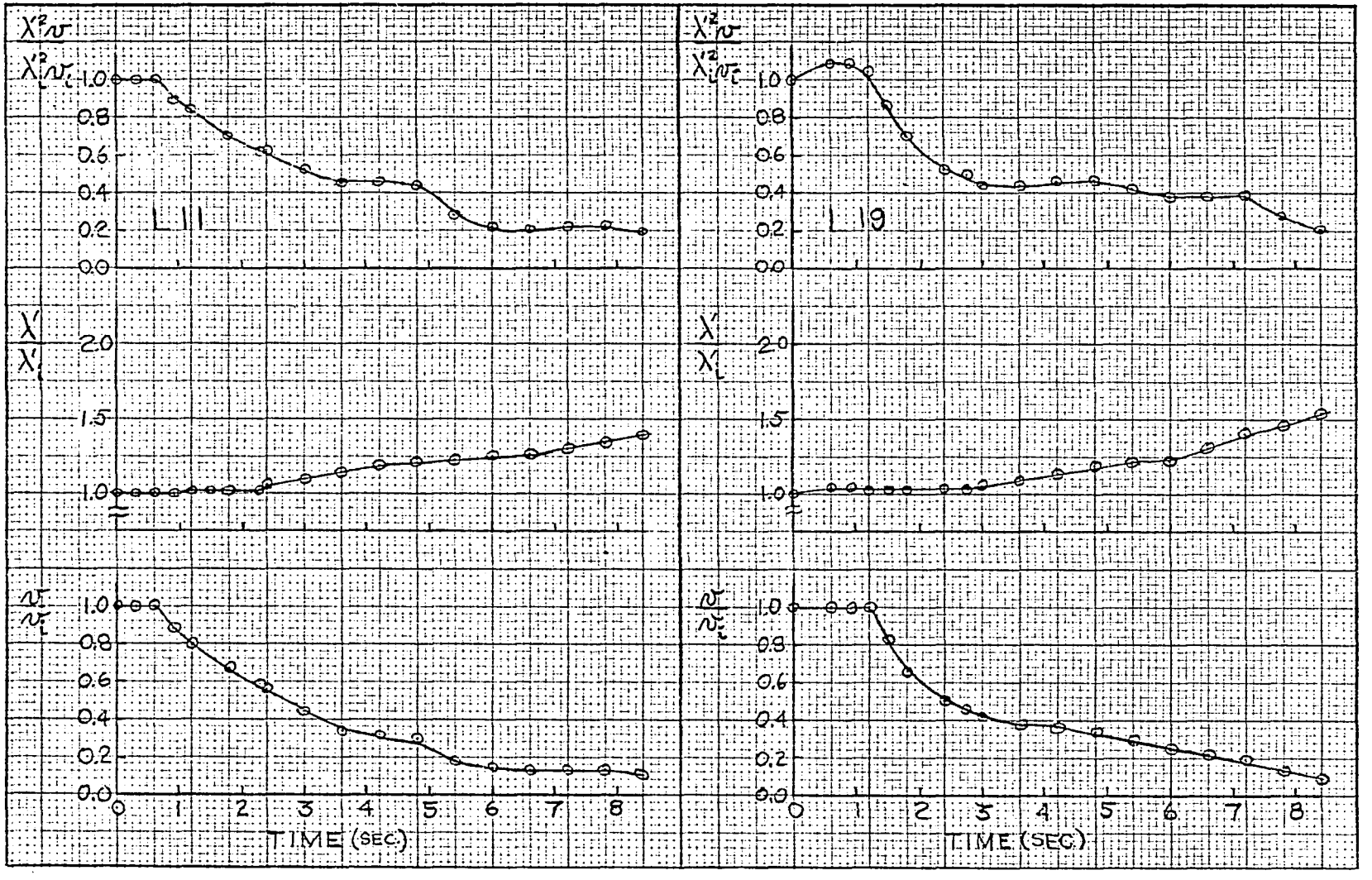

Fig. 31. Data for velocity decrease tests.

TABLE 3 (VELOCITY DECREASE TESTS)

TEST	v_i	v_f	$\frac{v_f}{v_i}$	χ_i	$\frac{\chi_f}{\chi_i}$	$\chi_i^2 v_i$	$\frac{\chi_f^2 v_f}{\chi_i^2 v_i}$	Δt	Δd	$\frac{v_d}{v_i}$	$\frac{v_d - v_i}{\Delta t}$	STRUCT. UNIFORM-ITY
#	$\frac{\mu}{SEC.}$	$\frac{\mu}{SEC}$	·	μ	·	$\frac{\mu^3}{SEC.}$	·	SEC.	μ	·	$\frac{\mu}{SEC.^2}$	#
L 10	18.80	16.30	0.87	1.46	1.03	40.1	0.92	---	---	---	---	---
J 10	31.34	15.04	0.48	1.41	1.33	62.3	0.85	0.30	9.2	0.85	-15.67	2
M 13	13.79	3.92	0.28	1.79	1.37	44.0	0.54	1.02	10.8	0.64	-4.87	3
J 7b	21.47	3.60	0.17	1.50	1.06	48.3	0.19	---	---	(0.17)	---	7
J 7a	22.72	2.66	0.12	1.65	1.60	61.5	0.34	1.68	22.6	0.31	-9.33	6
L 22	19.59	1.88	0.10	1.46	2.16	41.6	0.45	1.23	21.2	0.70	-4.78	1
L 11	13.63	1.25	0.09	2.07	1.43	58.4	0.21	1.68	17.4	0.59	-3.32	5
L 19	15.67	1.25	0.08	1.83	1.69	52.7	0.23	1.56	15.5	0.46	-5.42	4

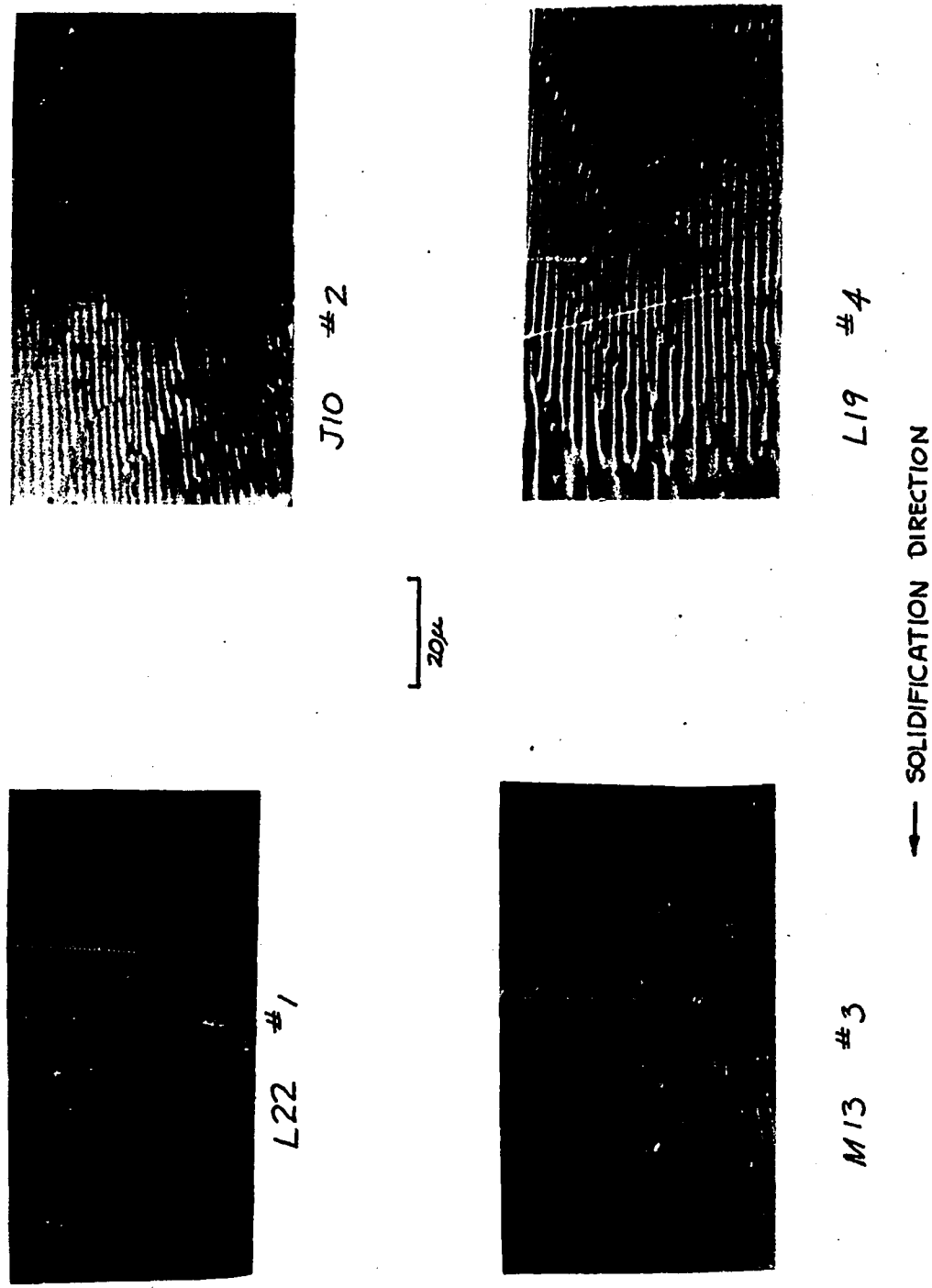

Fig. 32. Micrographs taken from movie film for each test showing structure uniformity no. (velocity decrease tests).

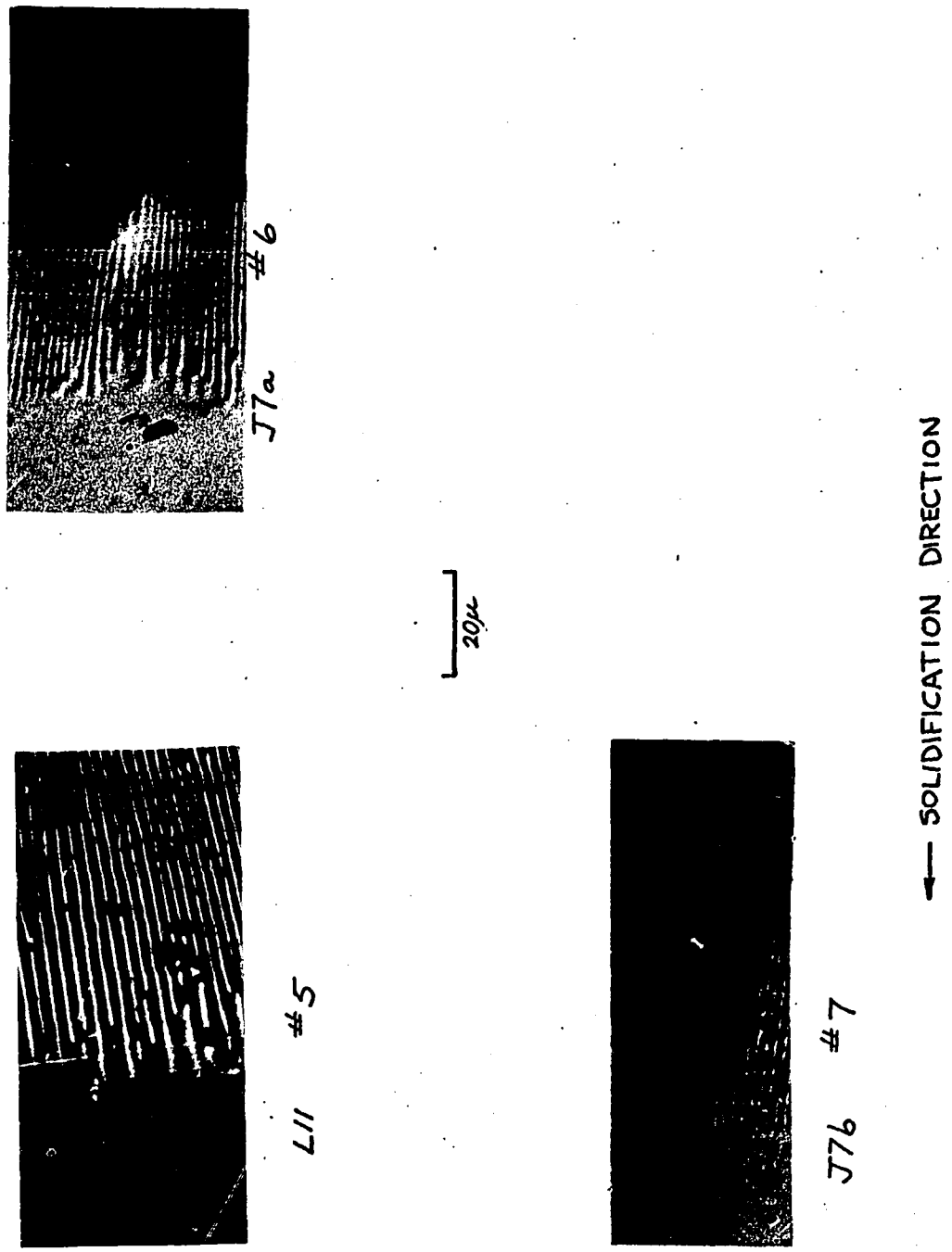

Fig. 33. Micrographs taken from movie film for each test showing structure uniformity no. (velocity decrease tests).

end of each test. These micrographs have again been numbered according to increasing uniformity of the lamellar structure to the right (cold) side of the place where the lamellar spacing began to increase. The same points mentioned in Part 2 of this Section are considered in this ordering. From these micrographs one can see that lamellar spacing increases are accomplished by the termination of individual lamellae. In these micrographs, one can definitely see places where dark (β-γ-β composite) lamellae terminate and places where light (α) lamellae terminate. They appear to be pinched off by the adjacent lamellae. There is no definite preference for either of these in the micrographs. It is also possible for increases in lamellar spacing to occur if the lamellae are not parallel. If the lamellae fan out in the growth direction they can increase their width continuously. This only occurred when the gross interface was convex with respect to the liquid. Spacing increases of this type were observed but were excluded from this work.

The first point to be noticed about these data is that in no case did the final value of $\lambda'^2 v$ return to its original value. With the exception of tests L 10 and J 10 this is felt to be due to the fact that the solidification was not observed long enough. Complete changes in lamellar spacing require a legitimate distance to occur. For all of these tests the final velocities were less than 4μ/sec, whereas the final velocities

for tests L 10 and J 10 were 16.30 and 15.04μ/sec. respectively. Hence only in tests L 10 and J 10 would one hope that the tests had been observed long enough. The value of the parameter $\frac{\lambda'^2_f v_f}{\lambda'^2_i v_i}$ = .85 for test J 10 gives one an idea of the lower limit which the lamellar spacing can have for a steady velocity. That is, after a velocity decrease, the lamellar spacing only has to increase to the point where $\frac{\lambda'^2 v}{\lambda'^2_i v_i}$ = .85. Further changes could be accomplished by the slower process of lamellar fault motion. One might speculate that if the final velocity is greater than .85 times the initial velocity, that no spacing change would occur. This is the case for test L 10.

The second point to be noticed is that no definite stages were seen in the lamellar spacing increases. This lack of observation however does not definitely preclude the existence of stages since in all the tests where the change in velocity was large enough to require staging, the final velocity was so slow that the tests probably were not observed long enough to see stages if they occurred.

The third point regards the initial response of the lamellar spacing to a velocity decrease. If the interface velocity was reduced to zero in a short enough time, no change in lamellar spacing was observed. Also in test J 7b no change in spacing was seen when the velocity had decreased to a final steady velocity of 3.6μ/sec. ($\frac{v_f}{v_i}$ = .17). It is assumed that the spacing would have finally responded if the test had been

observed longer. For this test then the value of $\frac{\Delta v_d}{\Delta v_i}$ will be set equal to .17. The values of $\frac{\Delta v_d}{\Delta v_i}$ for all of the tests in which the velocity change was large enough to cause a spacing change (this excludes L 10) are graphed against their structure uniformity number, their average accelerations, and $\frac{\Delta v_f}{\Delta v_i}$ in Figure 34. It is seen that the acceleration and the total velocity change have no simple effect on the values of $\frac{\Delta v_d}{\Delta v_i}$, but the higher the uniformity number, the smaller the value of $\frac{\Delta v_d}{\Delta v_i}$. Hence the more uniform the lamellar structure, the larger the velocity decrease required to initiate the change in lamellar structure.

Attempts to formulate a mechanism of lamellae termination for a perfect lamellar structure, which is consistent with all of the above observations have been unsuccessful. That no such mechanism might exist is at least partially substantiated by the fact that for the extremely uniform structure of test J 7b, no change in lamellar spacing was found. A mechanism which accounts for only the pinching off of the β-γ-β composite can be speculated upon using the same type of analysis used in Part 2. As the interface velocity decreases from a steady value, the solute composition in front of each phase decreases, the temperature of the interface increases, and the shape of the interfaces of the lamellae becomes more convex into the liquid. Because it has been observed (40) that the α phase slightly leads the gross interface using a quench technique,

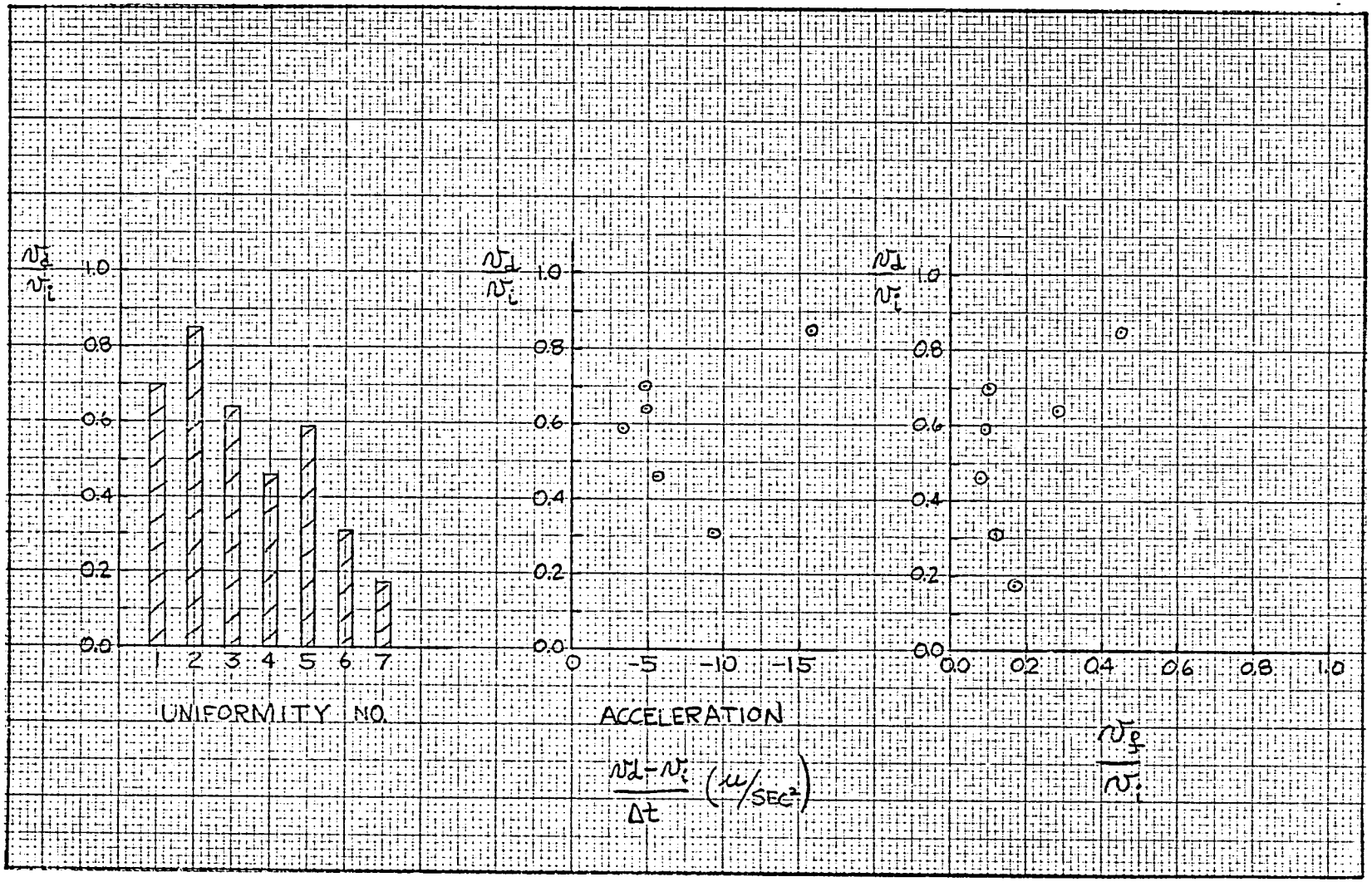

Fig. 34. Correlation of v_2/v_i with structure uniformity no., acceleration, and v_f/v_i (velocity decrease tests).

and because the increased convexity will cause the widest (α) phase to protrude into the liquid more than the others, overgrowth of the α lamellae might be possible. This overgrowth might cause the pinching off of the β-γ-β composite. This mechanism does not allow for the pinching off of α lamellae, however.

There are no observations made here which contradict the ideas of Jackson and Hunt (33) about the termination of individual lamellae due to "boundary layer instabilities." In fact, the observation that the more uniform the structure the larger the velocity decrease required to initiate the spacing increase supports their idea that for eutectic compositions these instabilities occur at positions of irregularity in the lamellar structure. Also "boundary layer instabilities" cause different phases to be pinched off depending on the relation of the average liquid composition at the interface to the eutectic composition. This is consistent with the observation that at different places on the interface, different phases are pinched off.

4. Oscillating interface velocities ---- Three tests were performed in which the interface velocity (always non-negative) oscillated. The interface velocity v, the apparent lamellar spacing λ' and the product $\lambda'^2 v$ are plotted as functions of time for each test in Figures 35 and 36. One can see that for none of the tests did the product $\lambda'^2 v$ remain constant. For

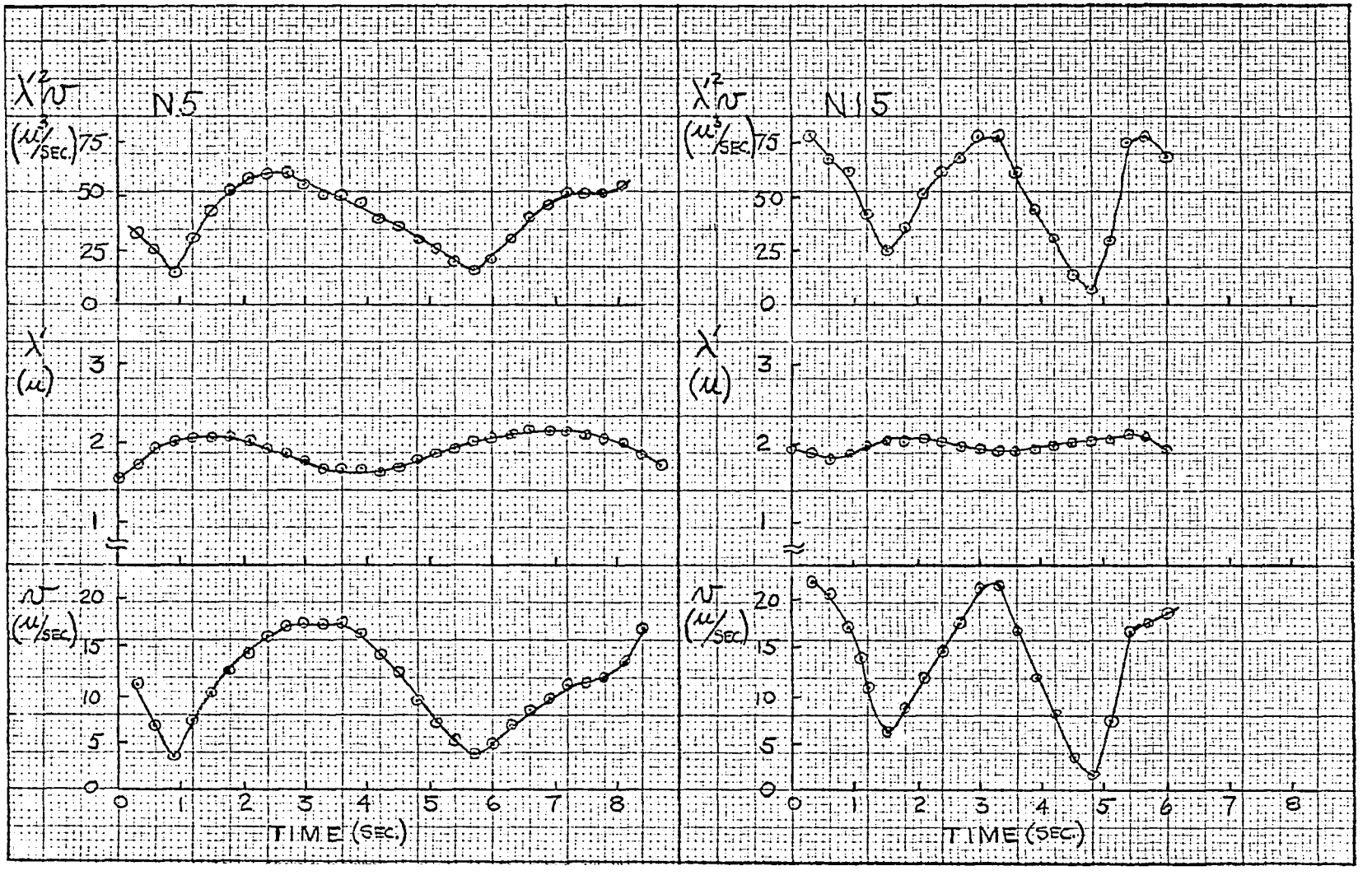

Fig. 35. Data for oscillating velocity tests.

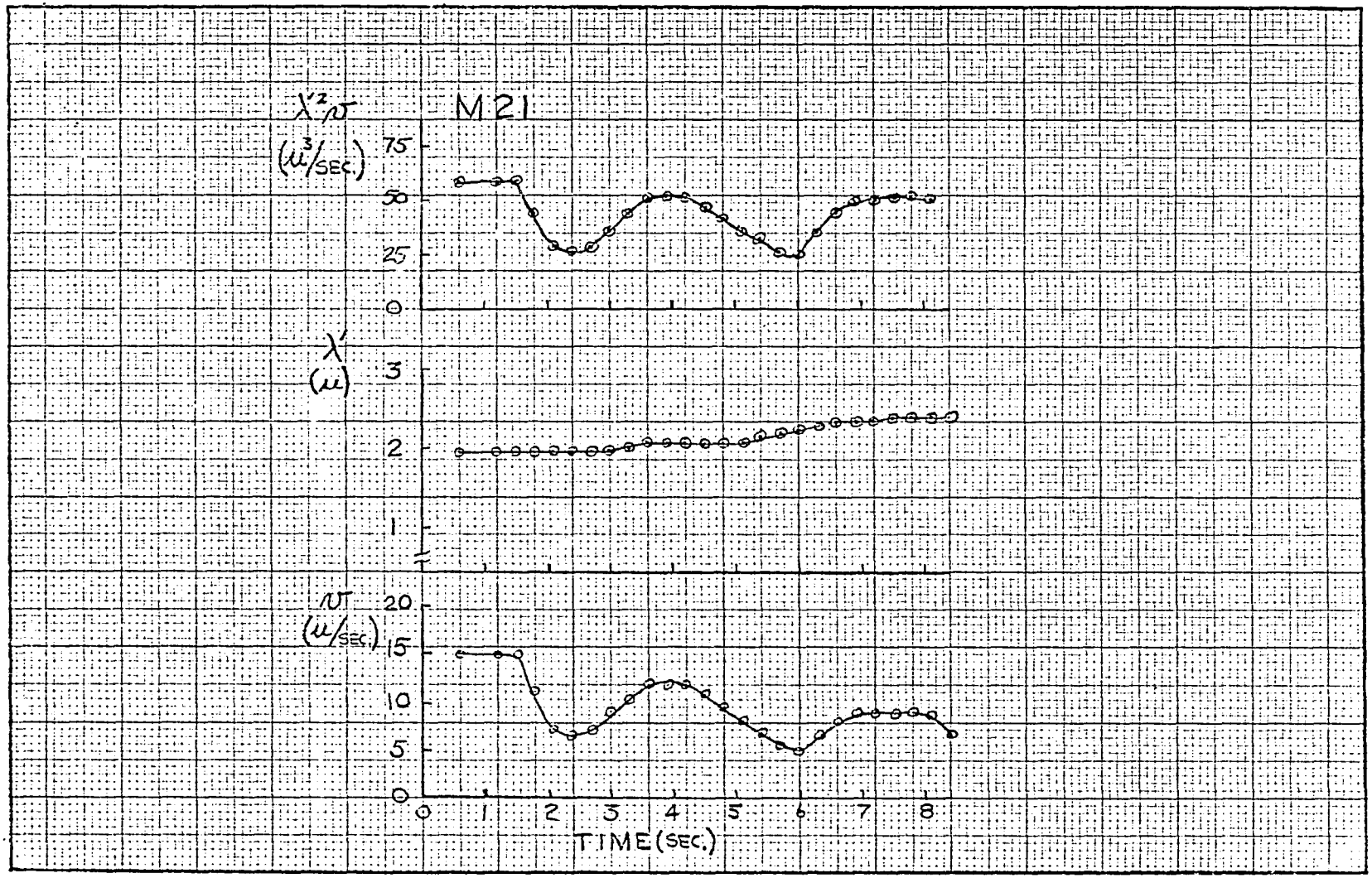

Fig. 36. Data for oscillating velocity tests.

tests N 5 and N 15 the instants of maximum and minimum spacing do not correspond to the instants of minimum and maximum velocity respectively. This fact is of course indicative of the delay in lamellar spacing change in response to interface velocity changes. In test M 21, the oscillations in velocity are the smallest of the three tests. Although the lamellar spacing is not perfectly constant, it is obvious that the changes in spacing have nothing to do with the oscillations in velocity. In fact, the slight increase in spacing seen in this test is caused by the slight increase in the values of the velocity over the course of the entire test. This failure of the lamellar spacing to react to the oscillations in velocity is consistent with the statements made previously regarding the magnitude of the velocity changes required to initiate the changes in lamellar spacing. Figure 37 shows cross-hatched regions which contain those values of $\frac{v_d}{v_i}$ that caused changes in lamellar spacing by the termination or formation of individual lamellae. Also shown is a plot of

$$\frac{\Delta T}{\Delta T_e} = \frac{1}{2}\left[\left(\frac{v}{v_i}\right)^{\frac{1}{2}} + \left(\frac{v}{v_i}\right)^{-\frac{1}{2}}\right]$$

Test M 21 is supposed to take place in the central region. Picking a value of $v_i = 8.31\ \mu/\text{sec}$, $\frac{v_{max}}{v_i}$ and $\frac{v_{min}}{v_i}$ for the oscillations of test M 13 are 1.41 and .79 respectively. These values are almost within the central region. The exact width of the central region for any test is of course a function

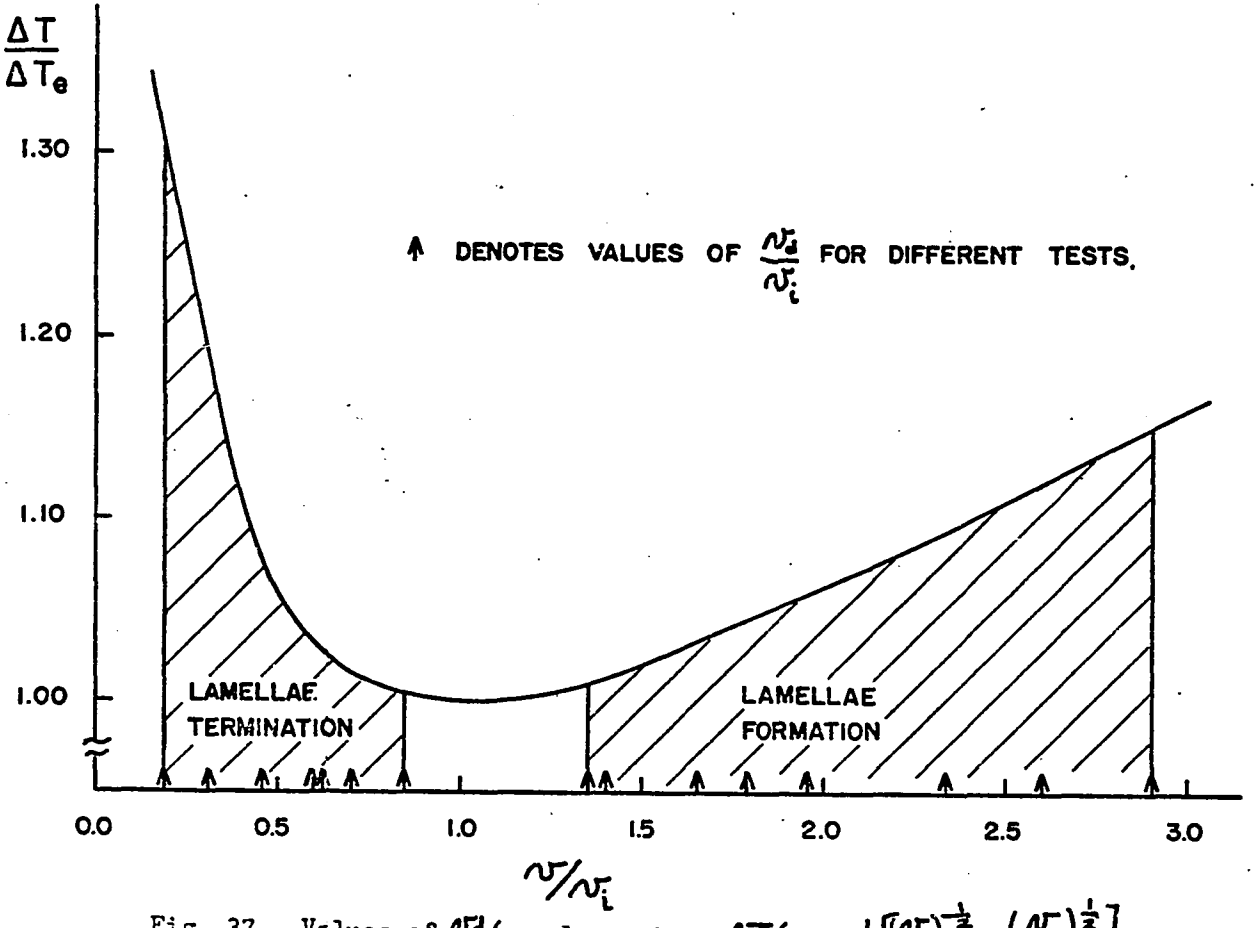

Fig. 37. Values of ν_d/ν_i along with $\Delta T/\Delta T_e = \frac{1}{2}\left[\left(\frac{\nu}{\nu_i}\right)^{-\frac{1}{2}} + \left(\frac{\nu}{\nu_i}\right)^{\frac{1}{2}}\right]$

of the uniformity of the lamellar spacing.

The $\frac{\Delta T}{\Delta T_e}$ curve shows that the change in lamellar spacing, whether caused by lamellae formation or termination, might be initiated when the velocity reached a value at which the undercooling of the interface exceeded by a certain amount the undercooling that the interface should have if the lamellar spacing satisfied the extremum condition for that velocity. This shows that for a variety of tests the uniformity of the lamellar structure is much more important in determining the value of $\frac{\lambda_d}{\lambda_i}$, than is the change in undercooling.

IX. CONCLUSIONS

Experimental Technique -- A topography is produced on the free surface of a solidifying foil of the Pb-Sn-Cd ternary eutectic through which the liquid-solid interface and the lamellar microstructure can be continuously observed when examined through an optical microscope using oblique illumination. A relatively planar liquid-solid interface, which is perpendicular to the surface of the foil and whose velocity is controllable, can be obtained by heating the foil with an electric current through part of the wire loop used to support the foil. The solid microstructure of a solidified foil of the Pb-Sn-Cd ternary eutectic is the same at the surface of the foil as it is in the interior of the foil and as it is in bulk ingots.

Non-steady Solidification of the Pb-Sn-Cd Ternary Eutectic -- For the solidification of foils of Pb-Sn-Cd ternary eutectic, changes in lamellar spacing corresponding to large changes in liquid-solid interface velocity occur by the termination of individual lamellae for spacing increases, and by the nucleation of new lamellae for spacing decreases. In either case no particular lamellar phase is favored for the termination or formation.

For large changes in the liquid-solid interface velocity from an initially steady value, the lamellar spacing produced at the interface does not change exactly when the velocity does. For the types of velocity changes performed in this work, the parameter which best describes the conditions which initiate the spacing change is the ratio of the interface velocity to the initial interface velocity, rather than the details of the velocity change. The critical value of this parameter at which the spacing begins to change depends strongly on the uniformity of the lamellar structure in the region solidified before the spacing change. The more uniform the lamellar structure, the further the critical value of the parameter is from unity.

When the final interface velocity is greater than four times the initial velocity, the lamellar spacing produced at the interface does not decrease uniformly in time but decreases in stages to its final value.

The total change in lamellar spacing accomplished by the termination or formation of individual lamellae and caused by a change in interface velocity from one steady value to another, is never large enough to return the value of $\lambda'^2 v$ to its original value.

It is possible to produce a lamellar structure with constant lamellar spacing with an oscillating solidification velocity.

In the opinion of the author, the results obtained through the solidification of eutectic foils are representative of phenomena occurring in bulk ingots. For uniform lamellar structures, the nucleation of new lamellae is controlled not only by the formation of concavities in individual lamellar interfaces, but also is directly controlled by the temperature of the interface and the composition of the liquid at different points on the interface. The termination of individual lamellae caused by interface velocity decreases is adequately described by the basic ideas of Jackson and Hunt concerning "boundary layer instabilities."

Bibliography

(1) G. A. Chadwick, Eutectic Alloy Solidification, Progr. Mater. Sci., 12, 1963, 97.

(2) H. W. Kerr & W. C. Winegard, Journal of Metals, 18, 1966, 563.

(3) R. W. Kraft, Advances Mat. Research, 5, 1971, 83.

(4) F. Guthrie, Phil. Mag. Ser 4, 49, 1875, 274.

(5) see F. L. Brady, J. Inst. Metals, 28, 1922, 372.

(6) W. Rosenhain & P. Tucker, Trans. Roy. Soc. (London), 209A, 1909, 89.

(7) G. Tammann, A Text Book of Metallography, Chem. Cat. Co., (New York), 1925.

(8) F. E. E. Lamplough & J. T. Scott, Proc. Roy. Soc. (London), 90A, 1914, 600.

(9) C. H. Desch, Metallography, Longmans Green (New York), 1918.

(10) R. Vogel, Z. Anorg. u. Allgem. Chem., 76, 1912, 425.

(11) F. L. Brady, J. Inst. Metals, 28, 1922, 369.

(12) A. M. Portevin, J. Inst. Metals, 29, 1923, 239.

(13) G. Tammann & G. Moritz, Z. Anorg. u. Allgem Chem., 214, 1933, 414.

(14) A. A. Bochvar & K. V. Gorev, Ann. Sec. Anal. Phys. Chim., Inst. Chim. Gen. (USSR), 8, 1936, 283.

(15) W. C. Winegard, S. Majka, B. M. Thall, & B. Chalmers, Can. J. Chem., 29, 1951, 320.

(16) C. S. Smith, A History of Metallography, Univ. Chic. Press, Chic., 1960.

(17) G. Phragmen, J. Inst. Metals, 77, 1950, 489.

(18) P. W. Bridgman, Proc. Am. Acad. Arts & Sciences, 60, 1925, 303.

(19) R. B. Pond & S. W. Kessler, J. Metals (Trans. AIME), 3, 1951, 1156.

(20) F. Weinberg & B. Chalmers, Can. J. Phys., 29, 1951, 382.

(21) F. Weinberg & B. Chalmers, Can. J. Phys., 30, 1952, 488.

(22) M. E. Glicksman, in Solidification, ASM. (Metals Park), 1971.

(23) K. A. Jackson & J. D. Hunt, Acta Met., 13, 1965, 1212.

(24) A. Rosenberg & W. C. Winegard, Acta Met., 2, 1954, 603.

(25) M. E. Glicksman & R. J. Schaefer, Acta Met., 14, 1966, 1126.

(26) D. P. Woodruff & A. J. Forty, Phil. Mag., 15, 1967, 985.

(27) V. de L. Davies, J. Inst. Metals, 92 (1963-1964), 127.

(28) H. E. Cline, Trans. Met. Soc. AIME, 239, 1967, 1489.

(29) N. Takahashi & K. Ashinuma, J. Inst. Metals, 87, 1958-1959, 19.

(30) E. Scheil, Z. Metallk., 37, 1946, 1.

(31) C. Zener, Trans. AIME, 167, 1946, 550.

(32) W. A. Tiller, in Liquid Metals and Solidification, ASM, Cleveland, 1958.

(33) K. A. Jackson & J. D. Hunt, Trans. Met. Soc. AIME, 236, 1966, 1129.

(34) J. J. Kramer & W. A. Tiller, J. Chem. Phys., 42, 1965, 257.

(35) J. W. Cahn, unpublished, see Reference 33.

(36) C. Li & H. W. Weart, J. Metals, 14, 1962, 86.

(37) H. W. Kerr, J. A. Bell, W. C. Winegard, J. Aust. Inst. Metals, 10, 1965, 64.

(38) D. J. S. Cooksey & A. Hellawell, J. Inst. Metals, 95, 1967, 183.

(39) I. Crivelli-Visconti, Metallurgia Italiana, 60, 1968, 822.

(40) J. P. Chilton & W. C. Winegard, J. Inst. Metals, 89, 1961, 162.

(41) J. D. Hunt, Ph.D. thesis, Cambridge University, 1963.

(42) A. S. Yue, Trans. Met. Soc. AIME, 224, 1962, 1010.

(43) J. D. Hunt & J. P. Chilton, J. Inst. Metals, 92, 1963, 21.

(44) V. de L. Davies, J. Inst. Metals, 93 (1964-1965), 10.

(45) J. D. Hunt & J. P. Chilton, J. Inst. Metals, 91 (1962-1963), 338.

(46) A. Moore & R. Elliot, Joint Conference on Solidification of Metals, Iron & Steel Institute, Brighton, England, 1967, Paper B/I/5.

(47) I. Crivelli-Visconti, Metallurgia Italiana, 60, 1968, 431.

(48) F. R. Mollard & M. C. Flemings, Trans. Met. Soc. AIME, 239, 1967, 1526.

(49) F. N. Rhines, Phase Diagrams in Metallurgy, McGraw-Hill, New York, 1956, 161.

(50) A. Stoffel, Z. Anorg. Chem., 53, 1907, 167.

(51) D. D. Double, P. Truelove, & A. Hellawell, unpublished, see Reference 3.

Vita

William James Boettinger was born on July 22, 1946 in Baltimore, Maryland. He attended the Baltimore Polytechnic Institute from 1960 to 1964. From 1964 to 1968, he attended the Johns Hopkins University and completed his B.E.S. degree in Mechanics with general honors. During his undergraduate years at Hopkins he was elected to Tau Beta Pi and Pi Tau Sigma.

From 1968 to date, he pursued graduate study in the Department of Mechanics at the Johns Hopkins University with an NDEA IV Fellowship and a Kennecott Refining Company Fellowship. During that time he also served as a Research Assistant to Professor R. B. Pond and a Junior Instructor for Assistant Professor W. F. Hartman. As a graduate student he was the recipient of the 1971 ASTM Student Award for the Middle Atlantic States, and was elected to Alpha Sigma Mu. He is a member of the Maryland Institute of Metals and a joint student member of AIME and ASM.